GAS TREATMENT UTILIZING PULSED DISCHARGE PLASMA

January 1996

DOCTOR OF ENGINEERING

KAZUO SHIMIZU

TOYOHASHI UNIVERSITY OF TECHNOLOGY

GAS TREATMENT UTILIZING PULSED DISCHARGE PLASMA

January, 1996

DOCTOR OF ENGINEERING

Kazuo Shimizu

TOYOHASHI UNIVERSITY OF TECHNOLOGY

Dedicated to my parents

論　文　要　旨

本論文は放電プラズマを用いた有害ガス（主にＮＯｘ）浄化の研究結果を報告するものである。

直流コロナ放電に対するパルスストリーマ放電の優位性の一つは電子の持つエネルギーを他の中性ガス分子のエネルギーと比較して高くできることである。本研究では電子のエネルギーをパルス放電時の電子電流の測定および窒素の2 nd positive band (337.1 nm)の発光分析から調べた。電子電流の測定は窒素ガス、メタンガス中で行い、これらから低エネルギー電子の存在が確認できた。

窒素ガス中の発光分析からはプラズマ化学反応を誘起、促進するための活性ラジカルを生成するために十分なエネルギー（十数eV程度）を持つ高エネルギー電子が存在することが確認できた。発光強度の変化から非熱平衡プラズマ中のE/N（Ｅは電界強度、Ｎはガス密度）により大きく影響を受けることも認められた。パルスストリーマ放電中では大気圧下での平均電界強度10 kV/cm以上（平均E/N値40 Td）の高電界が得られ、これを直流コロナ放電で得ることは困難である。また、パルスストリーマ放電が直流コロナ放電に比べてはるかに広い空間をプラズマ化できるという優位性を、空気を用いてオゾン濃度の分布を測定することで実験的に評価している。

本ガス浄化を実用化するためには、放電電力の低減化、ＮＯｘ除去反応の一層の促進が必要であり、乾式、半湿式、湿式、極低温反応器などの非熱平衡プラズマ反応器およびオゾン注入法の特徴を調べた。また、ガス温度やガス組成などにおけるＮＯｘ除去時のエネルギー消費低減化の条件を実験的に検討した。その結果、エチレンの添加がＮＯの酸化反応を大幅に促進すること、湿式反応器が放電プラズマ中でＮＯｘの吸収除去を促進すること等を見出し、これによりガス浄化のエネルギー効率を高く出来ることを示している。

放電プラズマ中でのNOx除去反応プロセスにおける炭化水素化合物および水蒸気濃度の影響を実験的に調べるとともに、反応副生成物の同定を行ない、有害な物質を生成しないことを確認している。炭化水素化合物（エチレン）添加時、および無添加時の放電副生成物をＦＴＩＲにより分析したところ、比放電電力が高く（300 J/g程度）長時間の放電プラズマ処理では酢酸（CH_3COOH）が認められた。比放電電力の低い場合（30 J/g程度）は副生成物としてアセトアルデヒド（CH_3CHO）およびホルムアルデヒド（ＨＣＨＯ）が認められた。これらの存在から、ＮＯｘ除去は炭化水素化合物のプラズマ化学反応過程中に生成する活性ラジカル（ＯＨ、HO_2など）の再生産により促進されると考えられる。

パルス電圧印加の湿式反応器を用いることで、NOx除去効率（80%）ならびに比放電電力（120 J/g以下）を実用的なレベルとすることが可能であることを示した。

ABSTRACT

In this work polluted gas treatment (mainly NOx) utilizing discharge plasma has been investigated.

To clarify the relatively high electron energy of non-thermal plasma, estimation of electron energy was carried out by light emission of N2 second positive band (337.1 nm) with spectroscopy. Also, a more direct method i.e. electron current measurement was carried out with nitrogen or methane gas as a carrier gas. The N2 second positive band could be produced through the collisions of high energy electrons. Higher E/N value gave the higher light emission signal peak suggesting that the electron energy was significantly affected by E/N value of given pulse voltage. Also, the high average electric field due to pulse discharge at NTP (10 kV/cm ≅ E/N of 40 Td) can be hardly achieved by dc corona discharge. The superiority of pulsed streamer discharge compared to that of dc corona discharge was evaluated by measuring ozone concentration. It was confirmed that pulsed streamer discharge generates very large volume of plasma compare to that of dc corona.

Main part of this work is experimental study of NOx removal utilizing discharge plasma. Dry, semi-wet, wet, and very low temperature plasma reactors with and without ozone injection method were proposed to decrease NOx removal energy consumption. Gas conditions such as temperature and composition, that affected the NOx removal energy consumption, were experimentally investigated.

Using dry type reactor, addition of hydrocarbon agent (ethylene) has shown excellent results on NOx removal study for gas temperatures above 200 °C. By-product analysis was carried out with FTIR, when hydro carbon agent was added to simulated flue gas. Relatively high power consumption (about 300 J/g) and long discharge exposure time yields acetic acid as one of the by-products. At low power consumption, acetaldehyde and formaldehyde were confirmed. From the existence of these by-products, it was observed that NOx removal process was enhanced by active radicals re-production (OH, HO_2 etc.) and chain reaction during plasma discharge.

Energy considerations were studied to estimate these techniques suited for practical use of gas cleaning. In the range of this study, the wet type reactor is the most efficient one to treat the pollutant gases from the point of power consumption which was within 120 J/g energy and resulted in 80% NOx removal efficiency.

CONTENTS

1. INTRODUCTION

1.1 Necessity of new technology for environmental problems

In Japan, treating the flue gas from the thermal power plants is being carried out with conventional combustion modification including two stage burner or low NOx burner and chemical treatment such as selective catalytic reduction and non selective catalytic reduction. These methods have shown good results and nitrogen dioxides, sulfur dioxide, and suspended particulate matter are under good control at the thermal power plants.

However, these conventional methods are not economical and suitable for small plant or mobile emission sources. Therefore nitrogen dioxide, suspended and oxidants exhausted from mobile emission sources are far from desirable level. Still, conventional chemical process or even novel method like E-beam process [1-5] was used with ammonia or lime to neutralize the acid pollutant like NOx or SOx. Relatively large scale power plants can be handled these chemical agents, but for small plants or mobile emission sources, they are not only economical but also sometimes dangerous.

In addition, recently interest for environmental problems is still increasing and calls for co-generation system which enables efficient use of fossil fuels, reduction of carbon dioxide emissions and production of electrical and thermal energy on-site.

These situations are the motivation to develop new small pulsed discharge plasma technique without ammonia or lime especially at crowded city area where co-generation system can be installed. A compact exhaust gas cleaning system on vehicles is also desirable. Further, development of new air purification techniques for reduction of chlorofluorocarbons (CFCs), volatile organic compounds (VOCs), bad

odors or microbes/viruses in households etc., will improve the working and living environments.

The Non-thermal electron beam (E-beam) irradiation process is one of the new exhaust gas treatment systems being developed [1-5].

In this method, the energy of the electron beam is used directly to dissociate and ionize the background gas. During the ionization by the high energy beam, a shower of secondary electrons is produced, which further produce a cascade of ionization and dissociation. This cascading effect produces energetic active radicals, results a large volume of plasma that promotes chemical reactions aiding the removal of pollutants. From the results of basic studies pilot-plant tests have been done in Japan [1-3], Germany [4,5], and other industrial countries, the electron beam process is considered to have an excellent potential for the simultaneous removal of NOx and SOx from high-sulfur, coal-fired utility boiler combustion gases.

However, the necessity of thick X-ray shielding and high initial cost has limited the use of this method for gas cleaning. These limitation make this excellent method can apply for the large scale plants or coal-fired utility boiler only. This situation has motivated studies into alternate plasma-based technologies such as those utilizing electrical discharges i.e. "*non-thermal plasma*" or "*non-equilibrium plasma*" (sometimes simply called "*discharge plasma*"). This electrical discharges can be produced in many different forms depending on the geometry of the reactor and the electrical power supply. Many reactor designs use electrodes, such as small diameter wires, needles or sharp edged metals that promote strong electric fields. The reactors are driven by direct current (DC), alternating current (AC; not only driven by commercial frequency but also high frequency ranged tens of kHz to MHz) or pulsed power sources.

Recently, non-thermal plasma (or non-equilibrium plasma) offers a novel approach to clean exhaust gases [6-10]. Radicals produced by the discharge plasma lead to chemical processes similar to that in E-beam process. Other discharge plasma such as surface discharge or partial discharge of the packed bed reactor was used not only for the removal of NOx but also for the removal of VOCs or CO_2 [11-13]. This technique involves low initial cost and small power source unlike the E-beam method. Poisonous gaseous and solid pollutants can be removed simultaneously using non-thermal discharge plasma. There are several kinds of plasma discharges, of which, the pulsed streamer discharge is

mainly used for NOx removal and is being dealt with in the present thesis.

In the latter half of this chapter various kinds of discharge will be introduced to help comprehending the plasma discharge.

1.2 Introduction to Plasma Discharges

In non-thermal plasma, temperature of electron is high but that of ion is low and gas temperature stays low. For gas cleaning, non-thermal plasma should be formed in large volume of gas at atmospheric pressure. There are several means to produce non-thermal plasma. Fig. 1.2.1 shows examples of reactors producing non-thermal plasma [14].

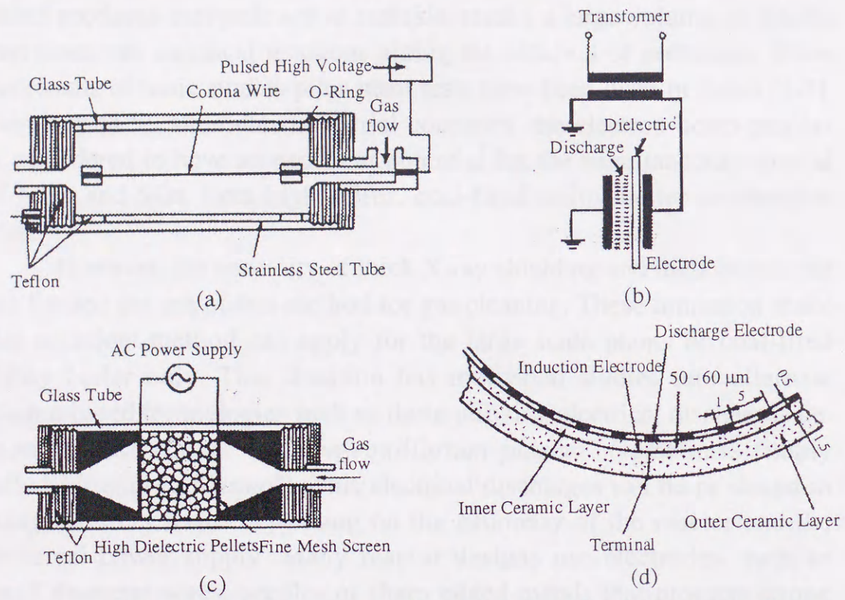

Fig. 1.2.1 Schematic of non-thermal plasma reactors.
(a) Pulsed streamer corona discharge , (b) Silent discharge ,
(c) Partial discharge, (d) surface discharge

1.2.1 Pulsed streamer discharge

One type of discharge that has shown very promising results is the pulsed streamer discharge (also called pulsed corona discharge). The industrial implementation of this reactor has the advantage of low retrofit cost since it can use the same wire-plate electrode geometry as in electrostatic precipitators (ESPs). Precipitators are commonly used for collecting particulate matter (PM) in the utility, iron/steel industries, paper manufacturing, cement industries and coal-fired utility boilers.

Fig. 1.2.1(a) shows the example of the pulsed streamer corona reactor. When a non-uniform electrode is energized with pulsed high voltage having fast rising time (less than 100 ns) and short pulse width (less than 1 μs), streamers are generated and propagate further in the electrode spacing since flashover voltage increases with decreasing pulse width. Pulsed streamer discharge can ionize larger volume of gases than that with DC discharges. In pulsed streamer discharge, electrons are accelerated and acquire energy to ionize gas molecules. The ionization energy is about 10 - 15 eV. Various active radicals are, therefore, formed in the non-thermal discharge plasma.

Since the mobility of ions is about one third of that of electrons, there will hardly be any movement of ions within the short period of pulse duration. Input electrical energy is, therefore, mainly used for acceleration of electrons. The non-thermal plasma promotes chemical reactions with high energy efficiency.

Pulsed corona reactors utilizing non-thermal plasma have been shown, both in laboratory and industrial scale, to be effective in the removal of many types of gaseous pollutants. Fig. 1.2.2 shows the pulsed streamer discharge.

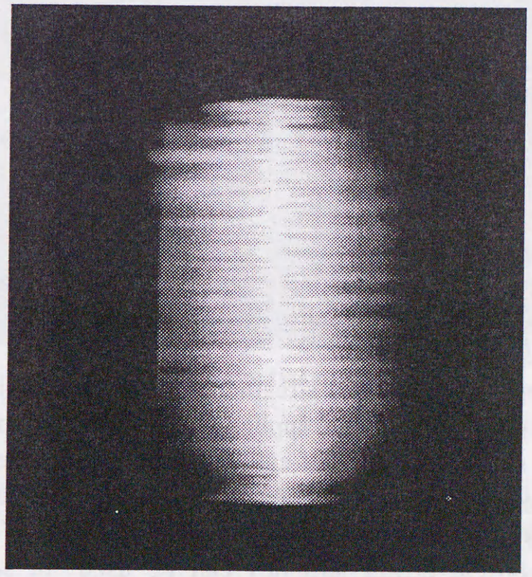

Fig. 1.2.2 Pulsed streamer discharge.
(Wire-cylinder , positive polarity, 25kV)

Industrial-scale experiments on the use of pulsed streamer discharge for the simultaneous removal of NOx and SOx from flue gas have been performed in Italy [15]. The core of this project is a series of experiments carried out by the Italian National Electricity Board (ENEL) at the coal-burning power station in Marghera, Italy. The ENEL tests have become the basis for the assessment of the electrical technology requirements of the pulsed corona process for applications to flue gas clean up in actual power plants.

Laboratory-scale experiments utilizing the pulsed streamer discharge have been studied in USA [16] to treat VOCs, such as toluene, methylene chloride and CFC-113.

Pulsed streamer discharge could be one of the most promising discharge in the non-thermal plasma technique. It does not have large system and is easy to handle. Further, capital cost is very low when compared to that of E-beam. Experiments shown in this thesis are based on this pulsed streamer discharge.

1.2.2 Silent discharge

When AC high voltage are applied between electrodes, one or both of which are covered with a thin dielectric layer, such as glass (A parallel-plate gap or cylindrical tubes are commonly used), micro pulsive discharges can be generated without breakdown. This type of discharge is called "*silent discharge*" and is also refereed to as "*dielectric-barrier discharge*". Silent discharge is a very mature technology, first investigated by Siemens in the 1850's for the production of ozone, and is still widely used for the ozone generation [17-20]. It is now routinely used to produce very large quantities of ozone for applications such as water purification, and the bleaching of textile and pulp. Fig. 1.2.1(b) shows the example of the silent discharge reactor.

Whereas in the pulsed streamer method the transient behavior of the plasma is controlled by the applied voltage pulse, the plasma that takes place in the silent discharge self-extinguishes when charge build-up on the dielectric layer reduces the local electric field. For some applications, this feature presents an advantage for the silent discharge approach since simpler electrical power supplies can be used. In some cases, the efficiency of the silent discharge reactor can be improved significantly by applying high-repetition-rate voltage pulses in a manner similar to that in pulsed streamer reactors.

1.2.3 Partial discharge of a packed ferroelectric pellet bed

When a AC voltage is applied across the packed pellet bed, the pellets are polarized, and an intense electric field is formed around each pellet contact point, resulted partial discharges inside a ferroelectric ceramic pellet-bed [21, 22]. The pellets are held within the tube arrangement by two metal mesh electrodes. Using pellet as the catalyst efficiency or selectivity of chemical reactions may be increased. Intensity of the partial discharge can be controlled either by changing dielectric constant of the pellet or frequency and shape of the applied voltage.

Fig. 1.2.1 (c) shows the example of the packed ferroelectric pellet bed reactor and Fig. 1.2.3 shows a picture of the partial discharge.

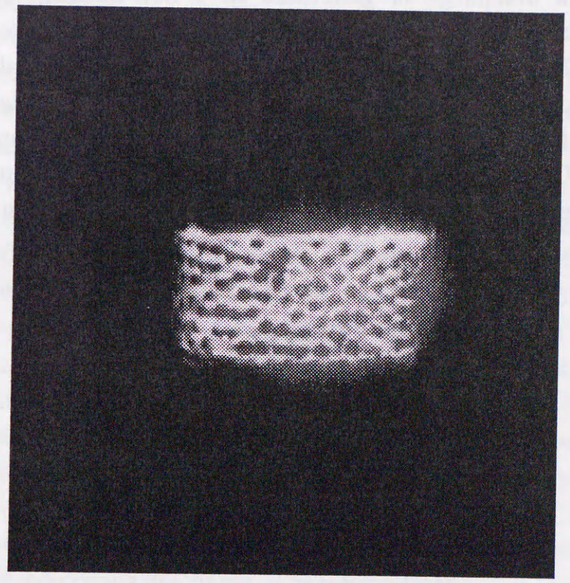

Fig. 1.2.3 Partial discharge.
(Packed bed , AC10kV , ε_s=4000)

Being relatively intense, this discharge plasma treatment is used for decomposition of VOCs recently, and many complicated by-products have been resulted [23].

1.2.4 Surface discharge

Surface discharge can be obtained by applying high frequency high AC voltage between a strip electrode on the surface of ceramic lamina and an electrode embedded in the lamina [24, 25]. This kind of discharge is being used for ozone generation as well as for decomposition of CFCs or VOCs. Since CFCs and VOCs are composed of various chemical species, decomposition process has been still uncertain [23, 26]. Fig. 1.2.1(d) depicts the example of the surface discharge reactor.

1.2.5 Corona discharge

Corona discharge is generated in a non-uniform electric field. Corona discharge has been widely used in electrostatic precipitators for particle collection. NO removal studies had also been carried out with DC corona discharge to oxidize NO and react with ammonia. The power efficiency, however, is low in comparison with pulsed streamer discharge [27]. For SO_2 removal, corona discharge with wet collection electrodes is effective because the ionic wind enhances SO_2 absorption to the water [28].

1.3 Scope of the present work

The non-thermal plasma techniques can be applied to the treatment of a wide variety of gaseous pollutants, and in some cases have the capability for the simultaneous removal of solid pollutants. In the present work pulsed streamer discharge was utilized for gas treatment.

In the previous sections, discharge plasma gas treatment techniques were introduced to comprehend the position of this work. Much work had been done using discharge plasma, however, the parametric study and other application which enables increasing the energy efficiency are not enough. Some of the advantages of this technique have been described in the forthcoming chapters. Main emphasis has been laid not only on pollutant (in many cases NOx) removal efficiency but also on energy efficiency considerations.

In this work, the effect of E/N and addition of hydrocarbons on NOx removal efficiency have been stressed. To decompose other stable green house effect gas, such as nitrous oxide (N_2O), very low temperature reactor has been shown as one of the novel plasma reactors.

Chapter 2 presents some numerical calculations about electron density and an experimental way to estimate electron energies required to ionize or dissociate the gas molecules. These results will help to comprehend the physics and characteristics of the discharge plasma. In the pulsed streamer discharge, mean energy of the electron is much higher than that of ion or other molecules. In order to apply pulsed streamer discharge to control or treat pollutant gas, one of the important factors to be considered is the effect of electron energy on gas molecules and hence an assessment of electron energy was carried out by electron current measurement. Also, time and space resolved optical emission spectroscopy, which is commonly used for diagnosis of non-thermal plasma in the pulsed corona discharge, was investigated.

Chapter 3 describes the NOx removal from simulated flue gas and diesel engine exhaust gases. Various novel plasma reactors will be introduced such as semi-wet reactor, wet reactor, spray reactor and low temperature reactor to decrease the energy consumption required to treat pollutant gases, namely nitrogen oxides. The effect of hydrocarbons on energy efficiency is also studied.

First, in order to confirm how discharge is affected by the dc voltage or pulsed streamer voltage, measurement of ozone concentration

is done for both types of the voltages. Because it is very difficult to measure the reactive region, instead of direct measurements of discharge volume, flue gas direction was changed and corresponding ozone concentration was measured. The gas flow direction is one of the important factors to study the discharge region that can produce the ozone for different applied voltages.

Later, NOx removal experiment using simulated gas will be introduced. With the dry reactor, addition of hydrocarbons (ethylene) is carried out to enhance the NOx oxidization. Once NO (about 90% of NOx in the actual exhaust gas) is oxidized to NO_2, it is easy to absorb this using the absorbant since NO_2 is soluble. Therefore wet type plasma reactor is developed to enhance the NOx removal efficiency. Also ozone injection method is conducted to save the energy required to remove NOx.

However, it is found that nitrous oxide (N_2O) is difficult to decompose or remove even with these plasma reactors. Therefore other plasma reactor i.e. low temperature reactor is developed to treat this stable gas under discharge plasma condition.

In addition, discharge plasma is demonstrated to treat very low concentration gases such as cigarette smoke or odor component gas.

An energy efficiency is compared with the type of the reactors or gas conditions and relative merits are discussed. It is confirmed that realization of this method will not be a difficult task from economic point of view.

In chapter 4, plasma chemical reactions promoted by the addition of hydrocarbons and water vapor are discussed with the data obtained in this work. From an analytical point of view, by-product measurements are introduced.

In chapter 3, effect of addition of the hydrocarbons (ethylene) was studied to enhance the NOx removal. Though the effect of hydrocarbons such as ethylene was significant, reports about its effect are very few. If the by-products after discharge plasma treatment were poisonous, hydrocarbon addition could not used for the actual exhaust gas treatment. To confirm the safety of this method, in this chapter, by-products analysis will be presented. And some chemical reactions with ethylene will be discussed to highlight the effects of hydrocarbons.

Final conclusions are presented in chapter 5.

2. ELECTRON DENSITY CALCULATIONS AND RELATED OPTICAL STUDIES

In order to investigate the streamer development or ion and electron density in the field, many theoretical and analytical models have been proposed by many authors [29-32]. In this chapter, some numerical calculations have been presented to comprehend the physics and characteristics of the discharge plasma. In the pulsed streamer discharge, mean energy of the electron is much higher than that of ion or other molecules. In order to apply pulsed streamer discharge to control or treat pollutant gas, one of the important factors to be considered is the effect of electron energy on gas molecules.

Assessment of electron energy was carried out by electron current measurement. Also, time and space resolved optical emission spectroscopy [33-35] which is commonly used for diagnosis of non-thermal plasma in the pulsed corona discharge, was investigated.

2.1 Calculations in the Laplacian field and streamer propagation mechanisms

2.1.1 Density of electrons and ions in the Laplacian field

To simplify the calculations the plasma reactor is assumed to be a simple wire-cylinder geometry without any dielectric barrier. Also other conditions described below are used.

(1) The wire diameter is set to be 0.2 mm, cylinder inner diameter is set to be 18 mm to simulate the reactor used in actual NOx removal experiment.

(2) Pulse voltage is given by equation (2.5) which is valid for pulse rise time of the order of 1 μs and width, 2-3 μs. Negative polarity is used.

(3) All the calculations correspond to Laplacian field. But in the actual condition this field gets distorted and Poison field should be used for calculations.

For a given pulse voltage, the Laplacian field E is given by the equation (2.1).

$$E(r) = \frac{V}{rLog\frac{R}{r_o}} \tag{2.1}$$

Where r_o and R are radius of wire and cylinder respectively.

The ionization coefficient α can be expressed as equation (2.2). This equation was derived from experiments, as α/p is uniquely determined by the ratio E/p for wide ranges of field strength and gas pressures where p = atomospheric pressure in Pa.

$$\alpha / p = A\exp[-B(p/E)] \tag{2.2}$$

Here A and B are constants depending on the gas used. The constants A and B are determined by curve fitting the experimental results on ionization and attachment data [36a]. Accordingly for $0.19 < E/p < 0.45$, the values are A = 4.778; B = 221. This equation is in good agreement with the experiment in many cases, but only over a limited range of E/p.

The attachment coefficient η is given by the equation (2.3).

$$\eta/p = C(E/p)^2 + D(E/p) + F \tag{2.3}$$

C, D and F are also determined by the curve fitting the experimental results on attachment data [36b]. These values are $C = 0.87 \times 10^{-5}$; D = 0.01298; $F = -541 \times 10^{-6}$. Since applied voltage (shown in Figs. 2.3.1 and 2.4.1(a), (b)) was a damped oscillation Vp can be expressed as below [36c].

$$Vp(t) \cong Vm\frac{t}{t_m}\exp[1-(t/t_m)] \tag{2.4}$$

where at t = tm, Vp(t)=Vm=peak value of the voltage. Now, the average value of Vp(t) is given by

$$\langle V_p \rangle = \frac{1}{t_d}\int_0^{t_d} V_P(t)dt$$

$$= V_m\frac{t_m}{t_d}\left[e^1 - e^{1-[t_d/t_m]}(1+[t_d/t_m])\right] \tag{2.5}$$

With these equations field E, the ionization coefficient α, and the attachment coefficient η can be determined. Therefore the electron density can be estimated with the equation (2.6).

$$N_e(r) = N_0\exp(\int_0^r(\alpha-\eta)dr) \tag{2.6}$$

Density of both positive ion Np and negative ion Nn can also be expressed with the following equations [36c].

$$N_p(r) = N_0\int_0^r \alpha(r')\left[\exp(\int_0^{r'}(\alpha-\eta)dr)\right]dr' \tag{2.7}$$

$$N_n(r) = N_0\int_0^r \eta(r')\left[\exp(\int_0^{r'}(\alpha-\eta)dr)\right]dr' \tag{2.8}$$

These calculated results are shown in Fig. 2.1.1.

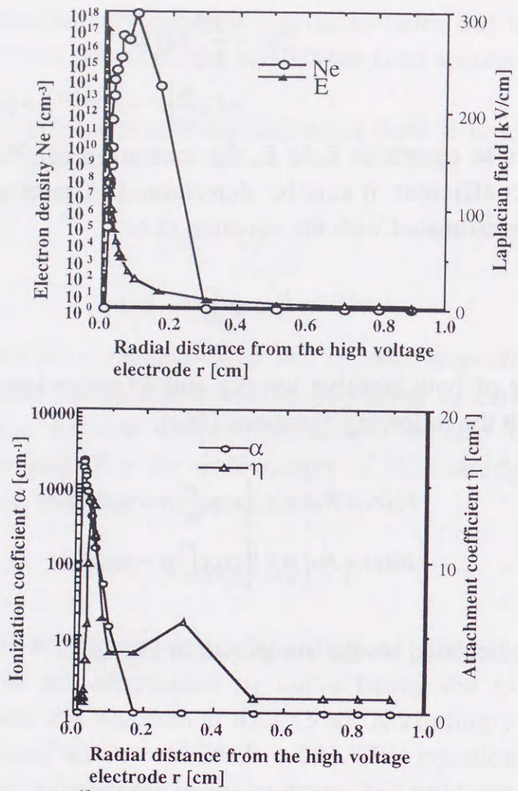

Fig. 2.1.1 Calculated values of Ne, E, α, η, N^+, and N^- as functions of radial distance from the high voltage electrode.

The radius at which α=η is the critical point. Ne was maximum at this radius having an order of 10^{18} [cm^{-3}]. From these calculated values,

radical density and removed NO molecules can be deduced as explained in the next section.

2.1.2 Relation between radical density and removed NO molecules

To begin with, the removed NO molecules were calculated. An initial NO concentration of 400 ppm is assumed (this is typical value when the experiment was carried out using the simulated gas). Assuming 50% removal, we get reduced number density:

$$0.5 \times 400\times10^{-6} \times 2.5\times10^{19} \text{ (molecules/cm}^3\text{)}$$
$$= 5.38 \times 10^{15} \text{ NO molecules were removed.}$$

This assumption suggests that active radicals under pulsed discharge plasma is of the order of 10^{15} molecules. As compared with the electron density, it was three order lower. This result suggests that all the electrons do not contribute to the removal of NO and they are trapped by neutral molecules to form ions or other active species.

It is to be noted that the parametric conditions used in the numerical calculations were not exactly the same as that used in the experiment. In the experiments the dielectric barrier may affect the production of the high energy electrons and the active radicals. That means the electron density could have been produced in the reactor during the pulsed voltage application. Hence the numerically computed electron density is less than that obtained from experiments.

Not only the high energy electrons but also some other active species such as ozone, O radical, and N radical play an important role to remove the NO molecules as mentioned in the appendix I. Since the produced high energy electrons collide during pulsed voltage application, radicals are generated. The place, where electrons collide with other back ground gas molecules, is located at the tip of the streamers [30]. That means the number of high energy electrons produced under plasma discharge depend on the number of generated streamers.

The streamer probability for the dc voltage was well documented [30], but not much data is available for the pulse case. The dc voltage results show that the avalanche size which corresponds to the electron density was related to the streamer probability. From the dc result, the electron density (~10^9) [36d, 36e] was less than the pulse case (~10^{18}).

Though the exact value could not be obtained with this data, pulse energization can produce more streamers than that with dc.

2.2 Experimental apparatus and measurements

2.2.1 Reactors

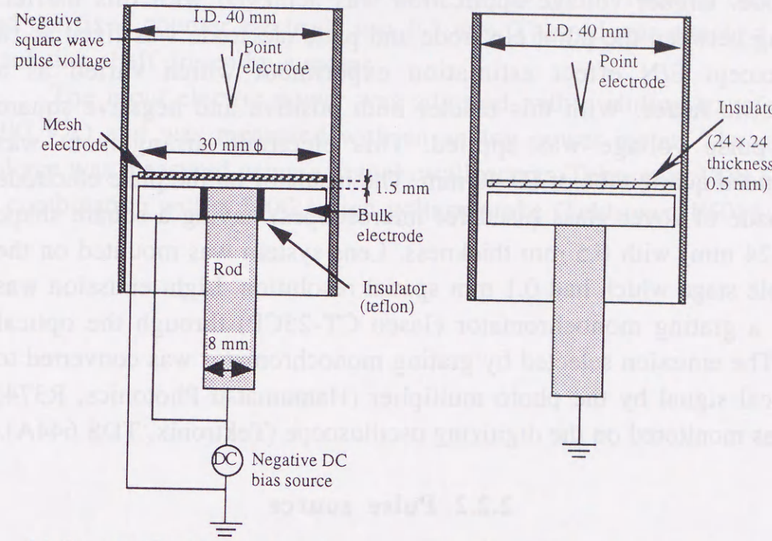

(a) Reactor for electron current measurement **(b) Reactor for light emission measurement**

Fig. 2.2.1 Reactors

To measure the electron current a point-to-plane reactor geometry was used. Fig. 2.2.1(a) shows the schematic diagram of the reactor. Spacing between point electrode and plane electrode was varied from 10 to 25 mm. Plane electrode was of diameter 30 mm consisting of a bulk electrode and mesh electrode. Mesh electrode was placed with 1.5 mm gap on bulk electrode. Mesh electrode was directly grounded to prevent the discharges causing a serious damage to the measurement apparatus. While bulk electrode consists of rod and plate separated by 1 mm thick Teflon insulator. Rod diameter was 8 mm. Whole electrode system was surrounded by a quartz tube to supply the gas. This bulk electrode was connected to the negative dc source giving bias between mesh electrode and bulk electrode, so that electrons without proper energy can not penetrate the mesh electrode. Only electron with enough energy can penetrate this electric barrier and is detected as electron current. Negative

polarity pulse voltage was applied to measure electron current in the system.

Fig. 2.2.1(b) shows the reactor used for light emission measurement. This geometry was similar to the one explained above. Only difference was instead of mesh electrode, it had insulator plate on the ground electrode. Higher voltage application was achieved with this barrier. Spacing between the point electrode and plate electrode was fixed at 18 mm except E/N effect estimation experiment which varied as a parametric factor. With this reactor both positive and negative square wave pulse voltage was applied. This electrode arrangement was surrounded quartz tube of ID 40 mm. The insulator on the plate electrode was made of cover glass (used for microscopes) having a square shape (24 × 24 mm) with 0.5 mm thickness. Lens system was mounted on the movable stage which had 0.1 mm spatial resolution. Light emission was fed to a grating monochromator (Jasco CT-25CP) through the optical fiber. The emission selected by grating monochromator was converted to electrical signal by the photo multiplier (Hamamatsu Photonics, R374) and was monitored on the digitizing oscilloscope (Tektronix, TDS 644A).

2.2.2 Pulse source

A rotating spark gap switch was used to generate square wave pulses of either polarity. The set up (Fig 2.2.2, it shows positive polarity only) consists of a step-up transformer (0.2/50 kV, 1 kVA) a rectifying high voltage diode (36 kV, 400 mA), and a filter capacitor (16 nF). The central electrode of the reactor was periodically connected to the dc. high-voltage supply and then disconnected and grounded, as the spark gap switch was rotating at constant speed [37].

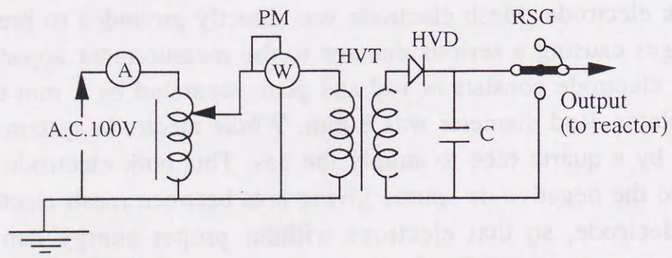

Fig. 2.2.2 Square wave pulse circuit (positive polarity)

PM: power meter (Yokogawa 2041), HVD: high-voltage diode (36 kV, 400 mA)

HVT: high-voltage transformer (0.2/50 kV, 1 kVA), RSG: roating spark gap switch

The durability of the switch was ensured by using sintered tungsten as the main material for the electrodes of the spark gap. A hemispherically capped metal rod (5 mm in diameter, 30 mm in length) was used as rotating electrode. The fixed counter electrode had similar shape. The minimum distance between the tip of the rotating electrode and the fixed counter electrode was 0.5 mm. The rod was attached to an insulating shaft driven by a motor.

The input electric power was adjusted with a sliding transformer (500 VA) and was measured with an analog power meter. The output voltage was measured using a digital oscilloscope (Tektronix, TDS 644A) in combination with a 1000:1 high-voltage probe (Tektronix, P6015).

2.3 Result of electron current measurements

2.3.1 Wave form and electron current characteristics

Fig. 2.3.1 shows the typical wave form of the applied voltage and electron current obtained with methane as carrier gas. Usually pulse voltage causes serious electro-magnetic noise (EM noise). Electron current might be a weak signal compared to these EM noise, charge current, or induced current. Therefore, in order to eliminate other signals precautions were taken and the procedures were as shown below.

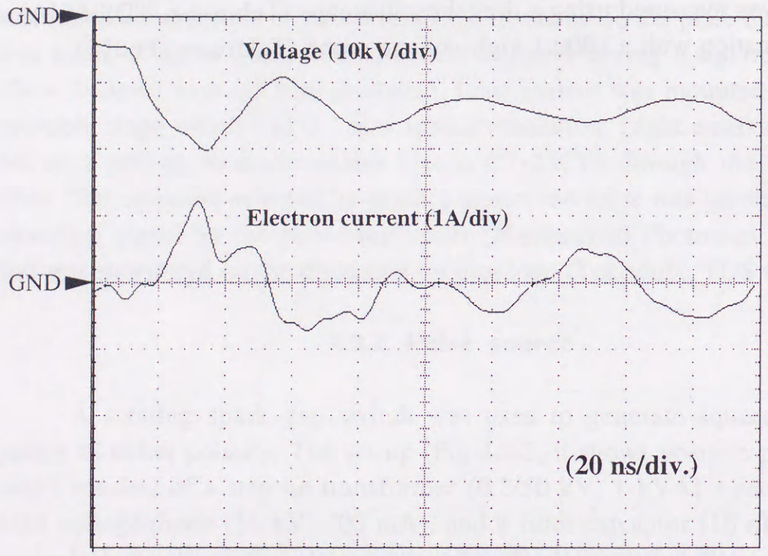

Fig. 2.3.1 Typical waveform of negative pulse voltage.
(Carrier gas : CH4, Input power : 10 W , Electrode spacing : 15 mm)

Current transformer (Tektronix, P6021) was used to measure the current including EM noise, charge current induced current, and electron current. First, current transformer 1 (CT1) in the Fig. 2.3.2 was measured followed by CT2, CT3 and CT4 measurements. Electron current can be expressed by the following equation:

$$\text{(Electron current)} = CT1 - (CT2 + CT3) \qquad (2.7)$$

Theoretically, electron current can flow only in CT4. However experimental result had shown that current values were much higher than

the calculated values because current through CT4 not only includes the induced current but also EM noise. In this experiment the value given by equation (2.7) was adopted as electron current value to eliminate the other signals such as EM noise.

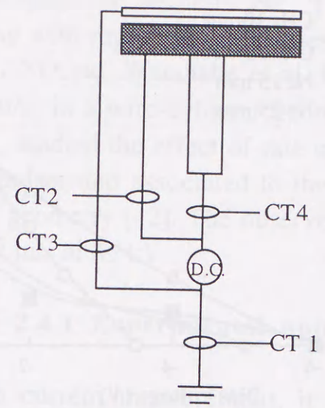

CT:current transformer

Fig.2.3.2 Current measurement circuit.

Nitrogen and methane were used successively as carrier gases. Both gas flow rates were set at 200 cc/min. In the case of methane, electrode spacing was adjusted between 10 and 25 mm. In nitrogen case, with 10 mm spacing, discharge was occurring and hence, the electrode spacing was adjusted between 15 and 25 mm. During the experiments, applied voltage was kept at -20 kV.

Fig. 2.3.3 shows the characteristics of electron current as function of bias voltage. This result shows several characteristics. With methane as carrier gas and no DC bias, electron current was higher than that of nitrogen. This may be due to the fact that nitrogen is electronegative in nature. Also within the bias voltage of -4 V (that corresponds to an electron energy of 4 eV), electron current of methane was higher than that of nitrogen. Usually electron attachment is ignored for molecules, so that in methane case only ionization effect should be considered. On the contrary, in nitrogen case low energy electrons are trapped by nitrogen atoms produced under discharge plasma which exhibit high electron affinity. Therefore, hardly any current was detected for a bias voltage of below -2 V. Note that for a given eV, ionization cross section is larger

for methane compared to that of nitrogen [38, 39]. Thus electron current for methane was higher than that of nitrogen.

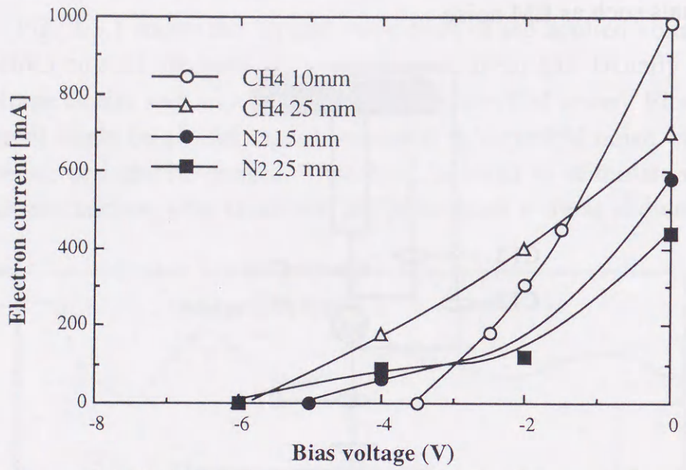

Fig. 2.3.3 Electron current as a function of bias voltage.

It was observed that the electron current was higher when the electrode spacing was narrow. This is due to the fact that, electrons were trapped by other molecules i.e. ions or neutral particles during their travel from the point electrode to the plate electrode. The results also suggested that higher E/N value gave the electrons higher energy. Higher electron current was resulted from higher E/N value when gap spacing was narrow and for the same applied voltage higher field was resulted which further increased electron current. This higher E/N value could only be resulted by pulsed streamer discharge, while dc voltage was tend to cause discharge and high E/N could not be achieved.

2.4 Light emission measurement

Light emission measurements were earlier carried out by different groups with the aim of studying the estimation of high energy electrons and the streamer propagation velocity etc. Teich [40] has reported emission spectroscopy with repetitive discharges for different gases like air, water vapor, N_2, NO etc. Watanabe et al. have measured streamer velocity (4.4×10^5 m/s) in a wire-cylinder geometry for positive pulses [41]. Creyghton et al. studied the effect of rate of rise and peak value of the applied positive pulses and associated to the E/N value on streamer velocity for a similar geometry [42]. The observed streamer velocity was about 5.1 to 8.3×10^5 m/s at 35 kV.

2.4.1 Experimental apparatus

In the electron current measurement, it was observed that for nitrogen gas the electron has energy less than 6 eV. It should be noted that the electrode configuration is different from the one used in the gas cleaning experiment i.e. point-to-plane instead of wire-cylinder. For the light emission measurements also a similar point-to-plane geometry was used as it is very difficult to carry out the experiments with wire-cylinder geometry. However to get the similar high field conditions existing in wire-cylinder geometry a glass barrier was used on the grounded point electrode. Also, to simulate the practical case, as far as possible, dry air medium was maintained inside the apparatus instead of nitrogen or methane.

Pulse voltage was used in this experiment. To confirm the polarity effect, experiment was carried out with both positive and negative voltages. N_2 second positive band (337.1 nm, threshold energy of 11.03 eV) was mainly investigated. Also N_2^+ first negative band (391.4 nm, threshold energy of 18.75 eV) was also investigated. This spectrum ensures that at least some electrons have had energy level greater than their each threshold energy. However due to the relatively high EM noise level with pulse power source (already mentioned in previous section) and weak signal level of N_2^+ first negative band because of electron affinity of oxygen especially in dry air compared to the pure nitrogen atmosphere. On the contrary the signal level of N_2 second positive band

was relatively stronger than that of the signal level of N_2^+ first negative band, results will be concentrated on N_2 second positive band.

Table 2.4.1 shows the threshold energy for ionization and dissociation related to this work.

TABLE 2.4.1 THRESHOLD ENERGY FOR IONIZATION AND DISSOCIATION.

Species	Ionization potential [eV]	Dissociation potential [eV]
N	14.53	——
O	13.62	——
N_2	15.59	9.76
O_2	12.06	5.12
O_3	12.3	1.04
NO	9.25	6.50
NO_2	11.23	3.11

2.4.2 Light emission of N_2 second positive band and streamer propagation

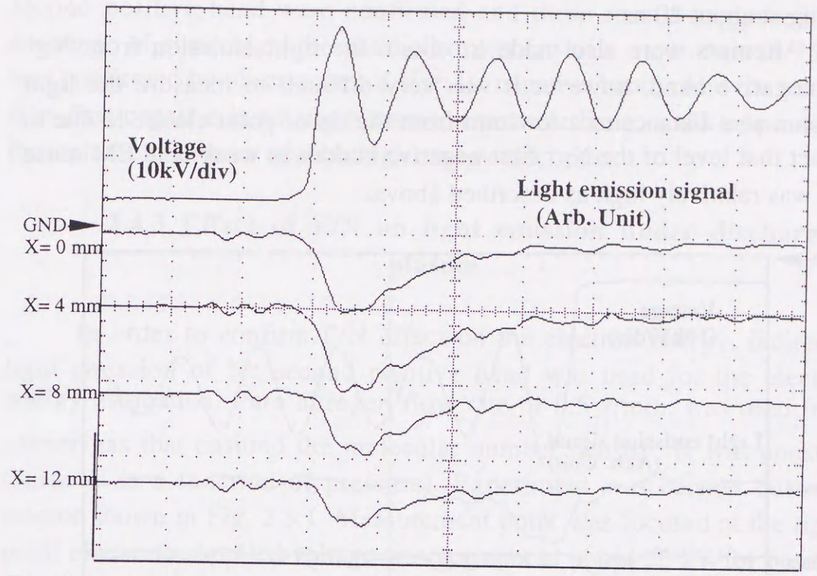

Fig. 2.4.1 (a) Rising part of positive square wave high voltage pulse and light emission of N_2 2nd positive band (337.1 nm).
(Observation point from the distance of needle electrode ; X(mm))

Fig. 2.4.1(a) shows positive voltage and its nitrogen light emissions. Input power was constant at 20 W. Gas flow rate was 2.4 ℓ/min. Gap spacing between point electrode and plate electrode was 18 mm both for positive and negative polarity case. Light emission signals were measured for every 2 mm distance from the tip of the point electrode along the point-to-plane axis. However, in Fig. 2.4.1(a), for convenience sake, the signals corresponding to that measured at a distance of 4 mm are shown.

Light emission occurred almost instantaneously as voltage began to rise, and continued for about 100 ns. Voltage rate of rise was about 0.85 kV/ns. The highest light emission signal was observed not on the tip of the point electrode, but 2 to 4 mm away from the point electrode, and it decreased as the streamer head went away from the tip of the point electrode. At the same time peak shifting was observed. This indicates

that streamer propagated from tip of the point electrode to the plane electrode. The streamer head propagation velocity was calculated and found to be about 0.9~1.0 × 10^6 m/s. Therefore, streamer bridged the spacing at about 20 ns.

Attempts were also made to obtain the light emission from N_2^+ first negative band, however it was very difficult to measure the light emission at a distance of a few mm from the tip of point electrode due to the fact that level of the N_2^+ first negative band was weak, and EM noise level was relatively high as described above.

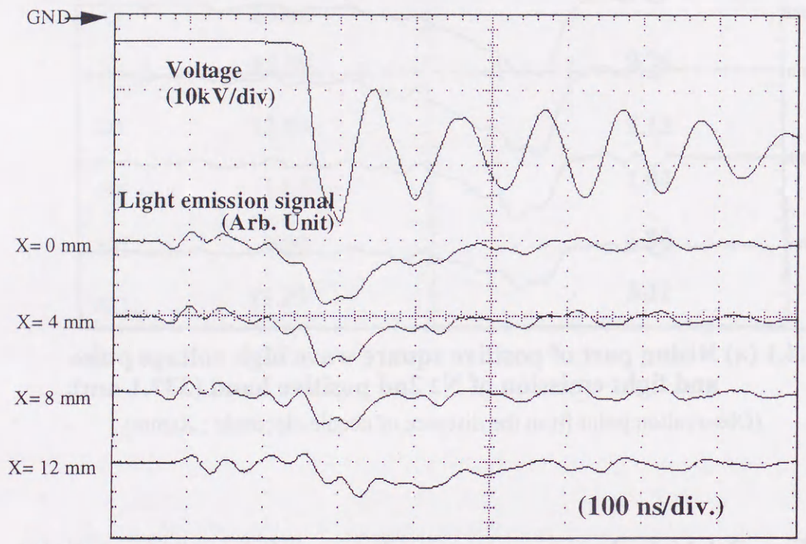

Fig. 2.4.1 (b) Rising part of negative square wave high voltage pulse and light emission of N2 2nd positive band (337.1 nm).

(Observation point from the distance of needle electrode ; X(mm))

Fig. 2.4.1(b) shows the result of the light emission when negative square pulse voltage was applied. Light emission peak was lower than that with positive voltage case. Especially near the cathode, light emission signal peak was very weak compared to the positive case. This is due to the fact that space charge suppresses the intense streamer propagation, and streamer head propagation velocity was calculated and found to be about 0.5~0.6 × 10^6 m/s. This value was about half of that with positive voltage case. In positive polarity case streamer propagation velocity was twice that with negative one, indicating the effect of polarity on the

streamer propagation velocity. A factor of uncertainty has crept into the signal measurements due to the presence of EM noise.

From these measurements, both N_2^+ first negative band and N_2 second positive band were confirmed and these results suggested that existence of some high energetic electrons (at least more than 18.75 eV was confirmed by observation of N_2^+ 1st negative band). And the state of $N2^+$ first negative band and N2 second positive band could be produced through the collisions of such high energy electrons.

2.4.3 Effect of E/N on light emission under discharge plasma

In order to confirm E/N effect on the electron energy, indirectly light emission of N2 second positive band was used for the electron energy estimation. Pure nitrogen flow rate of 0.5 ℓ/min. was used for a carrier gas that ensured the molecular number density; N was constant (since N is a function of pressure). Experiment was carried out with reactor shown in Fig. 2.3.1. Measurement point was focused at the tip of point electrode. Applied voltage was constant at about 25 kV for positive polarity and about 26.5 kV for negative polarity. Only gap spacing was changed between 15 and 25 mm to generate different E/N condition under discharge plasma.

TABLE 2.4.2 EFFECT OF E/N ON N2 SECOND POSITIVE BAND UNDER POSITIVE POLARITY PULSED DISCHARGE PLASMA.

Gap spacing [mm]	Applied field [kV/ cm]	E/N [Td]	Relative intensity of N_2 P.B.[%]
15	**16.5**	**65.8**	**100.0**
20	**12.6**	**50.3**	**98.7**
25	**10.1**	**40.3**	**91.0**
30	**8.4**	**33.5**	**88.5**
35	**7.1**	**28.3**	**16.0**

TABLE 2.4.3 EFFECT OF E/N ON N_2 SECOND POSITIVE BAND UNDER NEGATIVE POLARITY PULSED DISCHARGE PLASMA.

Gap spacing [mm]	Applied field [kV/ cm]	E/N [Td]	Relative intensity of N_2 P.B.[%]
15	**17.6**	**70.2**	**100.0**
20	**12.8**	**51.1**	**95.0**
25	**10.9**	**43.5**	**86.6**
30	**8.9**	**35.5**	**74.0**
35	**7.7**	**30.8**	**28.1**

Table 2.4.2 and 2.4.3 summarizes the effect of E/N on relative intensity of N_2 second positive band. These results show that wider the gap under constant applied voltage, lower the relative intensity of N_2 second positive band. In this experimental work, for both positive and negative polarity, when gap spacing was 35 mm, relative the relative intensity of N_2 second positive band was decreased to 16% for positive polarity and 28% for negative polarity. These results suggested that both positive and negative polarity had critical field values that could be maintained to produce energetic electrons that can contribute light emission of N_2 second positive band. The critical field value was found to be between 28.3 and 33.5 Td for positive polarity and between 30.8 and 35.5 Td for negative polarity, experimentally.

Therefore, to enhance the plasma chemical reaction for removal or for treatment of polluted gas under plasma discharge, high field value more than 10 kV/cm could be desirable. As mentioned in previous section 2.2, dc voltage hardly produce this high field under the atmospheric pressure and so, pulsed discharge plasma is necessary to enhance the plasma chemical reaction by generating abandon energetic electrons.

2.5 Main inferences

In this work, estimation was made for the electron density that could produce the active radicals or cause the chemical reactions under the plasma discharge. Though the modeling was different from the actual experimental set up, numerical calculation of the removed NO molecules was carried out. This result shows that electron density was much higher than the removed NO molecules. However, not all the high energy electrons contribute to the NO removal.

Also, an estimation of electron energy was carried out experimentally with direct measurement of the electron current and the light emission of mainly nitrogen second positive band.

The electron current measurement showed electron had higher energy when E/N value was higher. This higher E/N value might have resulted only by pulsed streamer discharge. Though the dc voltage was tend to cause breakdown in the gap, high E/N could not be achieved. The electron energy was also dependent on the gas composition because of the nature of the gas.

Through the light emission measurement, both N_2^+ first negative band and N_2 second positive band were observed. These results suggested the existence of some high energetic electrons (at least more than 18.75 eV was confirmed by observation of N_2^+ 1st negative band).

To conculde this chapter, superiority of the pulsed streamer discharge over the dc corona discharge is demonstrated. Because of the high electric field the energy levels of the electron densities were high enough to ionize or dissociate the gas molecules and produce the active radical species to enhance the plasma chemical reactions.

3. GAS TREATMENT EXPERIMENT

In the previous chapter, the electron energy in the pulsed streamer discharge was estimated. In this chapter, various kinds of plasma reactors are introduced to decrease the energy consumption required to treat pollutant gases, namely nitrogen oxides.

First, in order to confirm how discharge was affected by a dc voltage or a pulsed streamer voltage, ozone concentration was measured for both types of the voltages. Because it is very difficult to measure the reactive region, instead of direct measurements of discharge volume, flue gas direction was changed and corresponding ozone concentration was measured. The gas flow direction is one of the dominant factors to study the discharge region that can produce ozone for different applied voltages.

Later, NOx removal experiments using simulated gas will be introduced. With a dry reactor, addition of hydrocarbons (ethylene) is carried out to enhance the NOx oxidization. Once NO (about 90% of NOx in the actual exhaust gas) is oxidized to NO_2 which is easy to absorb this using the absorbant since NO_2 is soluble. Therefore wet type plasma reactor is developed to enhance the NOx removal efficiency. Also ozone injection method is conducted to save the energy required to remove NOx.

However, it is found that N_2O (nitrous oxide) is difficult to decompose or remove even with these plasma reactors. Therefore particular plasma reactor i.e. the low temperature reactor is developed to treat this stable gas.

In addition, discharge plasma is demonstrated to treat very low concentration gases such as cigarette smoke (containes both low concentration polluted gas and particles) or odor component gas such as ammonia.

Finally, the energy efficiencies are compared with the type of the reactors or gas conditions and relative merits are discussed.

3.1 Effect of gas flow direction to ozone generation in a plasma reactor

The importance of ozone generation in the corona discharge of an electrostatic precipitator is well recognized. Ozone is known as one of the most powerful oxidants and is very toxic to humans, plants, animals, and produce deterioration in many materials. Therefore, any electrostatic precipitator used in applications where the air will be directly breathed by humans or animals, or come into contact with sensitive plants and materials, must be designed to ensure that the ozone level does not exceed acceptable limits. The problem is exacerbated by the fact that both the precipitation collection efficiency and ozone generation rate are roughly proportional to the input power. Thus, there is a trade-off that should be considered in the design of these precipitators; the power input must be high enough to yield adequate collection efficiency but not so high as to produce hazardous levels of ozone.

Many studies have been reported to assess ozone generation from a coaxial geometry [43-46] and a point-to-plane [47, 48] discharge gap or discharge reactor. In these gaps the direction of gas flow carrying the ozone molecules was parallel to the discharge electrode. While the gas flow in real precipitator is normal to the discharge electrode.

It would be the first to report on effect of ozone generation in point-to-plane and wire-duct reactors influenced by the direction of gas flow in the reactor. Two directions, normal and parallel of gas flow to the discharge electrode in the reactor, were investigated. To confirm the effects of the electric field intensities, the reactors were applied by dc and repetitive square-pulse voltages of both polarities. Understanding ozone generation in point-to-plate reactor at first will illustrate the case in wire-duct reactors. This is why point-to-plane reactors are investigated along with wire-duct ones.

3.1.1 Experimental set-up

Two parallelepiped reactors of different size were tested to investigate the ozone generation in point-to-plane and wire-duct gaps. The voltage applied to the reactors was either a dc voltage or a repetitive square pulse of both polarities. The schematic diagram of the experimental set-up is shown in Fig. 3.1.1 and composed of high-voltage

supply, reactor, gas-flow system and instruments for measuring the applied high voltage, discharge current, input power, discharge power, ozone concentration and gas flow-rate.

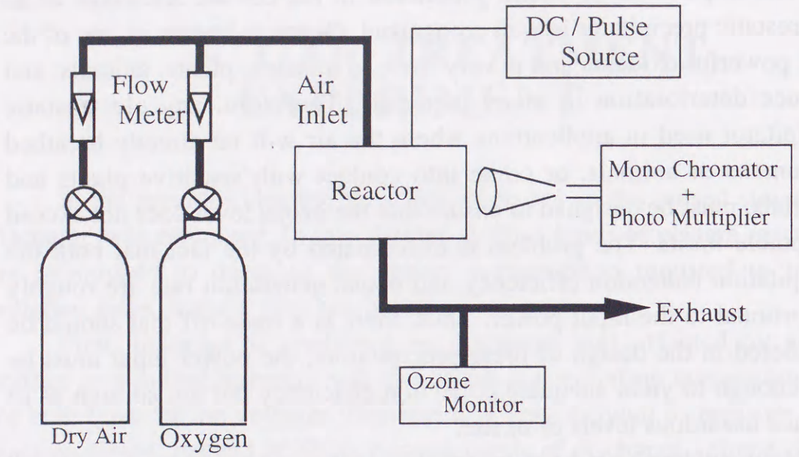

(a) experimental set-up

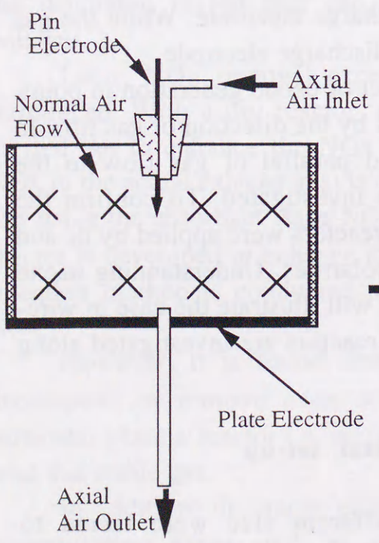

(b) Point-plane reactor

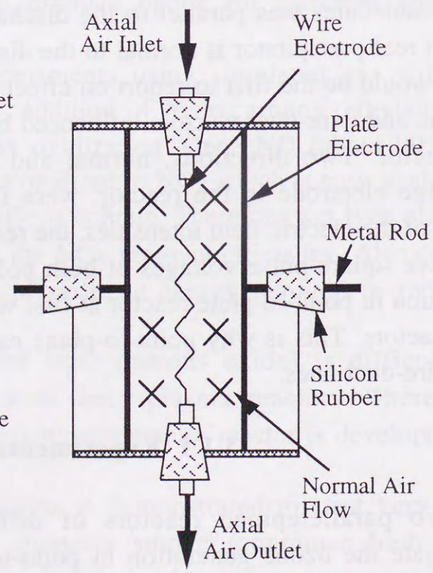

(c) wire-duct reactor

Fig. 3.1.1 Experimented set-up and details of investigated reactors and direction of air flow.

1)High-voltage supplies:

a)High-voltage dc supply: The high-voltage dc generator consisted of a set-up transformer(0.2 / 50 kV, 1 kVA), a rectifying high-voltage diode(36 kV, 400 mA) and a filtering capacitor (40 kV, 16 nF). The input electric power was adjusted with a regulating transformer(500 VA) and measured with an analog power meter(Yokogawa 2041). The output voltage of the supply was displayed on a digital oscilloscope(Tektronix TDS 644A, 2 GS/s) with a 1000:1 high voltage probe(Tektronix P6015). The corona current was measured by a grounded resistor, and an oscilloscope. The pulse power source was the same as used in previous subsection 2.1.3.

2)Reactors:

a)Point-to-plane reactor: The reactor had dimensions of 109 mm length, 72 mm breadth and 76 mm depth. The point was copper made and hemispherically-capped (1 mm radius) and the point-to-plane spacing was 18 mm to observe clearly the dependence of ozone generation on the corona modes which are easily distinguished by such points [49]. The plane was also made from copper and has 72×78 mm^2-area. Perpendicular to the gas-flow direction, reactor cross-sectional area is 76×72 mm^2 for normal flow and 109×76 mm^2 for flow parallel to the corona point.

b)Wire-duct reactor: The outer duct has dimensions of 187 mm length, 40 mm breadth and 60 mm depth. Two stainless-steel wires of diameters of 0.2 and 0.5 mm were tested. The active length of the wire (where discharge occured) was 132 mm. The ground electrodes, which were attached inside of duct walls were copper plates of area 187×60 mm^2. The plate-to-plate spacing of the duct was 40 mm and the discharge wire was suspended midway between the plates along the reactor.

With the application of pulse voltage to the reactor, a dielectric barrier (2 mm in thickness and 2.65 dielectric constant) was pasted on the ground plane in the point-to-plane reactor. For the wire-duct reactor, two dielectric barriers were pasted on each ground plate of the duct. This generates the so-called "silent discharge" in the reactor where the amplitude of the applied pulse could exceed the breakdown strength of the gas without proceeding to arcing. Silent discharge has

been proposed as one of excellent means for ozone generation [37,44, 50, 51].

3)Gas flow system:

The simulating air was adjusted by controlling the flow rate from dry N_2 and O_2 gas at volume ratio 4:1. The ozone concentration was measured with an ozone monitor (Ebara Jitsugo-EG-2001).

4)Technique

The concentration of the ozone generated in the investigated reactor was recorded for different values of the input power and different gas flow rates. The corresponding dc or pulse-voltage amplitude was also recorded. Either the corona current or the discharge power was recorded depending on the type of the applied voltage; dc or pulse voltage. The atmospheric temperature and relative humidity during the course of the present measurements were not controlled particurly, they were variable in the ranges 28-32°C and 40-45% respectively.

3.1.2 On the mechanisms of gas discharges in the investigated reactors

(a) Reactors applied by repetitive square pulse voltages:

With the application of positive square to the point-to-plane reactor, a detectable ionization of filamentary streamers of branched nature develops at the leading edge of pulse [30, 52]. (The typical voltage and current wave form will be shown in the subsection 3.3.2 (Fig. 3.3.2) of chapter 3 in this thesis.) These streamers easily penetrate the low-field regions and reach the ground plane associated with a current flow. But because of the dielectric barrier, only a short current pulse can propagate and no arc can develop. Thus, the dielectric barrier prevents electron emission from the ground plate which plays the main role in streamer-arc transition. The surface of dielectric barrier is charged where the streamer reaches its surface. This charging builds-up an electric field which extinguishes the current flow. This explains why the current wave form of Fig. 3.3.2 is a main pulse at the leading edge of the applied pulse voltage. Because of the overshooting of the applied pulse voltage, the main current pulse is followed by minor current pulse as shown in Fig. 3.3.2.

The duration of the applied pulse voltage is long (2 ms) enough for positive ion space-charge to accumulate, drift and distort the original field pattern in the gap. This results in a contraction of the spatial development of streamers towards the gap axis. The latter follows the pattern of the electric field lines along them the streamers propagate in the gap.

On the other hand, at the tail edge of the applied positive pulse, negative feathers start and propagate much less in radial and axial directions in comparison with their positive counter parts (streamers). This is the characteristic of negative feathers when compared with positive streamers [30, 52]. Moreover, the net voltage applied to the gap is smaller at the tail edge in comparison with that at the leading edge of the applied pulse as shown in Fig. 3.3.2. This makes positive streamers more dominating in comparison with negative feathers for applied positive pulse voltages. Subsequently, the net ion space-charge in the gap remains positive in polarity even with the charge cancellation by the negative ions produced by the feathers.

With the application of negative square pulses to the point-to-plane reactor, negative feathers develop at the leading edge and positive streamers at the tail edge of the pulse. However, the negative feathers are dominating and the net ion space charge in the gap is negative in polarity.

Whether the applied square pulse is positive or negative, streamers and feathers develop along the gap length without proceeding to arcing. Their spatial distribution is bound to the gap axis with limited propagation in the radial direction. This confirms with what was observed in the present measurements where the streamers / feathers met the dielectric barrier from the gap axis for 18 mm gap length. These streamers / feathers are sources of energetic electrons which can excite, dissociate and ionize the flowing gas molecules. Because the ionization level of oxygen is lower than that of nitrogen, chemical reaction rapidly occur leading to the formation of ozone rather than nitro-radicals [53].

With the application of square pulse to the wire-duct reactor, each point on the wire looks like a corona point to trigger streamers and feathers from the discharge wire to the duct plates covered by the dielectric barrier. The feathers of these discharges have the same apparance as discussed for point-to-plane reaction; namely, positive streamers dominate with the application of positive square pulses with net positive ion space charge accumulating in the gap. However, negative

feathers dominate with the application of negative square pulses with net negative ion space charge accumulating in the gap.

(b) Reactors applied by dc voltages:

With the application of dc voltages to the investigated reactors, corona takes place at the stressed electrode. The corona assumes different modes [30, 49, 52] depending on how high the applied voltage is above the threshold value. For positive polarity, the corona starts at threshold with the "onset-streamer" mode followed with further increase of the applied voltage by positive glow, pre-breakdown streamers and spark modes. For negative polarity, the corona starts at the threshold by "*Trichel-pulse*" mode followed with further increase of the applied voltage by negative glow and spark modes. The mechanisms of these modes are well reported [30, 49, 52] in the literature.

In the simulated gas, the majority of the ionized species will be due to the breakdown of oxygen as the energy required to ionize an oxygen molecule is less than a nitrogen molecule. This is why dc coronas generate mainly ozone and not oxides of nitrogen [53].

The ozone production takes place entirely in the ionization-zone around the corona electrode [43, 44] where the electric field is high enough for the electrons to multiply by ionization by collision. Compared with positive corona, the thickness of the ionization-zone is larger for negative corona and is of the same order as the radius of the corona electrode [54]. However, the thickness of the ionization-zone is a fraction of the corona electrode radius for positive corona.

3.1.3 Results and discussion

(a) Reactors applied by repetitive square pulse voltages:

Figures 3.1.2 and 3.1.3 show how the concentration of the generated ozone in the point-to-plane reactor increases with the input power for different axial gas flow-rates when the reactor is applied by positive and negative square pulses, respectively. The higher the flow rate the smaller is the ozone concentration at the same input power. This could simply explained by the increase of the contact time of the flowing gas with the reaction zone where streamers / feathers propagate and ozone is generated.

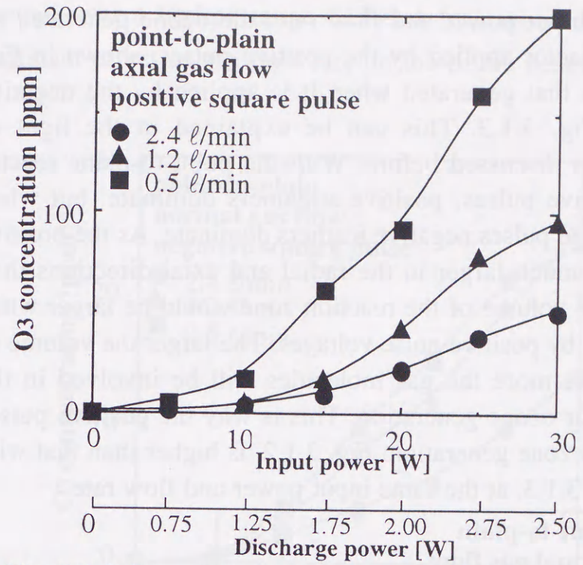

Fig. 3.1.2 Concentration of ozone generated in the point-to-plane reactor as a function of the input power for different axial gas flow rates.

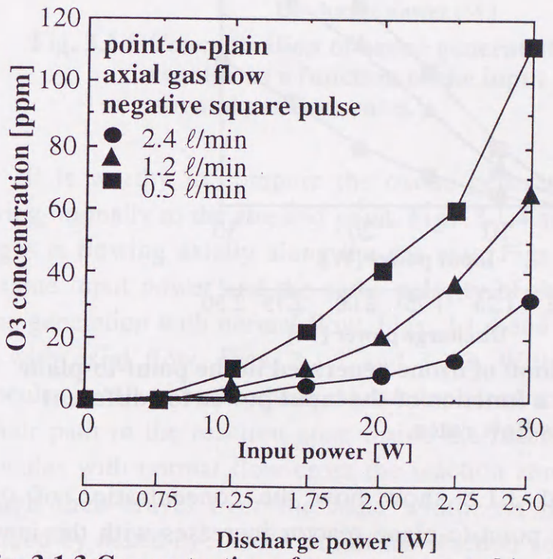

Fig. 3.1.3 Concentration of ozone generated in the point-to-plane reactor as a function of the input power for different axial gas flow rates.

For the same input power and flow rate, the ozone generated by the point-to-plane reactor applied by the positive pulses, shown in Fig. 3.1.2, is higher than that generated when it is applied by the negative pulses, shown in Fig. 3.1.3. This can be explained in the light of discharge mechanism discussed before. With the point-to-plane reactor applied by the positive pulses, positive streamers dominate, but when applied by the negative pulses negative feathers dominate. As the positive streamers propagate much larger in the radial and axial directions than negative feathers, the volume of the reaction zone would be larger when the reactor is applied by positive pulse voltages. The larger the volume of the reaction zone, the more the gas molecules will be involved in the chemical reactions for ozone generation. This is why the positive pulses is used for effective ozone generation. Fig. 3.1.2, is higher than that with negative pulses, Fig. 3.1.3, at the same input power and flow rate.

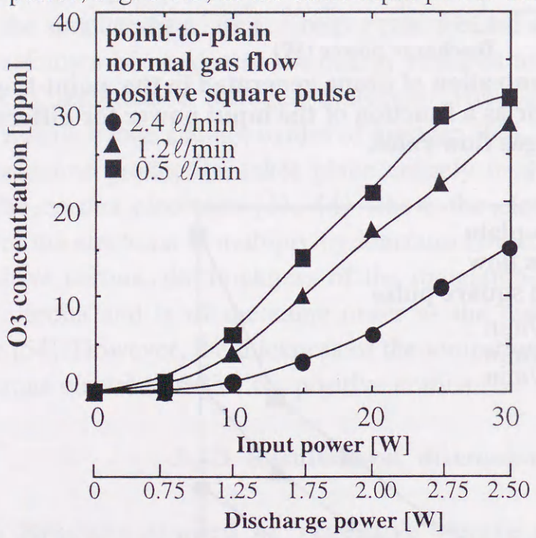

Fig. 3.1.4 Concentration of ozone generated in the point-to-plane reactor as a function of the input power for different normal gas flow rates.

Figure 3.1.4 and 3.1.5 show how the concentration of the generated ozone in the point-to-plane reactor increases with the input power for different normal gas flow rates when the reactor is applied by positive and negative square pulses respectively. The same as discussed for axial flow, the positive polarity is producing more ozone than the negative polarity for normal gas flow. But because the flow rate was

changed over a limited range (0.5~2.4 ℓm), it was hard to recognize a significant effect of gas flow rate on the ozone generation in Figs. 3.1.4 and 3.1.5.

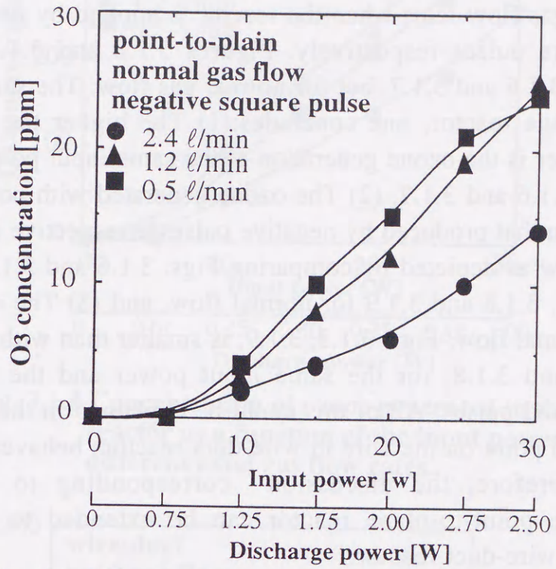

Fig. 3.1.5 Concentration of ozone generated in the point-to-plane reactor as a function of the input power for different normal gas flow rates.

It is worthy to compare the ozone generation when the gas is flowing normally to the stressed point, Figs. 3.1.4 and 3.1.5, to that when the gas is flowing axially along the gas axis, Figs. 3.1.2 and 3.1.3. For the same input power and the same polarity of the applied pulses, the ozone generation with normal flow, Figs. 3.1.4 and 3.1.5, is smaller than that with axial flow, Figs. 3.1.2 and 3.1.3. With axial flow, the gas molecules involved in the chemical reactions for ozone generation stay all of their path in the reaction zone inside the reactor. However, the gas molecules with normal flow cross the reaction zone and stay there just through their travel over the zone width. As discussed above and observed by naked eye, the width of the reaction zone is smaller than its length along the gas flow. Thus, the contact time of the flowing gas with the reaction zone is much longer with axial flow than that with normal flow. This explains why ozone generation with axial flow is larger than that with normal flow as depicted by comparing Figs. 3.1.2 and 3.1.4 for

positive pulses applied to the reactor and Figs. 3.1.3 and 3.1.5 for negative pulses applied to the reactor.

Figures 3.1.6 and 3.1.7 show how the concentration of the generated ozone in the wire duct reactor increases with the input power for different axial gas flow rates when the reactor is applied by positive and negative square pulses respectively. Figures 3.1.8 and 3.1.9 are analogous to Figs. 3.1.6 and 3.1.7, but for normal gas flow. The same as for the point-to-plane reactor, one concludes:(1) The higher the axial flow rate, the smaller is the ozone generation at the same input power as depicted by Figs. 3.1.6 and 3.1.7, (2) The ozone generated with positive pulses is higher than that produced by negative pulses, irrespective of the direction of gas flow as depicted by comparing Figs. 3.1.6 and 3.1.7 for axial flow and Figs. 3.1.8 and 3.1.9 for normal flow, and (3) The ozone generation with normal flow, Figs. 3.1.8, 3.1.9, is smaller than with axial flow, Figs, 3.1.7 and 3.1.8, for the same input power and the same polarity of the applied pulses. All of this could be explained in the light of the fact that each point on the wire in wire-duct reactors behaves as a corona point. Therefore, the discussion corresponding to Figs. 3.1.2~3.1.5 for the point-to-plane reactor can be extended to Figs. 3.1.6~3.1.9 for the wire-duct reactor.

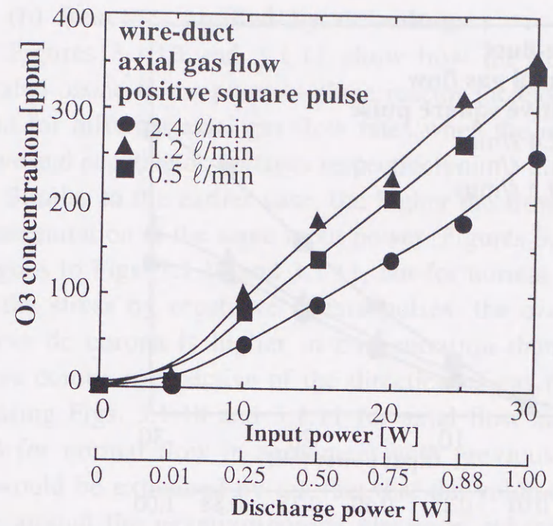

Fig. 3.1.6 Concentration of ozone generated in the wire-duct reactor as a function of the input power for different axial gas flow rates.

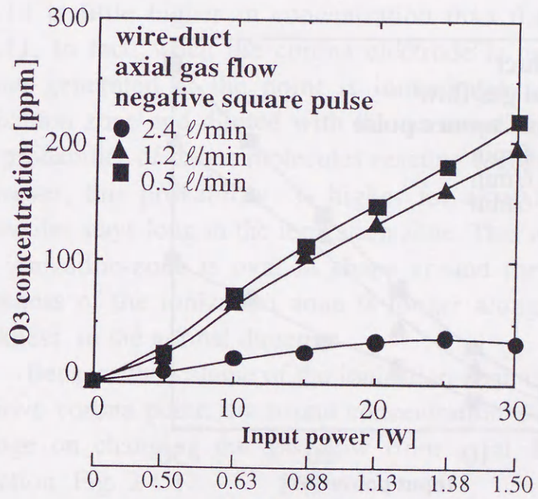

Fig. 3.1.7 Concentration of ozone generated in the wire-duct reactor as a function of the inout power for different axial gas flow rates.

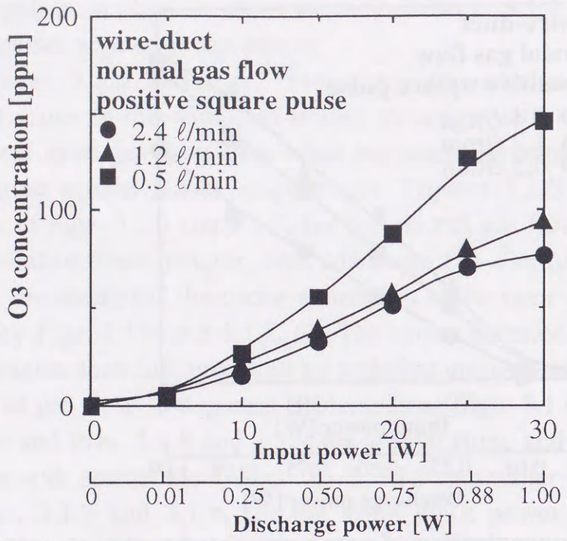

Fig. 3.1.8 Concentration of ozone generated in the wire-duct reactor as a function of the input power for different normal gas flow rates.

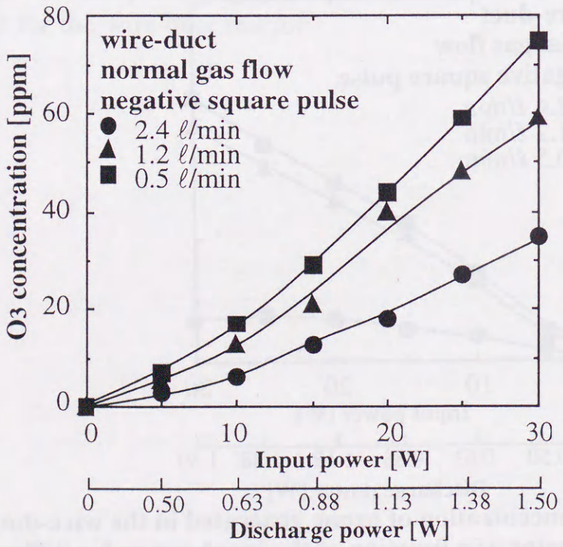

Fig. 3.1.9 Concentration of ozone generated in the wire-duct reactor as a function of the input power for different normal gas flow rates.

(b) Reactors applied by dc voltages:

Figures 3.1.10 and 3.1.11 show how the concentration of the generated ozone in the point-to-plane reactor increases with the corona current for different axial gas flow rates when the reactor is applied by positive and negative dc voltages respectively.

Similar to the earlier case, the higher the flow rate the smaller is the concentration at the same input power. Figures 3.1.12 and 3.1.13 are analogous to Figs. 3.1.10 and 3.1.11, but for normal gas flow. Different from the stress by repetitive square pulses, the ozone generated with negative dc corona is higher in concentration than that produced by positive corona irrespective of the direction of gas flow as depicted by comparing Figs. 3.1.10 and 3.1.11 for axial flow and Figs. 3.1.12 and 3.1.13 for normal flow in agreement with previous findings [43, 44]. This would be explained by the fact that the volume of the ionization-ozone around the negative corona electrode, where ozone production takes place, is larger than that around the positive corona electrode.

Contrary to the reactor when applied by negative square pulses, the ozone generated with negative dc corona for normal gas flow, Fig. 3.1.13 is little higher in concentration than that for axial flow, Fig. 3.1.11. In fact, when the corona electrode is normal to the gas flow, ozone generated at the point is immediately swept away from the ionization zone and diluted with the surrounding gas, thereby reducing the probability of ozone molecules reacting together for self-destruction. However, this probability is higher for axial flow where the ozone molecules stays long in the ionization zone. This is based on the fact that the ionization-zone is oval in shape around the corona point i.e. the thickness of the ionization zone is longer along the gap axis than its thickness in the normal direction.

Because the volume of the ionization-zone is very small around the positive corona point, the ozone concentration did not show significant change on changing the gas flow from axial, Fig. 3.1.10 to normal direction, Fig. 3.1.12.

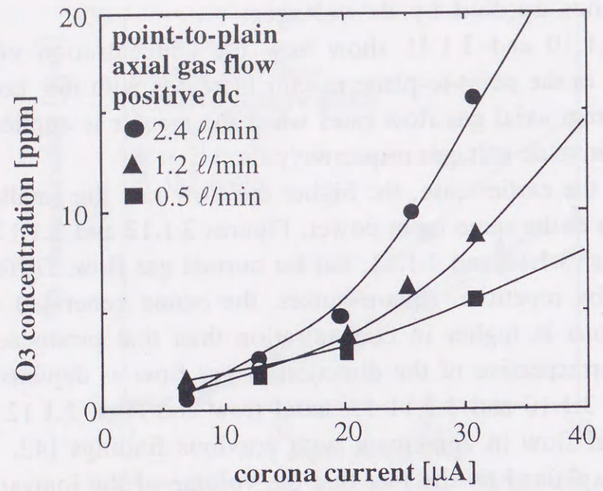

Fig. 3.1.10 Concentration of ozone generated in the point-to-plane reactor as a function of the discharge power for different axial gas flow rates.

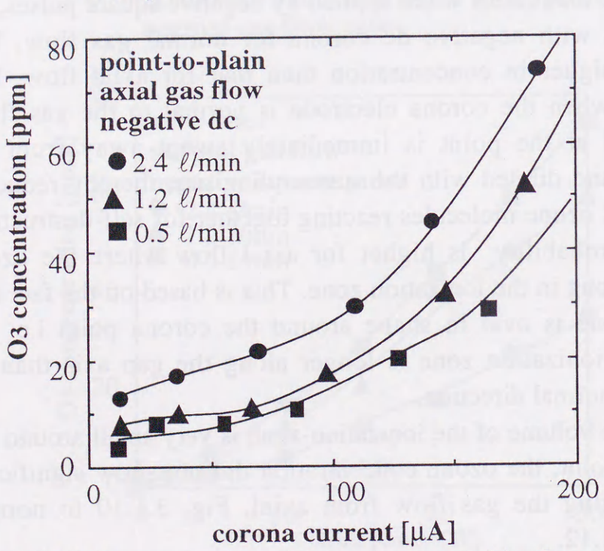

Fig. 3.1.11 Concentration of ozone generated in the point-to-plane reactor as a function of the discharge power for different axial gas flow rates.

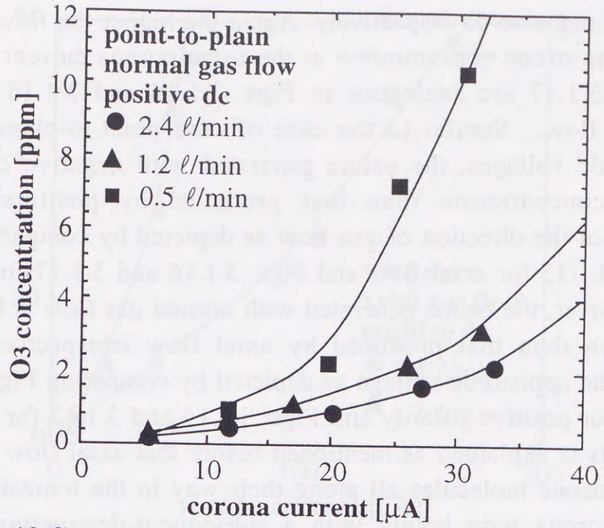

Fig. 3.1.12 Concentration of ozone generated in the point-to-plane reactor as a function of the discharge power for different normal gas flow rates.

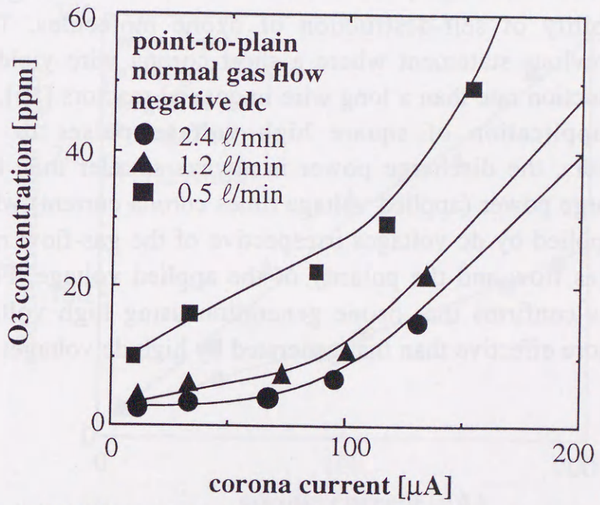

Fig. 3.1.13 Concentration of ozone generated in the point-to-plane reactor as a function of the discharge power for different normal gas flow rates.

Figures 3.1.14 and 3.1.15 show how the concentration of the generated ozone in the wire-duct reactor increases with the corona current for different axial gas flow rates when the reactor is applied by

positive and negative dc respectively. Again the higher the flow rate the smaller is the ozone concentration at the same corona current. Figures 3.1.16 and 3.1.17 are analogous to Figs. 3.1.14 and 3.1.15, but for normal gas flow. Similar to the case of the point-to-plane reactor applied by dc voltages, the ozone generated with negative corona is higher in concentration than that produced by positive corona irrespective of the direction of gas flow as depicted by comparing Figs. 3.1.14 and 3.1.15 for axial flow and Figs. 3.1.16 and 3.1.17 for normal flow. More over, the ozone generated with normal gas flow is higher in concentration than that produced by axial flow irrespective of the polarity of the applied dc voltage as depicted by comparing Figs. 3.1.14 and 3.1.16 for positive polarity and Figs. 3.1.15 and 3.1.17 for negative polarity. This is explained as mentioned before that axial flow result in the stay of ozone molecules all along their way in the ionization-zone along the corona wire length with a subsequent-destruction of gas molecules. With normal flow, ozone generated at the wire immediately swept from the ionization-zone (whose thickness is negligible with respect to the corona wire length) and diluted with the surrounding gas with little possibility of self-destruction of ozone molecules. This conforms with previous statement where a short corona wire yields a higher ozone production rate than a long wire in coaxial reactors [55].

With the application of square high voltage pulses to the investigated reactors, the discharge power is always smaller than that with the dc discharge power (applied voltage times corona current) when the reactors are applied by dc voltages irrespective of the gas-flow rate, the direction of gas flow and the polarity of the applied voltage, Figs. 3.1.2~3.1.17. This confirms that ozone generation using high voltage square pulses is more effective than that generated by high dc voltages.

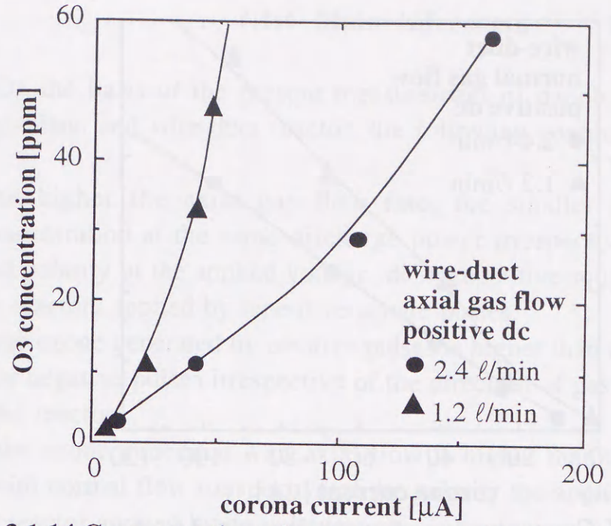

Fig. 3.1.14 Concentration of ozone generated in the wire-duct reactor as a function of the discharge power for different axial gas flow rates.

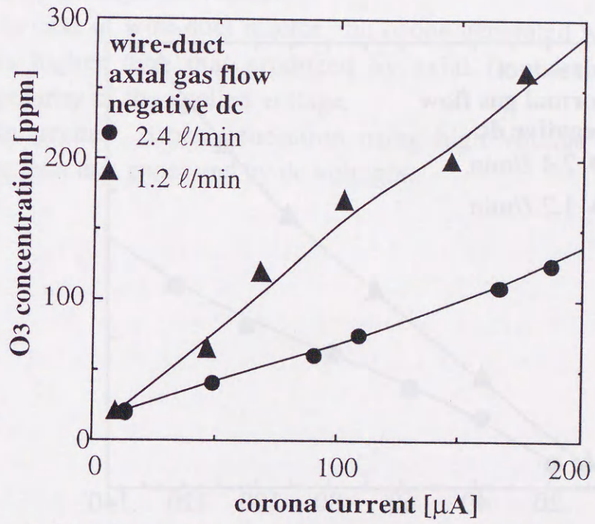

Fig. 3.1.15 Concentration of ozone generated in the wire-duct reactor as a function of the discharge power for different axial gas flow rates.

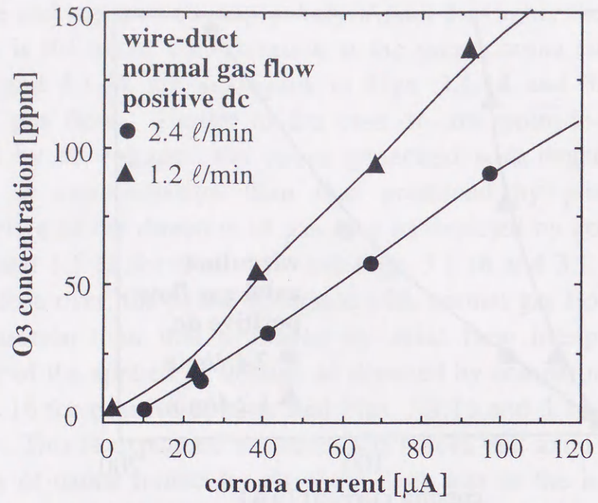

Fig. 3.1.16 Concentration of ozone generated in the wire-duct reactor as a function of the discharge power for different normal gas flow rates.

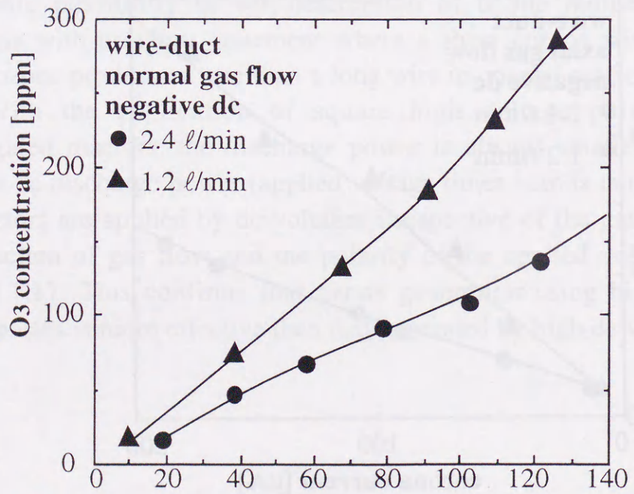

Fig. 3.1.17 Concentration of ozone generated in the wire-duct reactor as a function of the discharge power for different normal gas flow rates.

3.1.4 Main inferences

On the basis of the present measurement of ozone generation in point-to-plane and wire-duct reactor, the following conclusions may be drawn:

(1) The higher the axial gas flow rate, the smaller is the ozone concentration at the same discharge power irrespective of the type and polarity of the applied voltage; dc or repetitive square pulses.

(2) For reactors applied by repetitive square pulses:

(a) the ozone generated by positive pulses is higher than that generated by negative pulses irrespective of the direction of gas flow through the reactor.

(b) the ozone generated with axial flow is higher than that produced with normal flow irrespective of the polarity the applied pulses.

(3) For reactor applied by dc voltages:

(a) the ozone generated by negative voltage is higher than that produced by positive pulses irrespective of the direction of gas flow through the reactor,

(b) in case of wire-duct reactor, the ozone generated with normal flow is higher than that produced by axial flow irrespective of the polarity of the applied voltage.

In general, ozone generation using high voltage pulses is more feasible than that generated by dc voltages.

3.2 NOx removal using dry type reactor

The experiments reported in this section were aimed at evaluating the influence of several reactor and gas parameters and energy consumption on NOx removal efficiency. The study of the effect of hydrocarbon additives was one of the main objectives of the present research.

The results were obtained using a simulated flue gas, but the data of the test carried out with the exhaust of a diesel engine validated the conclusions.

3.2.1 Reactor and pulse power source

Two cylinder-type reactors of different sizes were employed in the experiments. The smaller one (uni-tubular reactor) consisted of a glass tube, the inner and outer diameters of 18 mm and 20 mm, respectively (Fig. 3.2.1). The outside of the tube was wrapped with a copper foil of 78 mm length as the ground electrode. A wire or a stainless steel tube situated on the axis of the tube, as a high voltage electrode. Three diameters of the high voltage electrode were used in the experiments: 0.1, 3.3 and 6.4 mm.

The larger reactor (Multi-tubular reactor) was composed of 73 elementary discharge tubes, assembled into a 70 mm diameter metallic cylinder, connected to the ground. The discharge tubes were energized in parallel. Each of them consisted of an electrode arrangement similar to uni-tubular reactor but of different dimensions. The outer and inner diameters of the reactor were respectively 7 mm and 5 mm. The length of the reactor was 450 mm and the diameter of discharge electrode was 0.5 mm.

Positive square wave pulse was used to treat simulated gas, and the details of the power source were explained in chapter 2.

Schematic diagram of the experimental set up including the power source and gas flow system was depicted in Fig. 3.2.2.

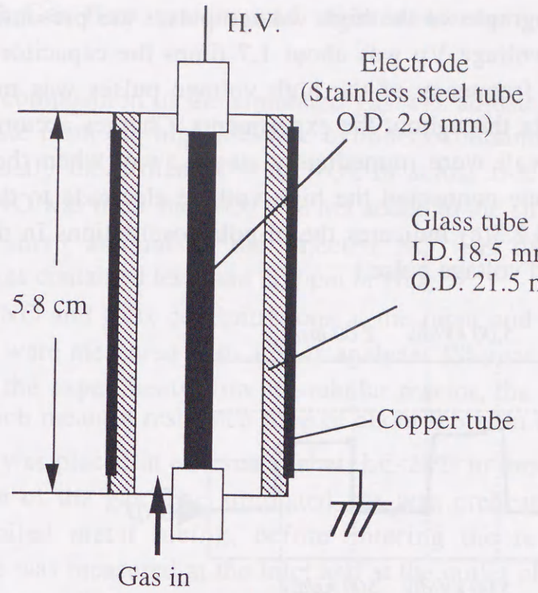

Fig.3.2.1 Plasma chemical reactor for flue gas treatment.

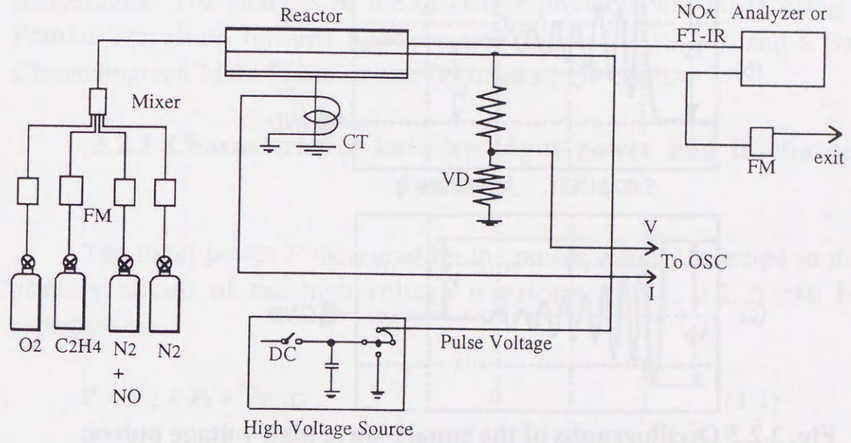

Fig.3.2.2 Schematic representation of the experimental setup.

F M: flow meter, C T: current transformer, V D: voltage divider, OSC: oscilloscope

The oscillographs of the high voltage pulses are presented in Fig. 3.2.3. The peak voltage Vp was about 1.7 times the capacitor charging voltage Vc. The frequency of the high voltage pulses was maintained constant at 250 Hz throughout the experiments. Charges accumulated on the inner glass wall were immediately swept away when the rotating spark gap electrode connected the high voltage electrode to the ground electrode. (Fig. 3.2.3(c) indicates the bi-polar oscillations in the falling part of the applied voltage pulse.)

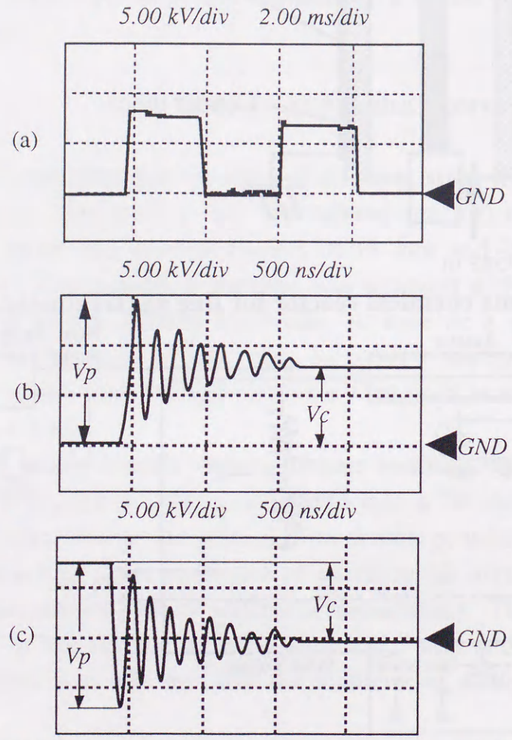

Fig. 3.2.3 Oscillographs of the square wave high voltage pulses;
(a) square wave pulse
(b) oscillations in the rising part
(c) oscillations in the falling part

3.2.2 Gas flow system and measurements

The composition of the simulated gas was adjusted by controlling the flow rate from the high-pressure cylinders containing NO, N_2, O_2, C_2H_4. Usually more than 90% of NOx in actual flue gas is NO and therefore, NO was used and NO_2 was not added to the simulated flue gas. However, small amount of the injected NO was oxidized and the simulated gas contained less than 20 ppm of NO_2.

The NO and NOx concentrations at the input and at the output of the reactor were measured with a NOx analyzer (Shimadzu NOA 305A). In most of the experiments with uni-tubular reactor, the flow rate was 2 ℓ/min., which meant a residence time of about 0.6 s. In some situations, the reactor was placed in an oven (Tabai, LC-222) in order to control the temperature of the gas. The simulated gas was preheated in the oven, using a coiled metal tubing, before entering the reactor. The gas temperature was measured at the inlet and at the outlet of the reactor and the measured value was slightly lower (within 5°C) than the oven temperature. The analysis of the discharge products was made using a Fourier Transform Infrared Spectrometer (Bio-rad, FTS-30), and a Gas Chromatograph Mass Spectrometer (Shimadzu, QP-2000A).

3.2.3 Characteristics between input power and discharge power

The input power P measured by the power meter connected in the primary circuit of the high-voltage transformer (Fig. 3.2.2) can be expressed as:

$$P = P_d + P_t + P_{RSG}\,, \qquad (3.1)$$

where P_d, P_t and P_{RSG}, respectively signifies the discharge power, the losses in the transformer and power dissipated in the rotary spark gap and pulsed high voltage circuit assembly. P_d can possibly be obtained by integrating the multiple of measured voltage and current wave forms. Accurate measurements of these wave forms, however, could not be made in the experiments because of large electromagnetic noises.

In order to evaluate the discharge power P_d, a second reactor was connected at the output of the high-voltage supply. No change in high-

voltage wave-shape was noticed in this situation. Hence, the conditions of energization of each reactor were similar to the case when only one of them was connected to the high-voltage supply and the reading P' of the power meter could be considered to represent the sum:

$$P' = 2P_d + P_t + P_{RSG} . \qquad (3.2)$$

It followed that, at a given value of the capacitor charging voltage Vc, the discharge power could be calculated as:

$$P_d = P' - P . \qquad (3.3)$$

Using this method a set of experiments was made with the uni-tubular reactor to evaluate the ratio between the input power and the discharge power at various levels of the capacitor charging voltage Vc. The measured quantities are represented in Fig. 3.2.4 and indicate that only about 30 % of the input power goes into the discharge.

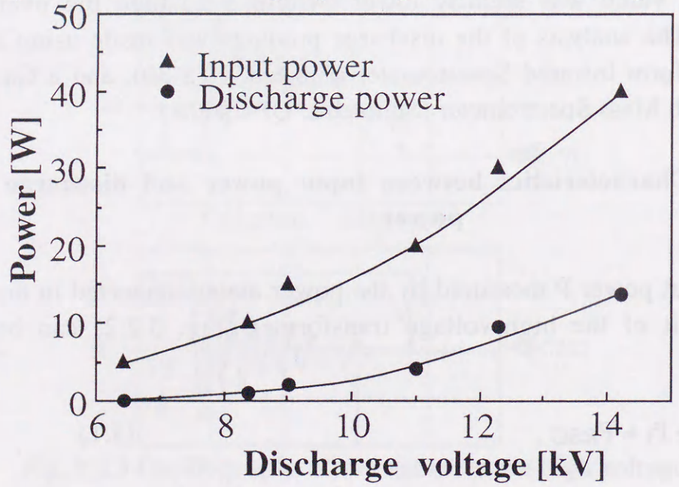

Fig. 3.2.4 The input power and the discharge power as functions of the capacitor charging voltage Vc.

P = Pd + Pt + PRSG
Pd - power going into the discharge
Pt - losses in the transformer
PRSG - power dissipated in the rotary spark gap

The loss in the transformer P_t, was found to be about 35 % of the input power P. P_t was mainly due to eddy currents, while the loss due to a

resistance of the winding was negligibly small. In the case of the uni-tubular reactor, with its P_d value less than 10 W, P_{RSG} was estimated to be about 35 % of P. It should be noted that large noises disturbed an accurate measurement of P_{RSG} from the voltage and current wave forms.

With multi-tubular reactor a quasi-linear relation was observed between P and P_d as shown in Fig. 3.2.5. In this case, with P_d-value of more than 20 W, P_d was about 60 % of P, and P_{RSG} was about 5 % of P. With larger reactors having lower impedance, the ratio of P_{RSG} to P should become small because the increase in arcing current through the RSG results in lower voltage drop across the spark gap.

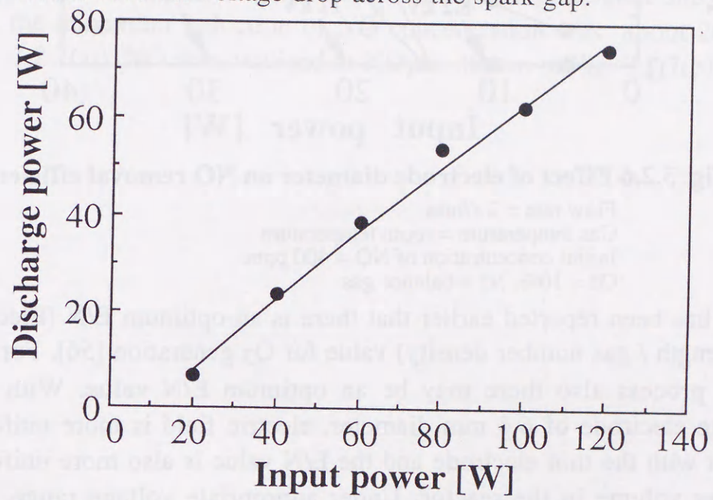

Fig. 3.2.5 The discharge power as a function of input power.

3.2.4 NOx removal without hydrocarbons

Initially experiments were carried out with the uni-tubular reactor to study the influence of the diameter of the high voltage electrode on NO removal efficiency. As shown in Fig. 3.2.6, a strongly non-linear relationship was observed between the input power and the removal efficiency of NO. For instance, in the case of 3.3 mm diameter of corona electrode the removal efficiency was almost zero for the input power of less than 15 W and then increased to a maximum when P was raised to 30 W. The removal efficiency slightly decreased as the input power was raised further. Higher removal efficiencies were obtained with the reactors employing large diameter high voltage electrodes.

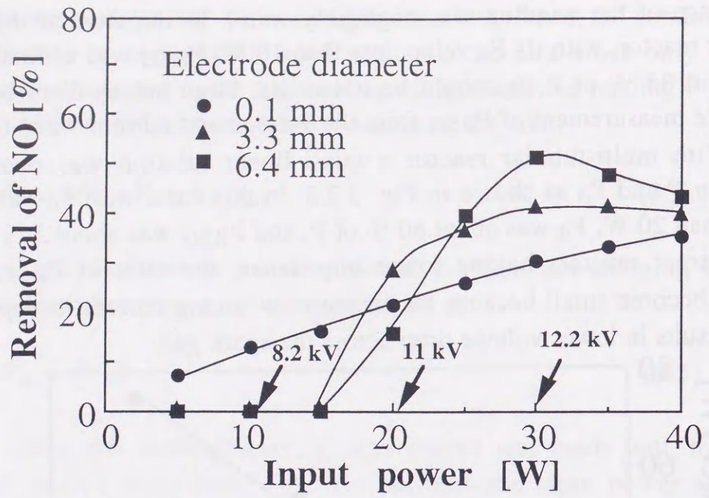

Fig. 3.2.6 Effect of electrode diameter on NO removal efficiency.

Flow rate = 2 ℓ/min
Gas temperature = room temperature
Initial concentration of NO = 400 ppm
O_2 = 10%, N_2 = balance gas

It has been reported earlier that there is an optimum E/N (Electric field strength / gas number density) value for O_3 generation [56]. For the DeNOx process also there may be an optimum E/N value. With the discharge electrode of 6.4 mm diameter, electric field is more uniform than that with the thin electrode and the E/N value is also more uniform for larger volume in the reactor. Under appropriate voltage range, the maximum efficiency of the NO oxidation could, therefore, be obtained with the discharge electrode of 6.4 mm diameter. The electron energy was estimated in the previous chapter 2. The results suggested that high field strength was required for NOx removal under discharge plasma.

From Fig. 3.2.6 of 0.1 mm diameter electrode, once voltage was applied corona was immediately occurred and NO was oxidized at lower input power (below 10 W level). On the contrary, with 6.4 mm diameter electrode, no corona was occurred at lower input power. However, once corona was initiated, field inside the reactor was higher than that 0.1 mm diameter electrode at the same input power (peak voltage was almost same for each electrode at same input power). This resulted in higher NO removal efficiency for 6.4 mm diameter electrode. Also, E/N or field strength was an important factor, rather than the peak of the pulse voltage or input power, to be considered while designing a reactor.

Another important factor that affects the DeNOx efficiency is the mode of discharge. When dense streamer channels are formed, oxidation of NO may be hampered due to an increase of local gas temperature around the streamer channel. This is similar to decrease in O_3 generation at higher temperatures [57]. When the power was increased, more dense streamers were formed and the DeNOx efficiency was decreased. However, further studies are necessary to find the optimum electrode configuration and E/N value.

The effect of the initial NO concentration was examined in a second set of experiments. Four gas compositions were simulated and in each case the maximum reduction of NO concentration was about 200 ppm (Fig. 3.2.7(a)). NO was oxidized to NO_2 as shown in Fig. 3.2.7(b).

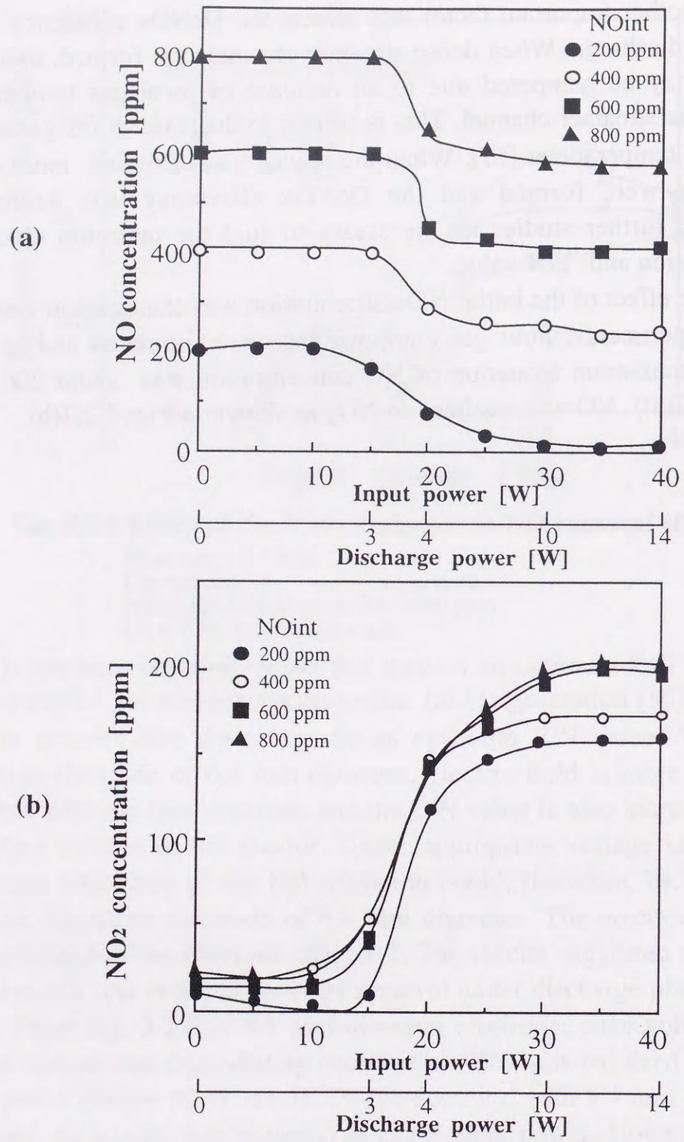

Fig. 3.2.7 Concentration of NO(a) and NO_2(b) as functions of input power for various initial concentrations of NO.
Flow rate = 2 ℓ/min
Gas temperature = room temperature
O_2 = 10 %, N_2 = balance gas

In the plasma process, NO in pure dry air is oxidized at first. When all the NO is converted to NO_2, reduction of NO_2 proceeds. This is a typical change observed for low initial concentrations of NO in pure dry air. When initial NO concentration is high, the oxidation becomes incomplete and NO and NO_2 exist together. In this case, the reduction of NO_2 is not effectively promoted by the discharge. In Fig. 3.2.7, the amount of NO oxidation was limited to 200 ppm. This may be due to the increase in local gas temperature around the streamer channel. When the power is increased, more dense streamer channels are formed limiting the production of O radicals and hence, reducing the NOx oxidation.

The increase in the gas temperature also caused a decrease in NO removal performance of the plasma process in dry air. Fig. 3.2.8 shows the magnitude of decrease in NO concentration as the gas temperature increases. Initial NO concentration was 400 ppm and the gas flow rate was 2 ℓ/min. At P=30 W and P=40 W, the magnitude of decrease in NO concentrations at room temperature were about 200 ppm. When the gas temperature was raised to 220 °C, the removal performance deteriorated, and only 100 ppm of NO was removed.

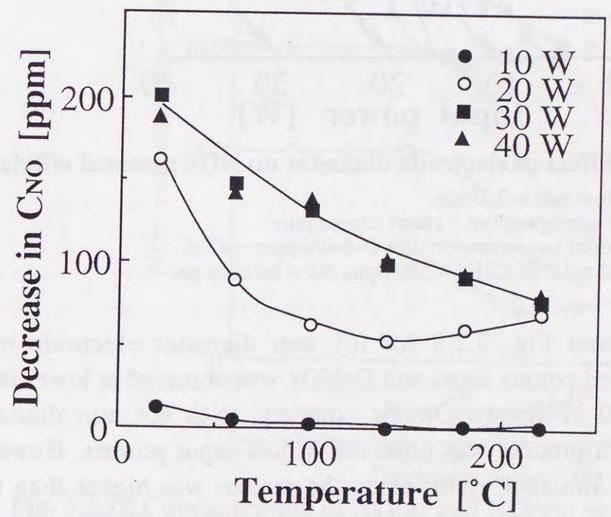

Fig. 3.2.8 Decrease of NO as a funtion of reactor temperature.
Flow rate = 2 ℓ/min
Gas temperature = room temperature
O_2 = 10%, N_2 = balance gas

3.2.5 NOx removal with hydrocarbons

The foregoing experiments were repeated with a hydrocarbons added to the gas. The curves in Fig. 3.2.9 show that the addition of C_2H_4 to the simulated flue gas increased the maximum removal efficiency of NOx and reduced the minimum input power needed for the reactor (e.g. From 30 W to 25 W, with 6.4 mm thick corona electrode) Further, an addition of 500 ppm of C_2H_4 significantly enhanced the NO oxidation, as shown in Fig. 3.2.10, leading to reduction of NOx.

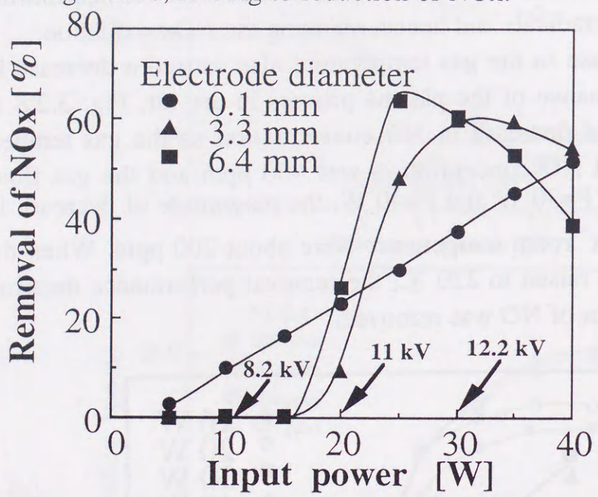

Fig. 3.2.9 Effect of electrode diameter on NOx removal efficiency.

Flow rate = 2 ℓ/min
Gas temperature = room temperature
Initial concentration of NO = 400 ppm
O_2 = 10 %, C_2H_4 = 500 ppm, N_2 = balance gas

As seen from Fig. 3.2.9 for 0.1 mm diameter electrode once voltage was applied corona starts and DeNOx was observed at lower input power (below 10 W level). On the contrary, with 6.4 mm diameter electrode, no such process was observed at low input powers. However once corona was initiated, field inside the reactor was higher than that with 0.1 mm diameter electrode at the same input power. This resulted in higher DeNOx efficiency for 6.4 mm diameter electrode. It is also observed that NOx removal was determined by E/N or field strength rather than by the input power or peak of the pulse voltage.

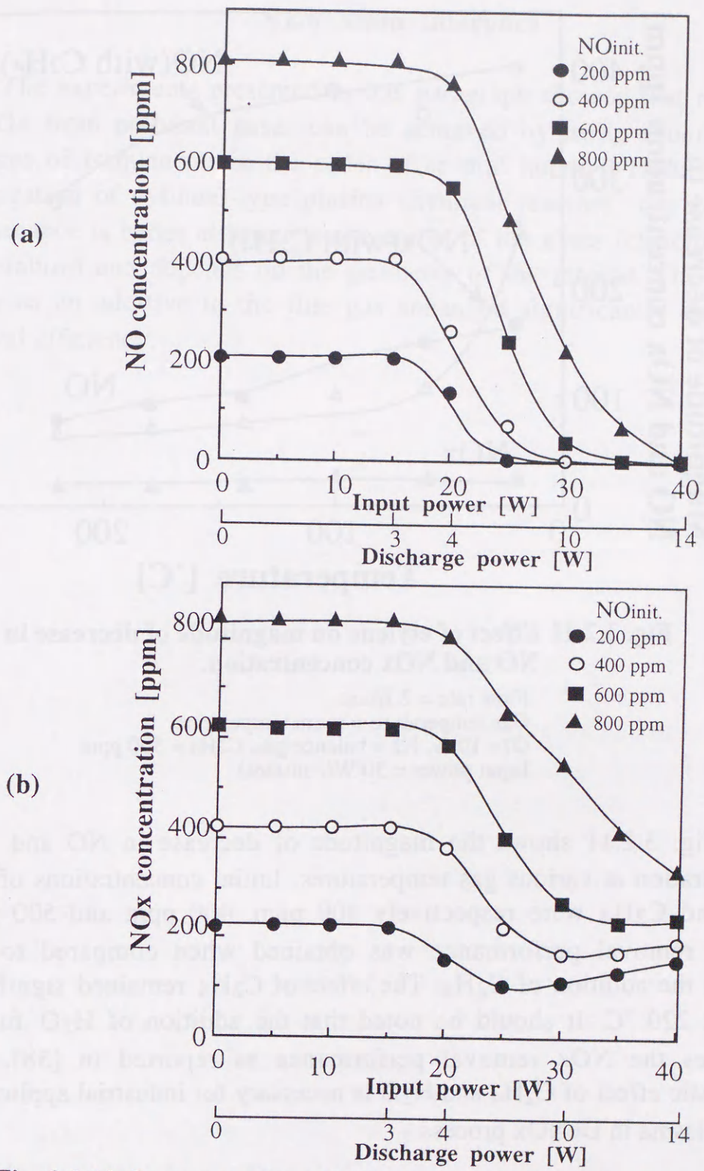

Fig. 3.2.10 Concentration of NO(a) and NO_2(b) as functions of input power for various initial concentrations of NO in the presence of ethylene.

Flow rate = 2 ℓ/min
Gas temperature = room temperature
O_2 = 10 %, N_2 = balance gas
C_2H_4 = 500 ppm

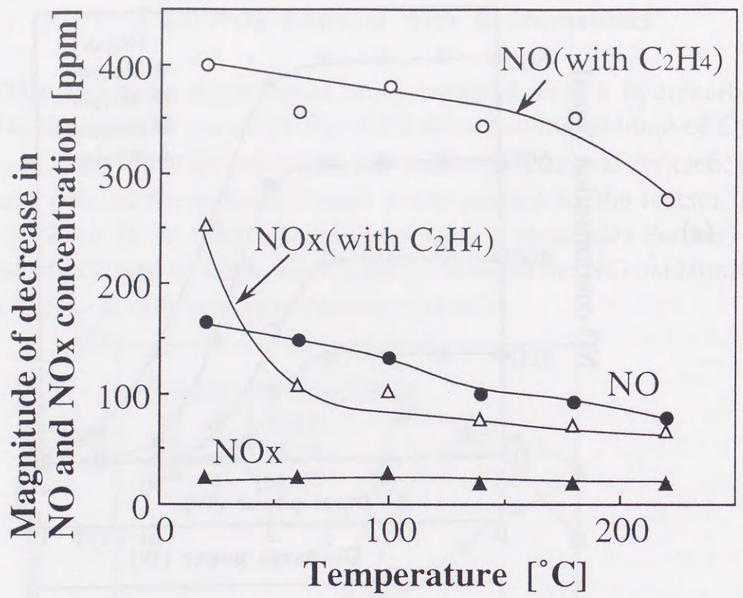

Fig. 3.2.11 Effect of etylene on magnitude of decrease in NO and NOx concentration.

Flow rate = 2 ℓ/min
Gas temperature = room temperature
O_2= 10 %, N_2 = balance gas, C_2H_4 = 500 ppm
Input power = 30 W(constant)

Fig. 3.2.11 shows the magnitude of decrease in NO and NOx concentration at various gas temperatures. Initial concentrations of NO, NOx and C_2H_4 were respectively 400 ppm, 400 ppm and 500 ppm. Higher removal performance was obtained when compared to that without the addition of C_2H_4. The effect of C_2H_4 remained significant even at 220 °C. It should be noted that the addition of H_2O further increases the NOx removal performance as reported in [58]. The synergistic effect of C_2H_4 and H_2O is necessary for industrial application of the plasma in DeNOx process.

3.2.6 Main inference

The experiments presented in this paragraph showed that removal of NOx from pollutant gases can be achieved by using square-wave voltages of frequencies in the order of several hundred Hertz for the energization of cylinder-type plasma chemical reactors. The removal performance is better at lower temperatures of the gases (close to room temperature) and depends on the geometry of the reactor. The use of C_2H_4 as an additive to the flue gas enhanced significantly the NOx removal efficiency.

3.3 NOx Removal Using Wet Reactor

In the pulse discharge, NO gets converted to NO_2 which can be absorbed by a liquie film maintained in the reactor. Such semi-wet reactors can also be used for collection of fine particles.

In this section, the performance evaluation of a dry type and several wet-type reactors in DeNOx efficiency. The resluts were analyzed and discussed.

3.3.1 Reactors

The plasma reactor consists of a cylindrical glass insulating tube (20 mm ID, 23 mm OD) with a centrally suspended discharge electrode and a thin copper foil wound on the surface of the glass as ground electrode. Four types of reactors were used as shown in Fig. 3.3.1: (a) Wet reactor: water or absorbent was injected from a nozzle to form a thin film on the inner wall of the reactor. An "O" ring was used to maintain uniformity of the film along the wall surface. (b) Semi-wet reactor: A cylindrical membrane filter was attached on the inner surface of glass tube to hold the water or absorbent film (c) Spray reactor: absorbent droplets were injected through the micro holes drilled on the discharge electrode (d) Dry reactor: a conventional cylindrical reactor.

The wet reactor, semi-wet reactor and dry reactor, all use a stainless steel wire (0.2 mm ϕ) of 210 mm length as the discharge electrode. For the spray reactor, an aluminum tube (2.5 mm ϕ) of 210 mm length was used as the high voltage (HV) electrode with about 160 holes drilled on its surface. Each hole is of 0.15 mm diameter, spaced 5 mm apart lengthwise. For the wet reactor and spray reactor, an electronic metering pump (Iwaki EX-C60) was used with repetition frequency of 120 pulses per second (pps). Absorbent was supplied with the flow rate of 84 ml / min in the plasma reactor. Analysis of the absorbent was done using a pH meter (Beckman, Φ10 pH meter) and an UV spectroscope (Shimadzu, UV-1200) to determine the NOx concentration. Pulse power source used in this experiment was the same as used in the section 3.2.

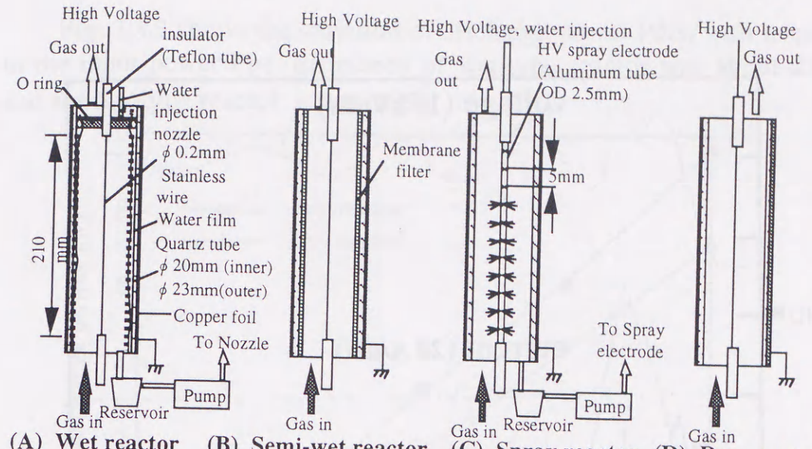

(A) Wet reactor (B) Semi-wet reactor (C) Spray reactor (D) Dry reactor

Fig. 3.3.1 Plasma reactors used in the experiment.

3.3.2 Waveforms and discharge power

Fig. 3.3.2 shows the pulse voltage and current wave forms measured for the wet reactor. Rise time of the voltage pulse was about 20 ns. A peak current (I_P) of 46.1 A was recorded for an input power (Pin) of 40 W. I_P of wet reactor and semi-wet reactor was found to be identical for the same input power. When water injection was stopped, the reactor behaved as a dry reactor and I_P was decreased to 22.5 A. This indicates that increase in capacitance of wet reactor due to the water film and increase in dielectric loss of water have, together, contributed to increase in I_P [59].

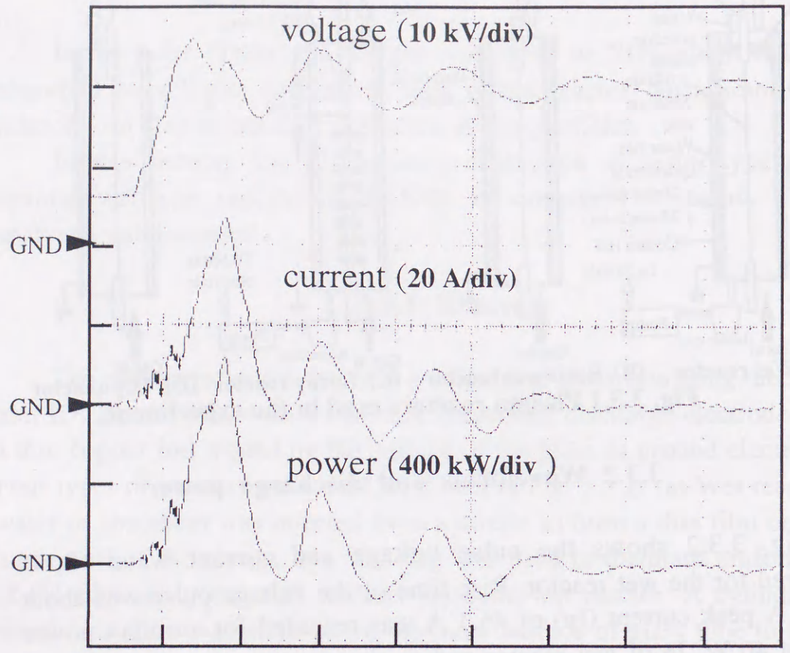

Fig. 3.3.2 Rising part of the square wave voltage , current and the discharge power : average of 256 waveforms.
(Wet reactor, time scale; 50 ns/div, input power 40W)

It has been well established that very narrow high voltage pulses, of the order of few nanoseconds, are capable of generating the so called non-thermal plasma [6-9]. The ionic space charge created by this plasma, during the pulse-on period, was immediately removed from the reactor when the discharge electrode was grounded by rotating spark gap [37]. This was reflected in the increase in discharge current which was very high compared to the displacement current due to glass dielectric. The above fact clearly indicates that in case of wet reactor the absorbent film need not be grounded.

In the spray reactor, I_P was directly proportional to the spray rate. This was due to the decrease in effective electrode separation with the extension of water column from the HV electrode. The I_P of spray reactor was about 10% higher than that of wet reactor or semi-wet reactor.

Fig. 3.3.3 shows the variation of discharge power Pdis, with respect to the input power P_{IN}. Efficiency of wet-type reactor was about 25% and for dry-type reactor, it was 18%.

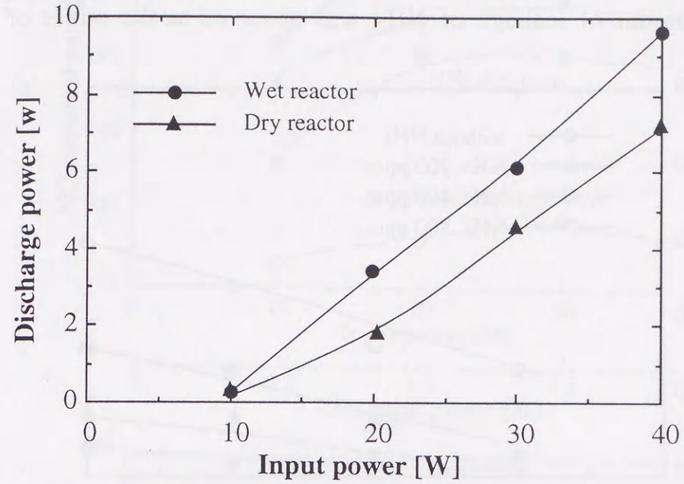

Fig.3.3.3 Comparison of discharge power of wet and dry reactors at room temperature.

In this thesis, graphs were drawn with respect to the input power instead of output (discharge) power owing to measurement inaccuracies caused by electromagnetic noise especially at low values of discharge power.

3.3.3 Performance of dry reactor

Experiments were conducted to study the effect of NH_3 and combined effect of H_2O vapor and NH_3 concentration on the DeNO and DeNOx efficiencies. Results were reported here for two temperature cases: room temperature and 150°C. NH_3 level was varied from 200-800 ppm. The initial concentrations of N_2, NO, O_2 and CO_2 were respectively 79.96%, 0.04%, 10% and 10%.

Studying the effect of NH_3 concentration, not much appreciable change in DeNO rate with respect to NH_3 was found for any temperature. This is because the conversion of NO to NO_2 depends on the concentration of free oxygen radicals and not on NH_3 [60a]. In case of DeNOx rate, though the temperature effect was negligible, the effect of NH_3 concentration was clearly distinct as shown in Fig. 3.3.4. This was so, particularly at high input power. Without any NH_3 additive, the

DeNOx rate was almost constant (~ 6%) for a given input power and increases to about 18-60% with the addition of NH_3. The chemical reactions that aid the increase in DeNOx rate were detailed in [60]. Certain amount of leakage of NH_3 was observed at the outlet of the reactor.

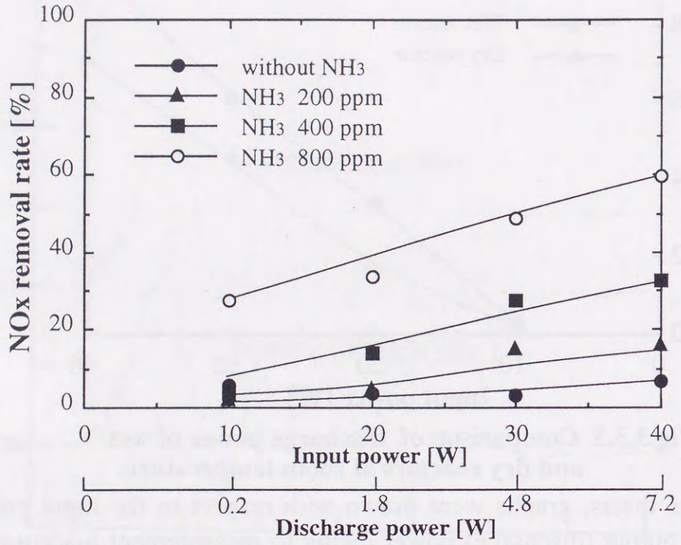

Fig.3.3.4 Performance of dry reactor at various NH_3 concentrations.

(Simulated gas composition: NO-400 ppm, O_2- 10%, CO_2-10%, balance gas-N_2, flow rate-2 l/min; temperature-25°C)

In the presence of NH_3 and water vapor, both DeNO and DeNOx rate were enhanced proportional to the temperature and input power. Fig. 3.3.5 presents the variation of DeNO and DeNOx rate with respect to the power input for different additives. The water concentration was 10% by volume and that of NH_3, 400 ppm. Maximum DeNO rate of 90% was obtained at 150°C for Pin of 20W. The corresponding DeNOx rate was 70%. Interestingly, there was no leakage of ammonia in this set of experiments. This was due to the absorption of NH_3 by H_2O.

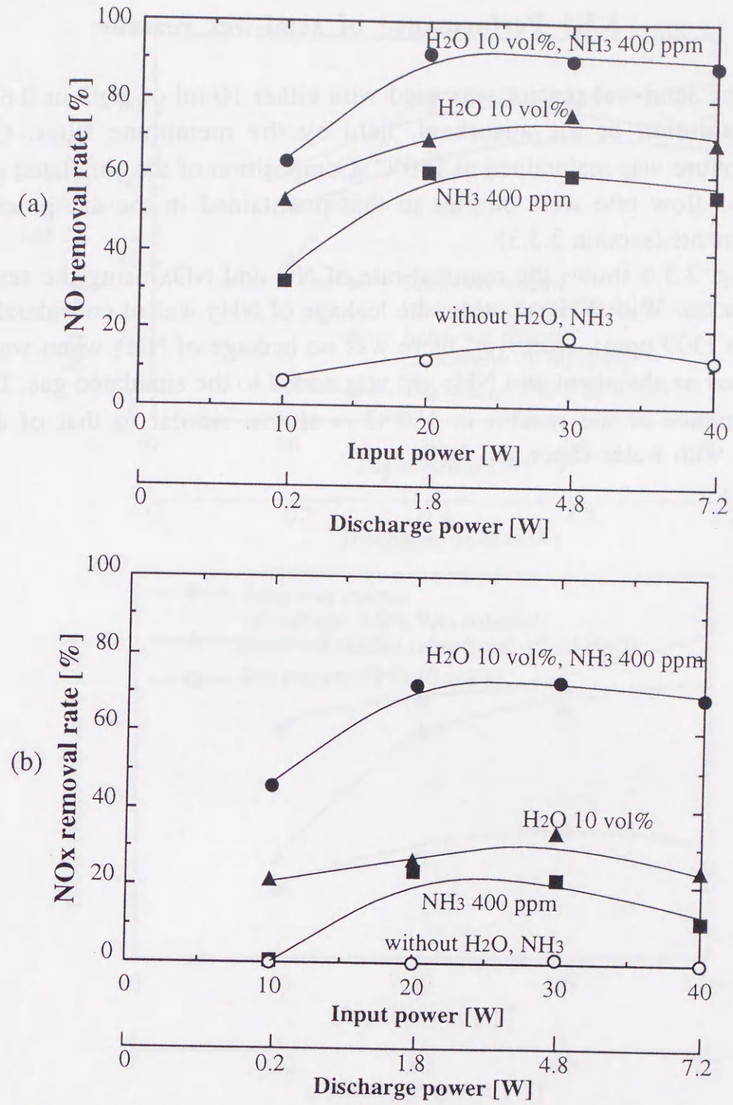

Fig.3.3.5 Performance of dry reactor with H_2O vapor and NH_3 as absorbents.

(a) NO removal rate (b) NOx removal rate

(Simulated gas composition: NO-400 ppm, O_2- 10%, CO_2-10%, balance gas-N_2, flow rate-2 l/min; temperature-150°C)

3.3.4 Performance of semi-wet reactor

The semi-wet reactor was used with either 10 ml of H_2O or 0.6 % NH_3 solution as the absorbent, held by the membrane filter. Gas temperature was maintained at 150°C. Composition of the simulated gas and gas flow rate were similar to that maintained in the dry-process experiments (section 3.3.3).

Fig. 3.3.6 shows the removal rate of NO and NOx using the semi-wet reactor. With NH_3 solution, the leakage of NH_3 was of considerable amount (300 ppm). However, there was no leakage of NH_3 when water was used as absorbent and NH_3 gas was added to the simulated gas. The performance of the reactor at 150°C is almost similar to that of dry reactor with water vapor and NH_3.

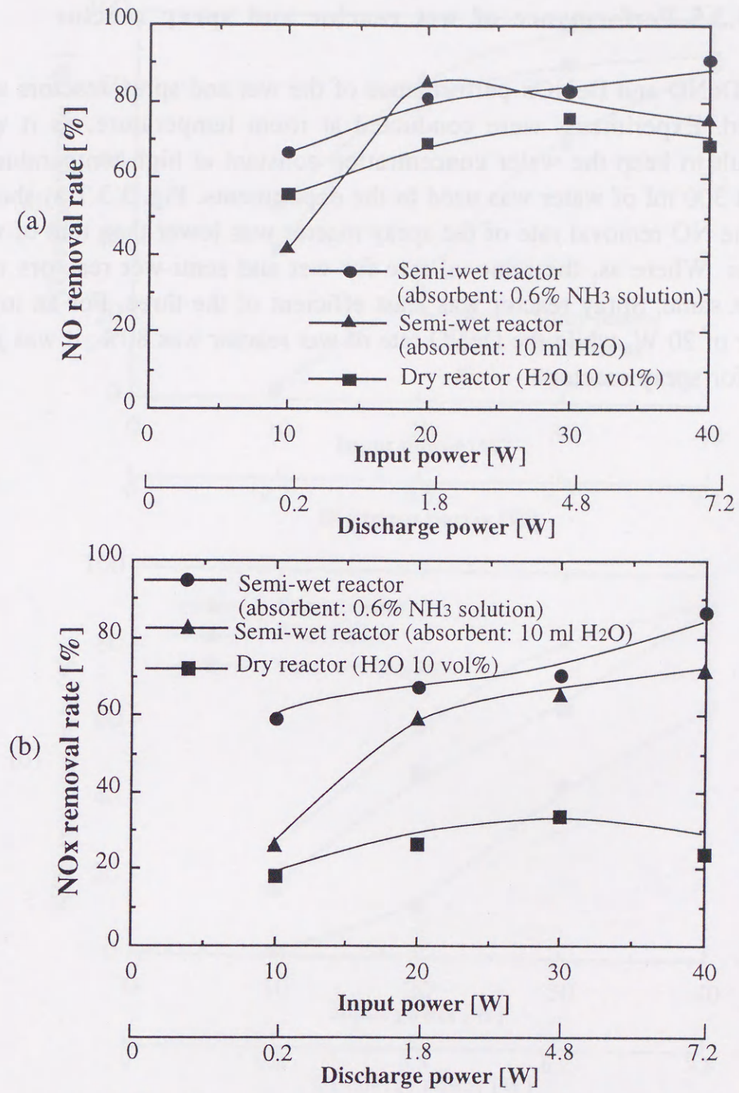

Fig.3.3.6 Performance of semi-wet reactor.
(a) NO removal rate (b) NOx removal rate
(Simulated gas composition: NO-400 ppm, O_2- 10%, CO_2-10%, balance gas-N_2, flow rate-2 l/min, temperature-150°C)

3.3.5 Performance of wet reactor and spray reactor

DeNO and DeNOx performance of the wet and spray reactors was studied. Experiments were conducted at room temperature, as it was difficult to keep the water concentration constant at high temperatures. About 300 ml of water was used in the experiments. Fig. 3.3.7(a) shows that the NO removal rate of the spray reactor was lower than that of wet reactor. Where as, the removal rate for wet and semi-wet reactors was almost same. Spray reactor was least efficient of the three. For an input power of 20 W, while the DeNO rate of wet reactor was 80%, it was just 30% for spray reactor.

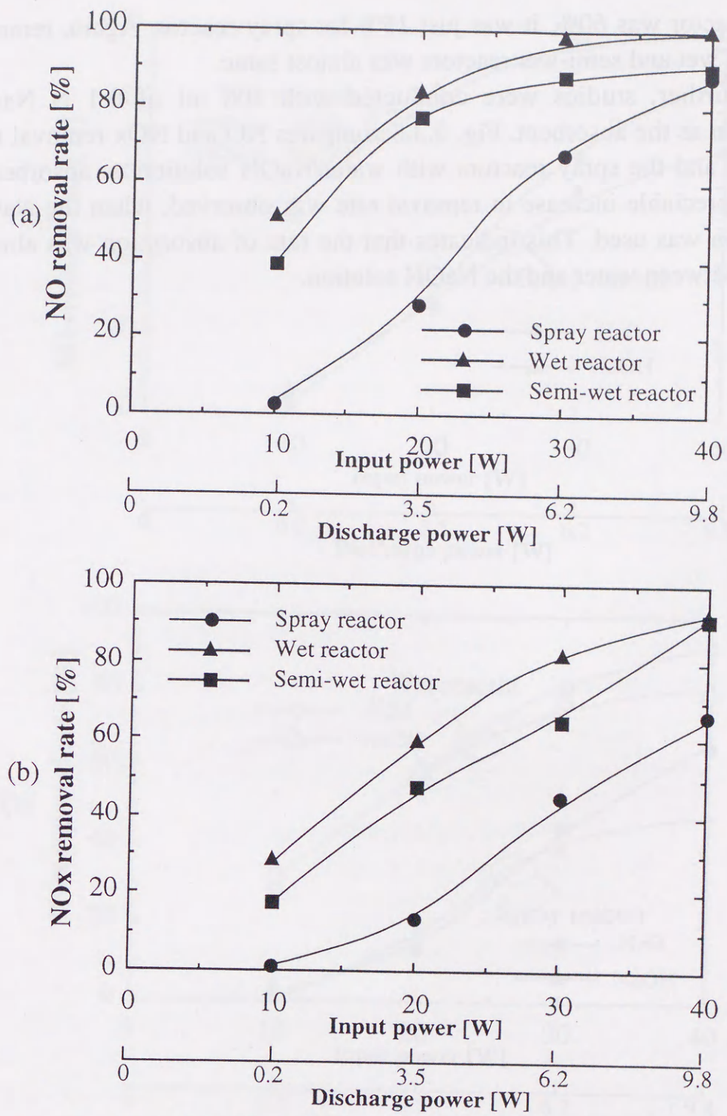

Fig.3.3.7 Performance of wet-type reactors with H_2O as absorbent.
(a) NO removal rate (b) NOx removal rate
(Simulated gas composition: NO-400 ppm, O_2- 10%, CO_2-10%, balance gas-N_2, flow rate-2 l/min; temperature-25°C)

Fig. 3.3.7(b) shows the NOx removal rate. It was observed that DeNOx performance of wet and semi-wet reactors was better than that of spray reactor. For an input power of 20 W, while the DeNOx rate of

wet reactor was 60%, it was just 15% for spray reactor. Again, removal rate of wet and semi-wet reactors was almost same.

Further, studies were conducted with 300 ml of 0.1 N NaOH solution as the absorbent. Fig. 3.3.8 compares NO and NOx removal rate of wet and the spray reactors with water/NaOH solution as absorbents. No appreciable increase in removal rate was observed, when the NaOH solution was used. This indicates that the rate of absorption was almost same between water and the NaOH solution.

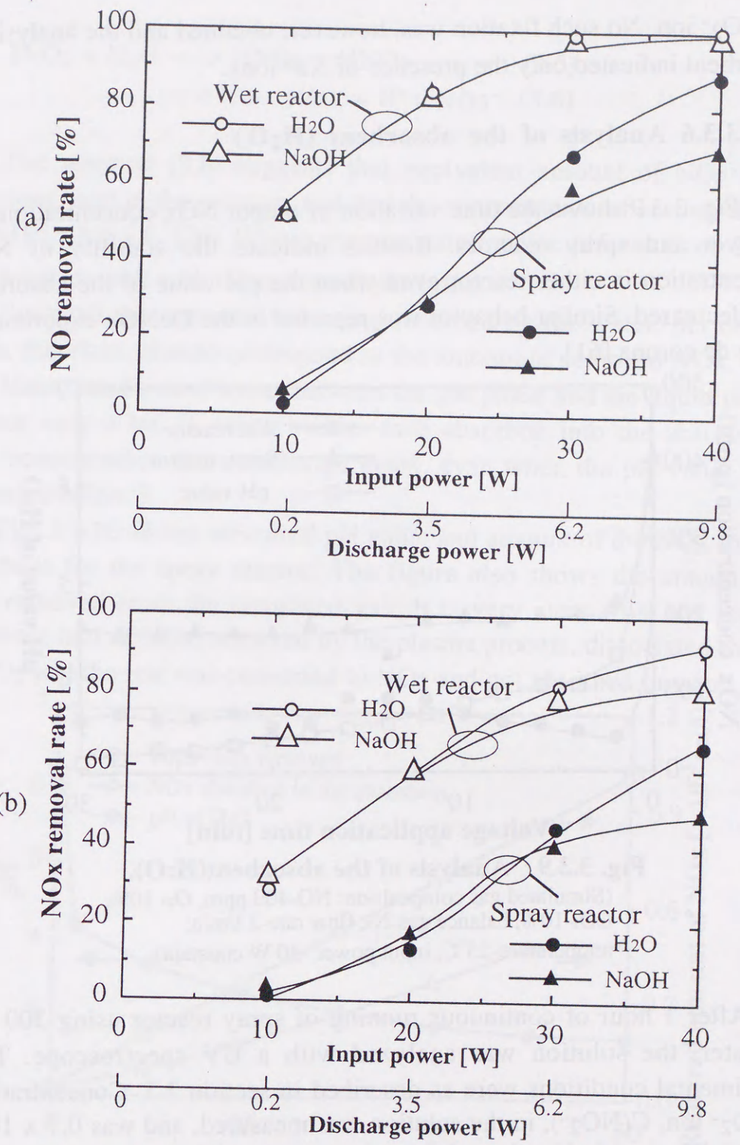

Fig.3.3.8 Performance wet and spray reactors with H_2O / NaOH solution as abosorbents.

(a) NO removal rate (b) NOx removal rate
(Simulated gas composition: NO-400 ppm, O_2- 10%, CO_2-10%, balance gas-N_2, flow rate-2 ℓ/min; temperature-25°C)

In this experiment, alkaline agent, like NaOH, was used with the aim of fixation of NO_2^- ion and to expect an enhancement of the absorption

of NO_2^- ion. No such fixation was, however, obtained and the analysis of absorbent indicated only the presence of Na^+ ions.

3.3.6 Analysis of the absorbent (H_2O)

Fig. 3.3.9 shows the time variation of output NOx concentrations of the wet and spray reactors. Results indicate the stability of NOx concentration in either reactor even when the pH value of the absorbent was decreased. Similar behavior was reported in the DeNOx experiments using dc corona [61].

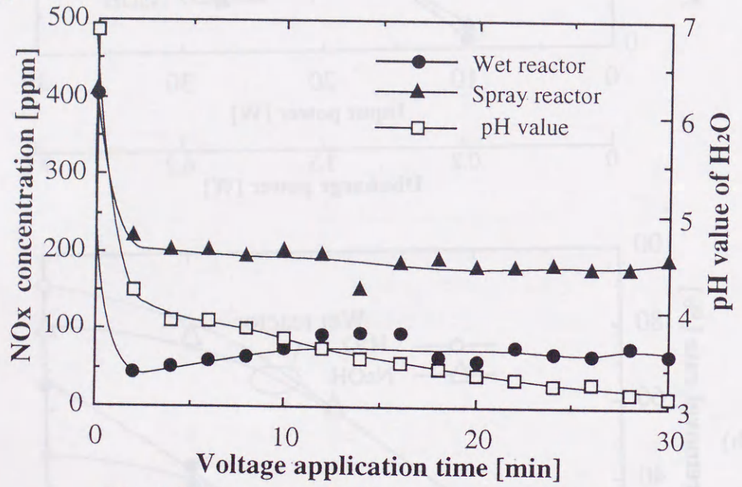

Fig. 3.3.9 Analysis of the absorbent(H_2O).
(Simulated gas composition: NO-400 ppm, O_2- 10%, CO_2-10%, balance gas-N_2, flow rate-2 l/min; temperature-25°C, input power -30 W constant)

After 1 hour of continuous running of spray reactor using 300 ml of water, the solution was analyzed with a UV spectroscope. The experimental conditions were as described in section 3.5. Concentration of NO_2^- ion, $C(NO_2^-)$, in the solution was measured, and was 0.7 x 10^{-3} mol / ℓ. Measured pH value of the solution was 2.83. Mol-concentration of H^+ ion of the solution was

$$C(H+) = 10^{-2.83} = 1.49 \times 10^{-3} \text{ mol } / \ell \qquad (3.4)$$

The value is 2 times that of the measured value of $C(NO_2^-)$.

NO_2(gas) was dissolved easily in the H_2O as the following reaction suggests:

$$2NO_2 + H_2O \text{ ----> } HNO_2 + HNO_3 \qquad (3.5)$$

$$\text{----> } H^+ + NO_2^- + H^+ + NO_3^- \qquad (3.6)$$

The reaction (3.6) suggests that equivalent amount of NO_2^- and NO_3^- ions exist in the solution, and that the concentration of H+ ion is 2 x 0.7 x10_3^- mol / ℓ. This H^+ ion concentration gives pH-value of 2.85, which agrees well with the measured pH value.

Since all the removed NOx was absorbed by the water, pH of the water, therefore, should correspond to the amount of removed NOx.

Mass transfer coefficient between the gas phase and the liquid phase did not vary a lot. In other words, once absorbed into the absorbent, NOx concentration did not change much, even when the pH value was decreased below 3.

Fig. 3.3.10 shows measured pH value and amount of the NOx in the absorbent for the spray reactor. The figure also shows the amount of NOx removed from the simulated gas. It is very clear from the graph that about half of NOx, removed by the plasma process, dissociated to N_2 and, O_2 and the rest was converted to NO_2 and got absorbed in water.

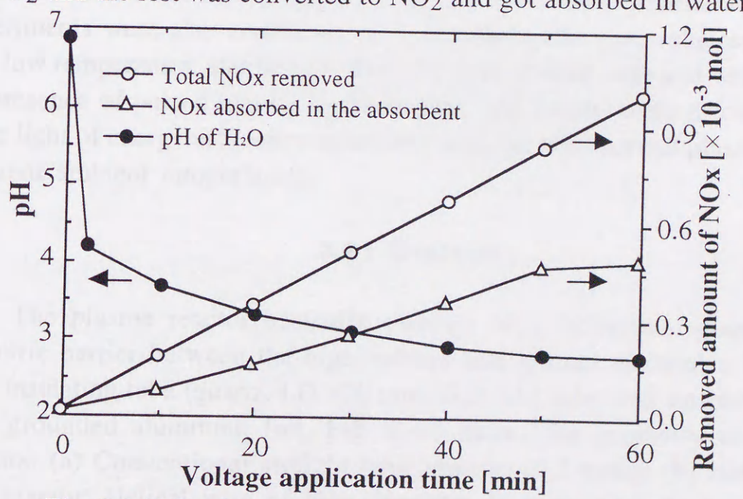

Fig. 3.3.10 Performance of spray reactor at various pH levels of H_2O.
[Experimental conditions: same as in Fig. 3.3.9]

3.3.7 Main inferences

DeNOx performance of the discharge plasma was experimentally compared using the wet-type reactors and the dry reactors, and following conclusions were obtained.

(1) Injection of ammonia and water vapor together enhanced the DeNOx performance of the dry-reactor, and no leakage ammonia was observed.

(2) The wet type reactors performed better compared with the dry reactor, and that the wet and the semi wet reactors were better than the spray reactor.

(3) In the wet-type reactors, DeNOx performances with water, ammonia solution and NaOH solution were about the same.

(4) When water is used, the DeNOx performance of the wet-type reactors stayed constant even pH value of the water dropped to less than 3.

(5) The experimental results suggest that about a half of NO removed by the plasma is dissociated to N_2 and O_2.

3.4 NOx Removal Using Low Temperature Corona Reactor

In most of the foregoing applications the plasma reactor was of the conventional dry type. Recently, it has been reported that the dry type reactor may not be adequate to remove certain stable gases present in the flue/exhaust gas [62]. In this regard, we carried out investigations on a simulated thermal power plant exhaust and found that such stable gases can be efficiently removed/precipitated by pulsed plasma treatment at very low temperature. The operation of corona reactors at low temperatures is quite a new finding, recently we reported in [63], and another important application of this low temperature plasma treatment. We, further, report the steps taken to improve the DeNO / DeNOx efficiency by modifying the plasma reactor design. Using the concept of wet-type reactor [64], field tests were carried out on the exhaust gas of a 8 kW diesel engine. Also, the conventional straight wire corona electrode was replaced by an helical wire electrode and performance of the reactor was studied. Selection of the helical wire was motivated by its excellent performance in other corona applications like ESP, ozone generators etc. Experiments were also conducted on a simulated flue gas, subjected to very low temperature, and DeNO / DeNOx were studied with and without the presence of pulsed plasma in the reactor. The results were discussed in the light of energy efficiency associated with the non-thermal plasma at different ambient temperatures.

3.4.1 Reactors

The plasma reactor basically consists of a cylindrical glass as dielectric barrier between the high voltage and ground electrodes. The glass insulating tube (quartz, I.D =20 mm, O.D =23 mm) was surrounded by a grounded aluminum foil. Fig. 3.4.1 shows the geometry of the reactors: (a) Conventional straight wire reactor: (0.2 mmϕ) (b) Helical wire reactor: Helical wire of loop diameter 10 mm, pitch 6 mm and electrode diameter 1.2 mm, was used. Both reactors were used for dry-type as well as for wet-type experiments. In the wet condition, an electronic metering pump (Iwaki EX-C60) was used with a repetition frequency of 120 pulses per second (PPS). Water was supplied with a

flow rate of 84 mℓ/min. in the plasma reactor. Pulse power source used was the same as mentioned in the previous section.

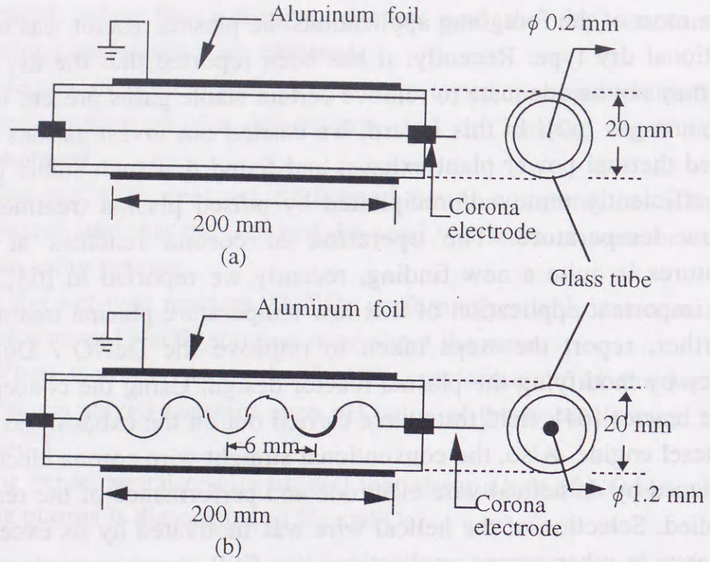

Fig. 3.4.1 Reactors used in the experiment.
(a) Straight wire reactor
(b) Helical wire reactor

3.4.2 Gas flow system and measurements

The paper reports the results of plasma treatment on three types of gaseous mixtures. They are:

1) Diesel engine exhaust for DeNO / DeNOx study: The exhaust gas from a 8 kW diesel engine (Kubota, G-3100S, displacement 855 cm3) was first treated by a fabric filter to remove the soot. A small quantity of the gas was then sampled at a flow rate 2 ℓ /min. and treated by the plasma reactor. Table 3.4.1 shows the gas composition of the diesel engine exhaust. Studies were conducted at or above room temperature.

TABLE 3.4.1 DIESEL ENGINE EXHAUST GAS COMPOSITION
(GAS TEMPERATURE 150-170°C)

NO (ppm)	NO_X (ppm)	O_2 (%)
100~120	110~160	18~18.5
CO (%)	CO_2 (%)	H_2O (vol%)
0.14~0.18	4.1~4.9	3.2~4.4

2) Simulated gas for DeNO / DeNOx study: The gas composition consists of an initial NO concentration of 940 ppm and O_2 (10% vol.). The gas flow rate was varied from 1 to 8 ℓ /min. to observe its effect on the reactor performance. Concentrations of NO and NOx were measured using a chemiluminescence NOx analyzer (Shimadzu NOA-305A). In this paper, NOx concentration indicates the sum of NO and NO_2 concentrations. Studies were conducted at or below room temperature. Table 3.4.2 shows the composition of the simulated gas used for DeNO / DeNOx studies.

TABLE 3.4.2 SIMULATED GAS COMPOSITION FOR DeNO &DeNOx

N2	NO (ppm)	O_2 (%)
Balance gas	940	10

3) Simulated gas for N_2O removal study: The gas composition consists of N_2O with an initial concentration of either 90 or 860 ppm, O_2 (10 % vol.), balance gas N_2, and CO_2 (10% vol) or H_2O. The addition of CO_2 or H_2O was to simulate the exhaust of thermal power plant. The gas flow rate was varied from 1 to 8 ℓ /min. Concentrations of N_2O and by-products were analyzed with a FTIR (Bio-Rad, FTS-30). The studies were conducted only at very low temperatures. Table 3.4.3 shows the composition of the simulated gas.

TABLE 3.4.3 SIMULATED GAS COMPOSITION FOR N2O REMOVAL

N_2	N_2O (ppm)	O_2 (%)
Balance gas	90, 860	10
(CO_2 (%)) or	(H_2O vol%)	
10	1	

During treatment of the diesel engine exhaust gas, the plasma reactor was installed in an oven (Tabai, LC-222) to facilitate control of gas temperature. In low temperature experiments on simulated gas mixtures, the reactor was immersed in a vessel containing either liquid nitrogen (-196 °C) or solid ethanol (-114 °C), as shown in Fig. 3.4.2. The measured gas temperatures were about -150 °C (with liquid N2) and -80 °C (with solid ethanol). A digital thermometer (Custom, CT-1200) having a type-K thermocouple (Custom, LK-700) was used for the measurement. Table. 3.4.4 shows the melting and evaporation points of the gases. Fusing and boiling temperature of NO_2 are -9°C and 21 °C respectively. If NO is oxidized effectively to NO_2 by the plasma treatment, NO_2 can be clustered and removed by cooling the gas.

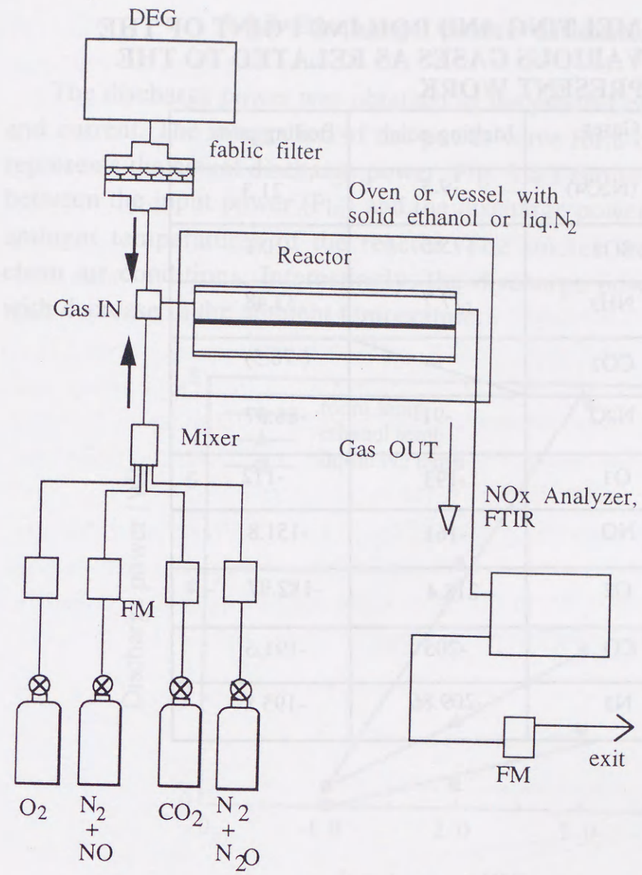

FM -flowmeter (kojima RK1200)
NO_X analyzer(Shimadzu NOA-305A)
DEG - Diesel engine

Fig. 3.4.2 Schematic representation of the experimental set up.

TABLE 3.4.4 MELTING AND BOILING POINT OF THE VARIOUS GASES AS RELATED TO THE PRESENT WORK

Gases	Melting point	Boiling point
NO_2 (N_2O_4)	-9.3	21.3
SO_2	-75.5	-10.1
NH_3	-77.7	-33.48
CO_2		(-78.5)
N_2O	-91	-88.57
O_3	-193	-112
NO	-161	-151.8
O_2	-218.4	-182.97
CO	-205	-191.6
N_2	-209.86	-195.8

3.4.3 Discharge power estimation

The discharge power was obtained as the product of discharge voltage and current. The integration of the power wave form over one full cycle represents the actual discharge power. Fig. 3.4.3 shows the characteristics between the input power (P_{in}) and the discharge power (P_{dis}) for various ambient temperatures of the reactor. The studies were performed for clean air conditions. Interestingly, the discharge power was decreased with decrease in the ambient temperature.

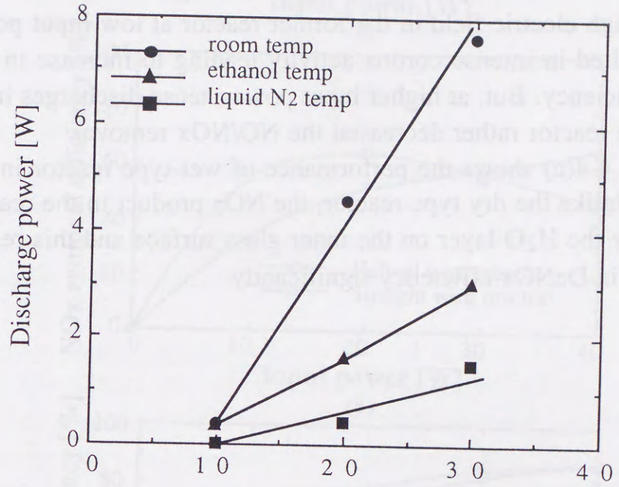

Fig. 3.4.3 Effect of ambient temperature on discharge power of the reactors.

3.4.4 DeNO/DeNOx study on diesel engine exhaust

The exhaust gas was treated both with the dry-type and the wet-type reactors. The sampled gas flow rate was maintained at 2 ℓ/min. (actual gas flow rate was 1500 ℓ/min.) during the studies. The exhaust gas temperature was about 150-200 ˚C and the sampled gas temperature was maintained at 150 ˚C while treating it with pulsed plasma. The pulse frequency was 240 pps. Input power was varied upto 40 W. The gas retention time in the reactor was 1.9 sec. Figs. 3.4.4(a-c) present the DeNO / DeNOx efficiency for the helical wire and the straight wire

corona electrodes as a function of input power. Figs. 3.4.4(a), (b) correspond to dry-type plasma reactors and Fig. 3.4.4(c), to wet-type plasma reactor. As seen from Fig. 3.4.4(a), both the corona electrodes, helical wire and straight wire, exhibited similar characteristics in the NO removal efficiency. However, in NOx removal, helical wire electrode performed better giving a maximum DeNOx efficiency of about 60% for an input power of 10 W (as against 40 W for 60% efficiency in straight wire case). One possible explanation for this behavior could be that in the helical wire case, the discharge gap (that between the wire and inner glass surface) was short compared to that with straight wire electrode. This results in high electric field in the former reactor at low input power and hence, resulted in intense corona activity leading to increase in DeNO / DeNOx efficiency. But, at higher input power, tense discharges inside the helical wire reactor rather decreased the NO/NOx removal.

Fig. 3.4.4(c) shows the performance of wet-type reactor in DeNOx at 150°C. Unlike the dry type reactor, the NO_2 product in the reactor was absorbed by the H_2O layer on the inner glass surface and this resulted in an increase in DeNOx efficiency significantly.

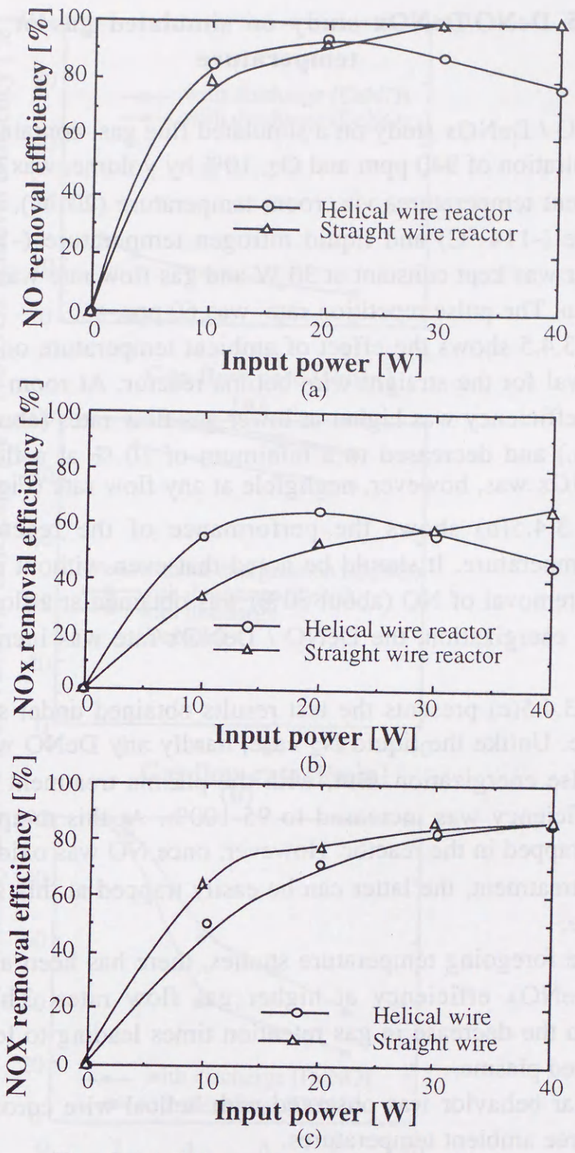

Fig. 3.4.4 Effect of corona electrodes on NO / NOx removal efficiency at different operating conditions (diesel engine exhaust).

(a) gas temp : 150°C , dry reactor (DeNO)
(b) gas temp : 150°C , dry reactor (DeNOx)
(c) gas temp : 150°C , wet reactor (DeNOx)

3.4.5 DeNO/DeNOx study on simulated gas at very low temperature

DeNO / DeNOx study on a simulated flue gas, containing an initial NO concentration of 940 ppm and O_2, 10% by volume, was carried out at three ambient temperatures viz. room temperature (20 °C), solid ethanol temperature (-114 °C) and liquid nitrogen temperature (-196 °C). The input power was kept constant at 30 W and gas flow rate was varied from 1 to 8 l /min. The pulse repetition rate was 60 pps.

Fig. 3.4.5 shows the effect of ambient temperature on the NO and NOx removal for the straight wire corona reactor. At room temperature, the DeNO efficiency was higher at lower gas flow rates (about 30 % at 1 to 2 l /min.) and decreased to a minimum of 10 % at a flow rate of 8 ℓ/min. DeNOx was, however, negligible at any flow rate (Fig. 3.4.5(a)).

Fig. 3.4.5(b) shows the performance of the reactor at liquid nitrogen temperature. It should be noted that even without energization, significant removal of NO (about 80%) was obtained at a flow rate of 2 l /min. With energization, the DeNO / DeNOx rate was increased to 95-100%.

Fig. 3.4.5(c) presents the test results obtained under solid ethanol temperature. Unlike the liquid N_2 case, hardly any DeNO was observed without pulse energization. But, with the plasma treatment the DeNO / DeNOx efficiency was increased to 95-100%. At this temperature, NO cannot be trapped in the reactor. However, once NO was oxidized to NO_2 by plasma treatment, the latter can be easily trapped at this solid ethanol temperature.

In the foregoing temperature studies, there has been a decrease of DeNO / DeNOx efficiency at higher gas flow rates. This could be attributed to the decrease in gas retention times leading to less exposure time to pulsed plasma.

Similar behavior was observed with helical wire corona electrode at all the three ambient temperatures.

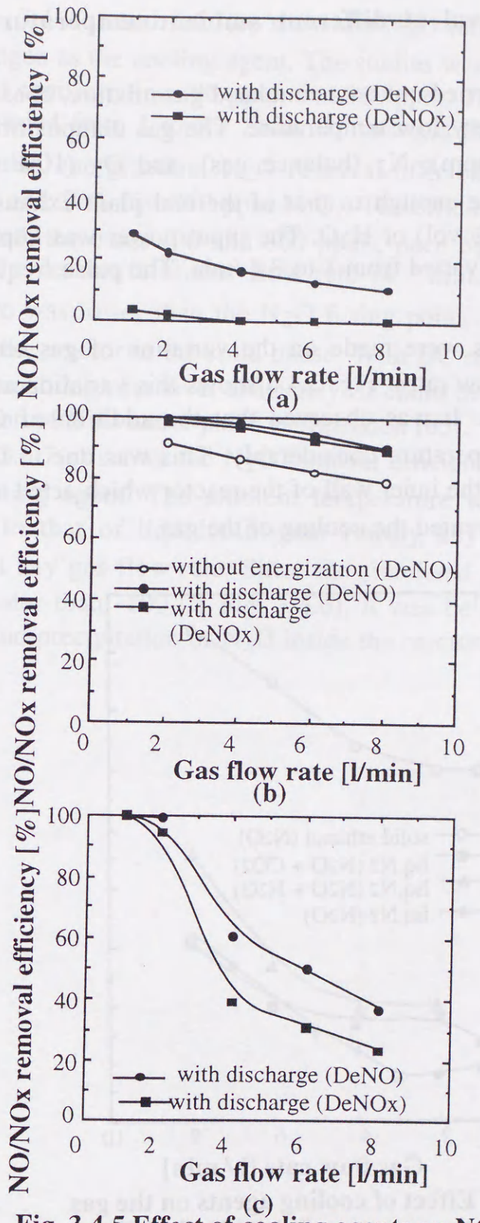

Fig. 3.4.5 Effect of cooling agents on NO/NOx removal efficiency with straight wire corona electrode.
(simulated flue gas).
(a) at room temp. ; (b) at liq.N2 temp.
(c) at solid ethanol temp.;

3.4.6 N_2O removal at different ambient temperatures

Studies were carried out on a simulated gas mixture, consisting of a stable N_2O gas, at very low temperature. The gas composition include N_2O (860 ppm/90 ppm), N_2 (balance gas), and O_2 (10% vol). The composition was close enough to that of thermal plant exhaust with an addition of CO_2 (10% vol) or H_2O. The input power was kept at 30 W and gas flow rate was varied from 1 to 8 ℓ /min. The pulse frequency was 60 pps.

Initially, studies were made on the variation of gas temperature with respect to gas flow rates. Fig. 3.4.6 shows this variation at different ambient temperatures. It was observed that the addition of CO_2/H_2O increases the gas temperature considerably. This was due to the frozen layer of CO_2/H_2O on the inner wall of the reactor which acted as thermal insulator and thus prevented the cooling of the gas.

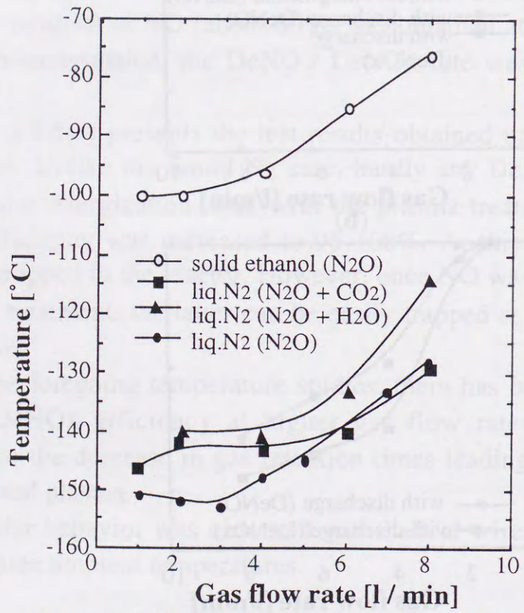

Fig. 3.4.6 Effect of cooling agents on the gas temperature (initial N_2O: 860 ppm).

Figs. 3.4.7(a) and 3.4.7(b) show the N_2O removal efficiency with liquid nitrogen as the cooling agent. The studies were conducted with two N_2O initial concentrations 90 ppm, and 860 ppm. The simulated gas flow rate was varied from 1 to 8 ℓ /min. Up to a gas flow rate of 4 ℓ /min., without pulse energization, N_2O removal efficiency was 70% (for 90 ppm N_2O) and 50% (for 860 ppm N_2O). The efficiency was increased to 90% for both the cases (90 and 860 ppm), once pulse energization was applied. The reason is at this flow rate (4 ℓ/min.) the simulated gas temperature was lower than the N_2O fusing point, and hence, N_2O was trapped in the reactor in the solid phase. With DC energization, we could not obtain such high removal efficiency. It could be due to the enhanced clusterization of N_2O under pulse energization [65].

Fig. 3.4.7(c) shows the N_2O removal efficiency with solid ethanol as the cooling agent. The ambient temperature was relatively higher compared to that of liquid nitrogen. Hardly any N_2O removal was observed at any gas flow rate. Since the simulated gas temperature was always greater than -100°C(Fig. 3.4.6), it was believed that there was practically no precipitation of N_2O inside the reactor.

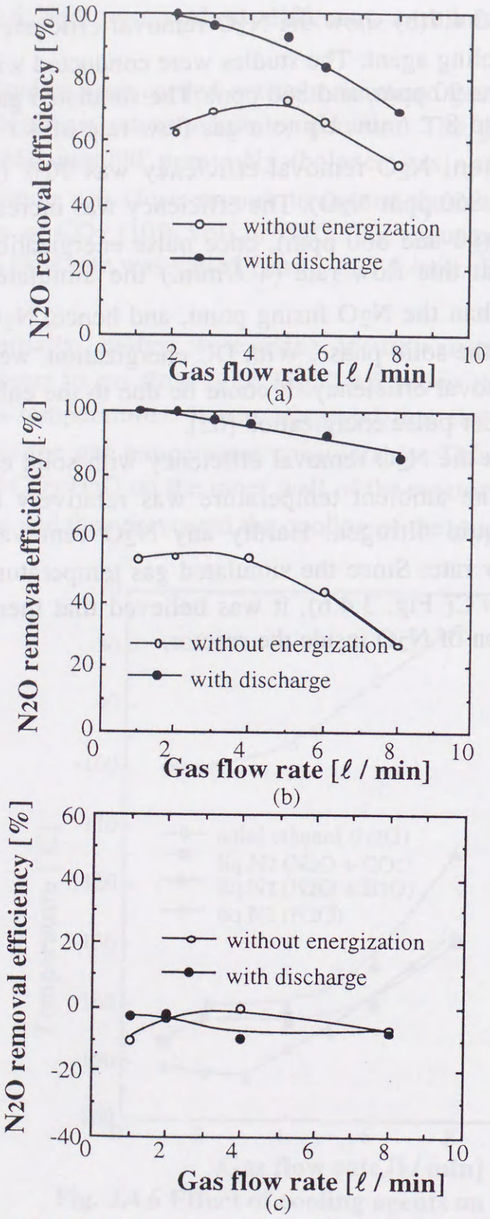

Fig. 3.4.7 N_2O removal efficiency at very low temperatures with straight wire corona electrode (without additives).
(a) cooling agent: liq.N_2 (b) cooling agent: liq.N_2
Initial N_2O: 860 ppm Initial N_2O: 90 ppm
(c) cooling agent: solid ethanol
Initial N_2O: 860 ppm

There was no improvement in the N_2O removal efficiency, when CO_2 / H_2O was added to the simulated gas, as shown by Fig. 3.4.8(a) and Fig. 3.4.8(b). N_2O removal efficiency, at higher gas flow rates, was higher than that without CO_2 / H_2O. The formation of layer of frozen CO_2 / H_2O inside the reactor wall, kept the gas temperature greater than the fusing point of N_2O (-91°C) and thus affected the removal efficiency.

The foregoing N_2O removal studies were reported for straight wire reactor. Similar results were observed with the helical wire reactor.

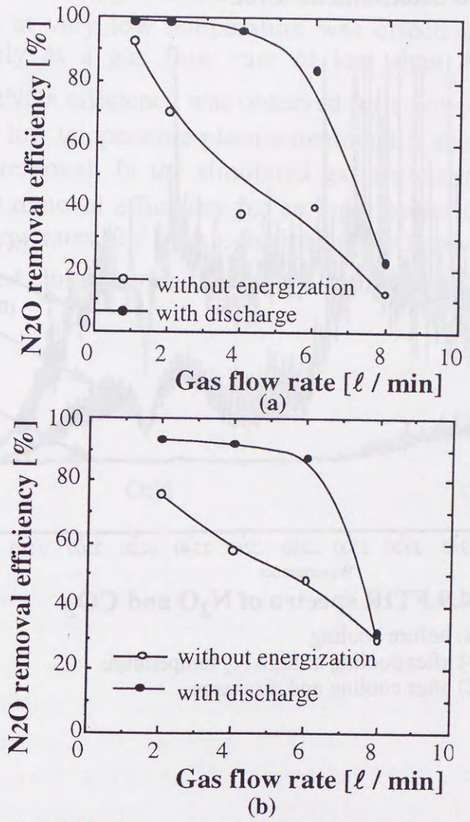

Fig. 3.4.8 N_2O removal efficiency at liquid N_2 temperature with straight wire corona electrode: effect of additives.
(a) initial N_2O (860 ppm) + H_2O
(b) initial N_2O (860 ppm) + CO_2

Fig. 3.4.9 shows the N_2O spectra analysis by FTIR. The simulated gas flow rate was 2 ℓ/min. Initial N_2O concentration was 790 ppm. CO_2 and O_2 concentrations were 10% by volume respectively. In the figure, spectrum-A corresponds to pre-gas treatment condition and spectrum-B, that after cooling with liquid nitrogen but no plasma treatment. As seen from the spectrum-B, the N_2O concentration was decreased to 240 ppm. Spectrum-C was obtained after the gas was cooled and pulse energization applied (input power = 30 W). The N_2O concentration was significantly reduced to 6 ppm. Also, there was a decrease in CO_2 but no quantitative measurement was done to determine its level.

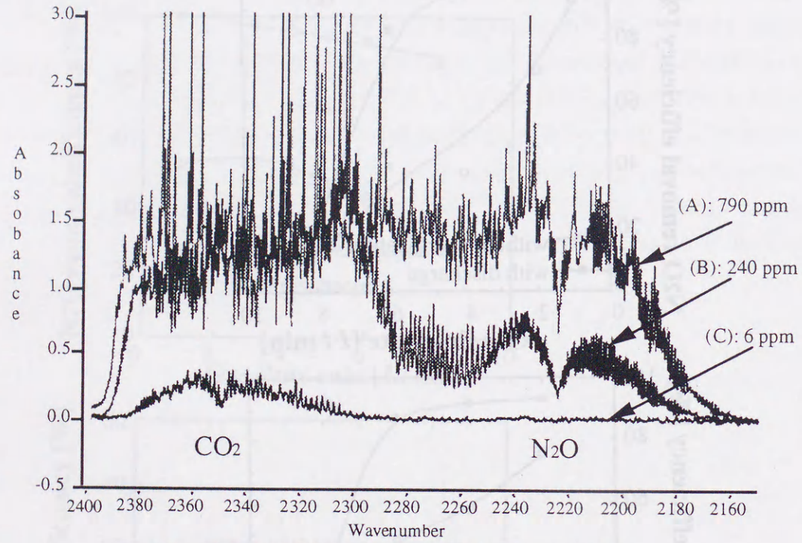

Fig. 3.4.9 FTIR spectra of N_2O and CO_2.

(A) before cooling
(B) after cooling at liqid N_2 temperature
(C) after cooling and discharge

3.4.7 Main inference

Studies were conducted on diesel engine exhaust gas using non-thermal plasma with dry type and wet type reactors. Further, plasma treatment was carried out on simulated gas mixtures, with the aim of removing NOx and N_2O, at very low temperature. The following conclusions were drawn from the studies conducted:

-Treatment of diesel engine exhaust in wet type plasma reactor resulted in 70% DeNOx efficiency at 150°C.

-In simulated gas treatment study for DeNO / DeNOx, the plasma treatment at very low temperature was effective for DeNO / DeNOx, particularly at a gas flow rate of less than 4 ℓ/min. About 90% DeNO/DeNOx efficiency was observed for a power input as low as 10 W.

-The low temperature plasma treatment is shown to be very effective for N_2O removal. In the simulated gas flow studies, we observed 95-99% N_2O removal efficiency for an input power of 30 W, particularly at low gas flow rates (2 ℓ /min.). Such high N_2O removal efficiency was due to enhanced clusterization of N_2O molecules in the pulse discharge.

3.5 NOx removal with O_3 injection

Effect of ozone injection during flue gas treatment has been studied recently [66]. However, not much work has been reported about the effect of ozone addition for treating small exhaust gas source i.e. diesel powered vehicle or co-generation system with diesel engines etc. A comparative study between plasma treatment [67] and ozone injection, to obtain fundamental data for ozone injection effect, is reported in this section.

3.5.1 Experimental apparatus

Fig. 3.5.1(a) shows the prototype ozonizer consisting of glass dielectric tube having an ID of 5 mm and OD of 7 mm. A stainless steel wire, acting as a discharge electrode, was suspended concentric to the tube. An aluminum foil was wrapped around the glass tube as a ground electrode. The effective reactor length was 300 mm. The reactor was surrounded by ice and thus, maintained at low temperature so as to absorb the heat produced during ozone production.

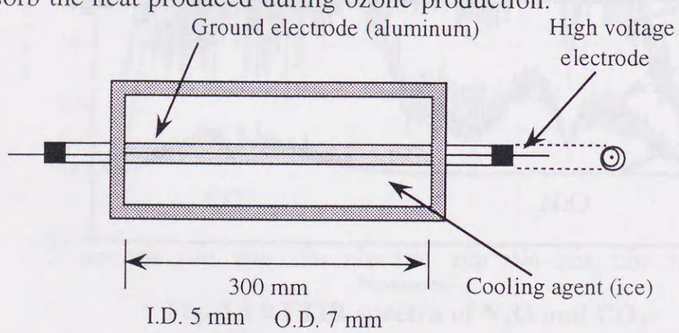

Fig. 3.5.1(a) Concentric type ozonizer.

Fig. 3.5.1(b) shows the gas flow system for the ozone injection experiment. Ozone from the ozonizer was introduced to the dry or wet type plasma reactor. The plasma reactor was fixed into the oven (Tabai, LC-222) to keep the gas temperature 150 °C. Material gas for ozone generation was either dry air or oxygen. High frequency inverted neon transformer (Sanyo, slight-10, 18 kHz) was used as a power source. Ozone concentration was measured with ozone monitor (Ebara, EG-2001) and NOx concentration was measured with NOx analyzer (Shimadzu, NOA-305A). NOx concentration was the sum of that of NO and NO_2. When NOx and ozone were existing simultaneously, error may

occur in the measured value. But, a careful analysis of the sample output gas with FT-IR (Bio-rad, FTS-30) indicated the absence of any such error.

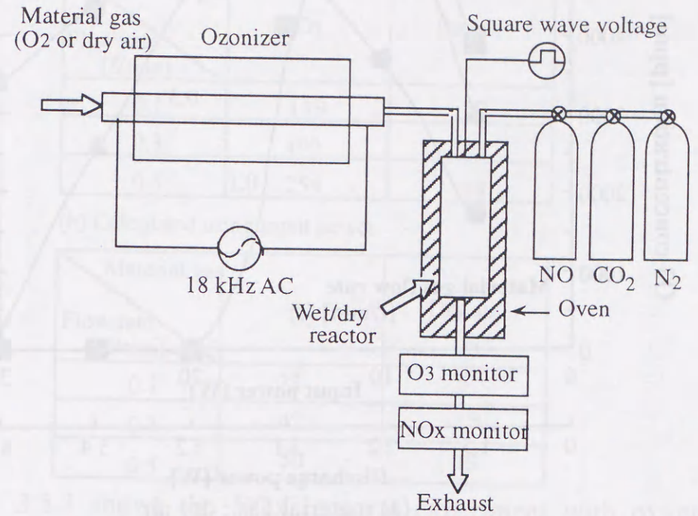

Fig.3.5.1(b) Schematic diagram of gas flow system.

3.5.2 Results obtained with dry plasma reactor

Material gas flow rate (for the ozonizer) was varied from 0.1 to 0.5 ℓ/min. The simulated gas consists of room air (8 ℓ/min.), CO_2 (1 ℓ/min.), and N_2 (0.5 to 0.9) ℓ/min. and was mixed with ozonizer output before introducing the whole mixture into the plasma reactor. Total gas flow rate was maintained at 10 ℓ/min. Variation of ozone concentration against input power was shown in the Fig. 3.5.2 for dry air case. Maximum ozone concentration of 6000 ppm was obtained at an input power of 10~20 W (equivalent discharge power of 2~5 W). The material gas flow rate was 0.1 ℓ/min. At higher input power the ozone concentration was decreased to almost zero ppm. Similar trend was seen at other material gas flow rates. This would be caused by the electrode heat, which dissolving the generated ozone greatly. With oxygen as the material gas, there was no decrease in ozone concentration at any input power. The ozone yield was shown in Table 3.5.1. When oxygen was used as material gas, ozone yield was 6 to 8 times that with dry air case.

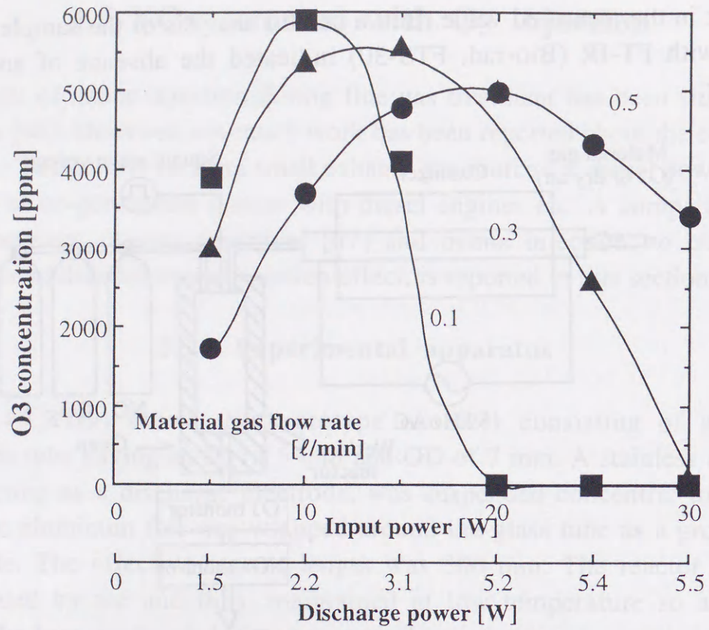

(a) material gas : dry air

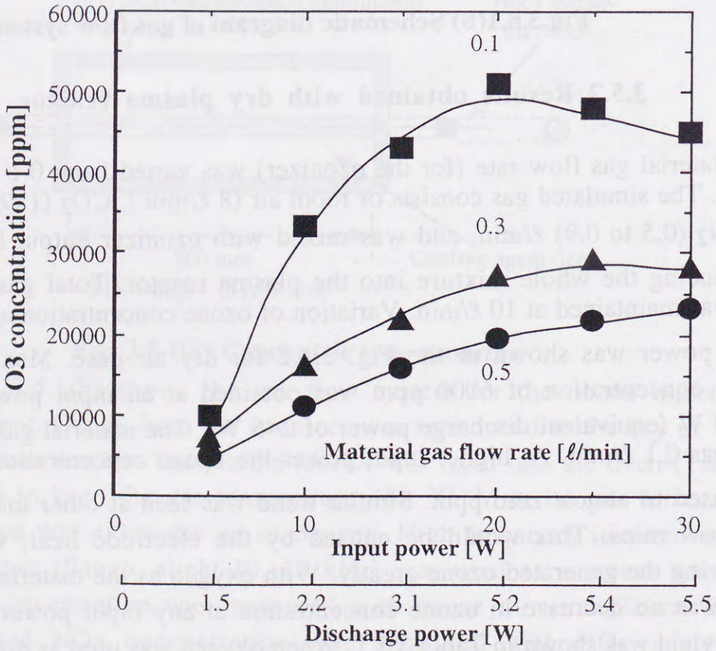

(b) material gas : oxygen

Fig. 3.5.2 O3 concentration characteristics

TABLE 3.5.1 OZONE YIELD FOR VARIOUS MATERIAL GAS FLOW RATES [O3 g/kWh]

(a) Calculated using discharge power

Material gas / Flow rate [ℓ/min]	O_2	Dry air
0.1	119	32
0.3	199	65
0.5	254	94

(b) Calculated using input power

Material gas / Flow rate [ℓ/min]	O_2	Dry air
0.1	28	6
0.3	42	15
0.5	50	18

Fig. 3.5.3 shows the NOx removal experiment with oxygen as material gas. NO initial concentration was 200 ppm. Total gas flow rate was 10 ℓ/min., gas temperature was 150 °C. NO was almost removed at any ozonizer material gas flow rate. 80% NOx removal efficiency was obtained for input power above 10 W.

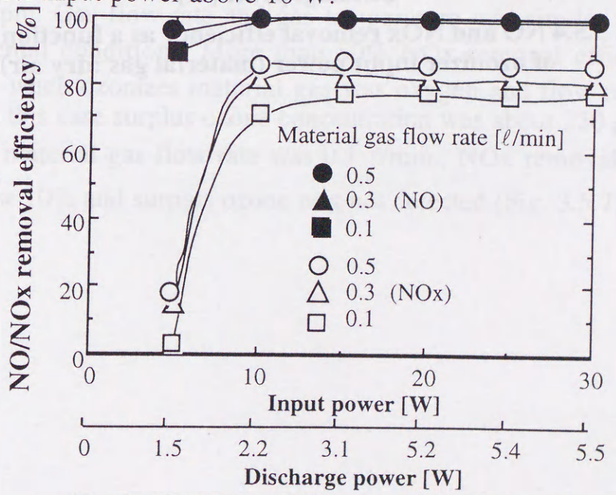

Fig.3.5.3 NO and NOx removal efficiency as a function of ozonizer input power (material gas : oxygen, initial NO concentration ; 200 ppm).

Fig. 3.5.4 shows the NOx removal efficiency with dry air as material gas. Experimental condition was same as the previous experiment. NO removal efficiency was 30, 60, and 90% corresponding to a material gas flow rate of 0.1, 0.3, and 0.5 ℓ/min. NO was oxidized and removed. The removed concentration was about 60, 120, and 180 ppm, respectively. The corresponding ozone concentrations were 60, 150, and 250 ppm, respectively. This means, the generated ozone concentration decides the oxidized NO concentrations.

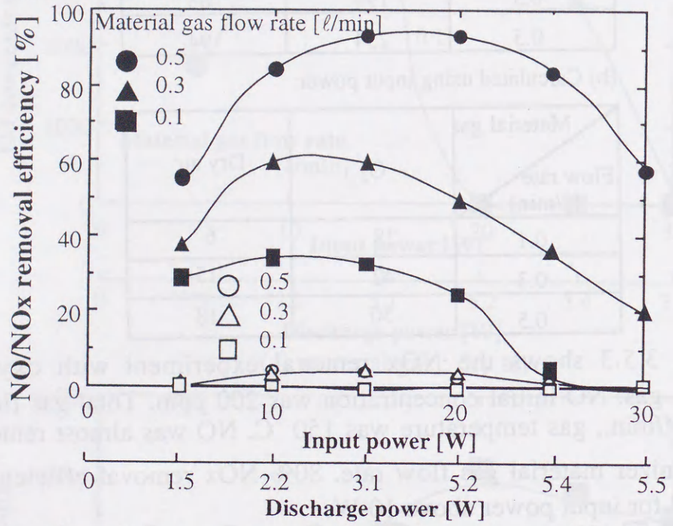

Fig. 3.5.4 NO and NOx removal efficiency as a function of ozonizer input power (material gas :dry air).

When oxygen was used as material gas (Fig. 3.5.3), surplus ozone production was confirmed as shown in Fig. 3.5.5. In this case more than 800 ppm ozone was present and it indicates that higher NO concentration could be treated with this ozonizer using oxygen material gas.

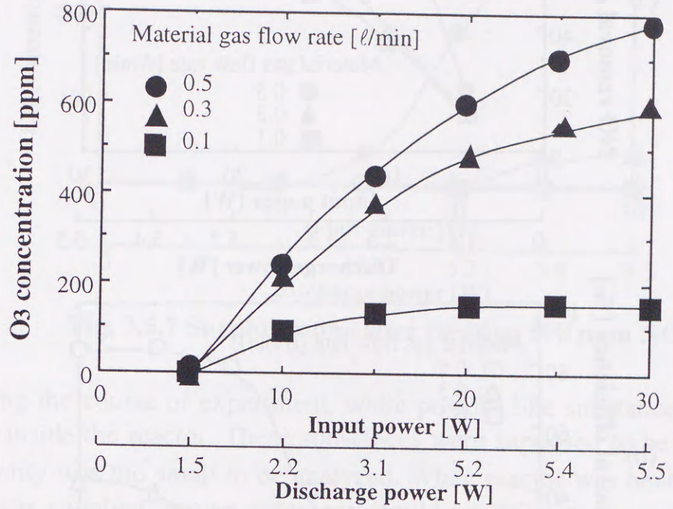

Fig. 3.5.5 Surplus ozone after treating 200 ppm NO.

Fig. 3.5.6 shows NOx removal efficiency for initial NO concentration of 500 ppm. Gas flow rate and gas temperature was similar to previous experimental conditions. More than 80% NOx removal efficiency was achieved when ozonizer material gas was oxygen and flow rate was 0.5 ℓ/min. In this case surplus ozone concentration was about 350 ppm. When ozonizer material gas flow rate was 0.1 ℓ/min., NOx removal efficiency was below 10% and surplus ozone was not detected (Fig. 3.5.7).

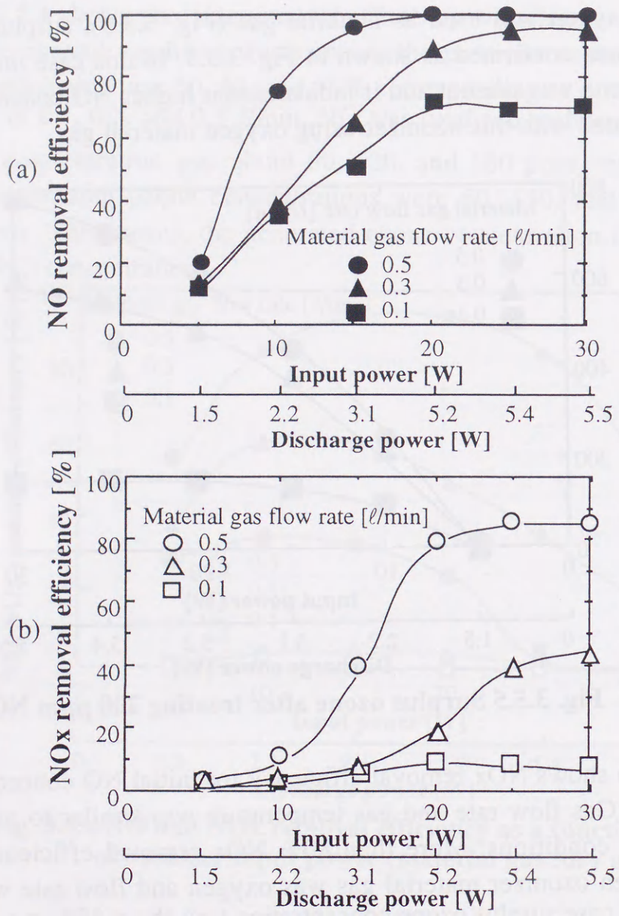

Fig. 3.5.6 NO(a) and NOx(b) removal efficiency as a function of ozonizer input power
(material gas : oxygen,initial NO concentration : 500 ppm).

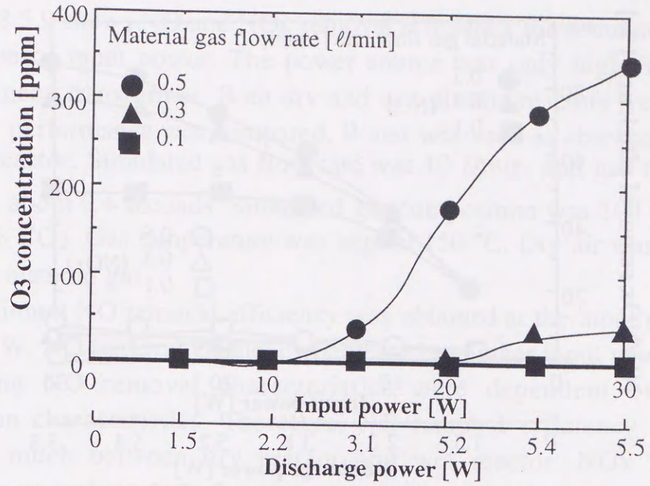

Fig. 3.5.7 Surplus ozone after treating 500 ppm NO.

During the course of experiment, white powder like substances were detected inside the reactor. These substances were supposed to be N_2O_5. The quantity was too small to be analyzed. When reactor was heated and dry air was supplied, brown color gas (could be NO_2) was confirmed. This gas was generated by N_2O_5 sublimation.

NOx removal results were shown in Fig. 3.5.8 for the NO initial concentration of 1000 ppm. Gas flow rate and gas temperature were maintained as before. Oxygen was used as ozonizer material gas. NO removal efficiency of 80% was achieved for material gas flow rate of 0.5 ℓ/min. However, NOx removal efficiency was below 10%. No surplus ozone concentration was confirmed, and this result suggested that even when oxygen is used as ozonizer material gas, NO or NOx removal efficiency will be decreased for high initial NO concentration.

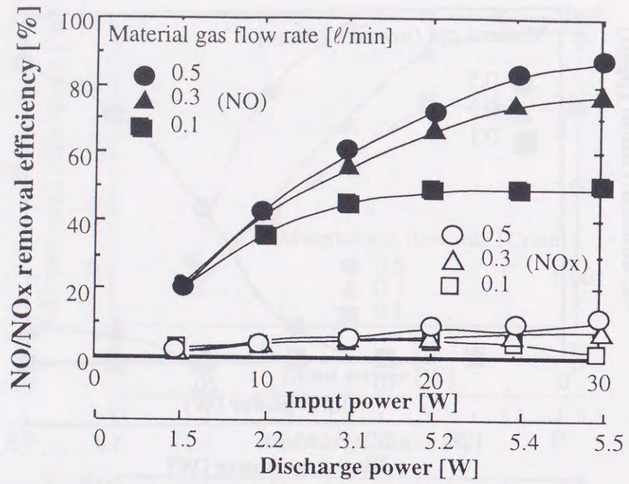

Fig. 3.5.8 NO and NOx removal efficiency as a function of ozonizer input power.
(material gas: oxygen, initial NO concentration : 1000 ppm).

3.5.3 Results obtained with wet plasma reactor

The experimental set up for the wet plasma reactor was described in in section 3.3.1 and that for ozonizer, in section 3.5.1. Only results have been shown here.

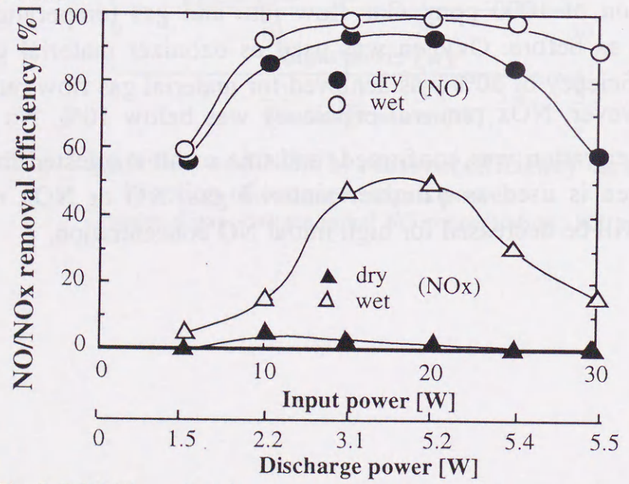

Fig.3.5.9 NO and NOx removal efficiency for simulated gas using ozonizer fed by dry air.

Fig. 3.5.9 shows NO and NOx removal efficiency for simulated gas as a function of input power. The power source was only high frequency inverted neon transformer. Both dry and wet plasma reactors were tested and their performance was compared. Water was used as absorbent liquid for wet reactor. Simulated gas flow rate was 10 ℓ/min. and gas residence time was about 0.4 seconds. Simulated gas composition was 200 ppm NO and, 10% CO_2. Gas temperature was kept at 150 °C. Dry air was used as ozonizer material gas.

Maximum NO removal efficiency was obtained at the input power of 15 to 20 W. NO removal efficiency decreased at higher input power. This interesting NO removal characteristics were dependent on ozone generation characteristics. Therefore, NO removal efficiency was not changed much between dry reactor and wet reactor. NOx removal efficiency was about 50% for wet reactor. However, in dry reactor case hardly any NOx removal was observed. This is due to the fact that NO_2 absorbance were not occurred in the dry reactor.

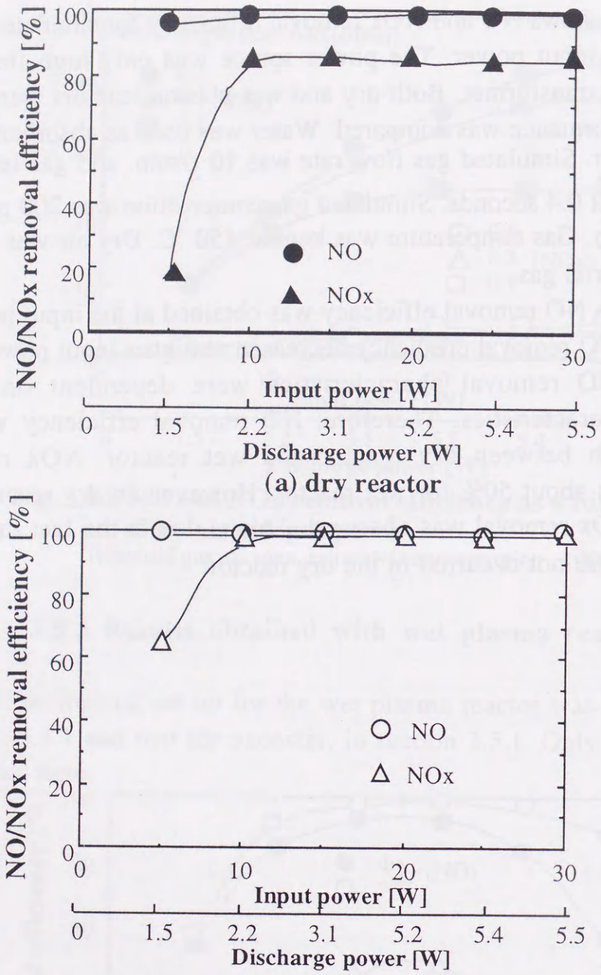

Fig. 3.5.10 NO and NOx removal efficiency using oxygen as material gas for ozonizer.

Fig. 3.5.10 shows the NO, NOx removal efficiency with ozone injection using oxygen as material gas (flow rate 0.5 ℓ/min.) for ozonizer. The simulated gas compositions and experimental conditions were similar to the previous experiment.

Fig. 3.5.10(a) shows dry reactor results and Fig. 3.5.10(b), that of wet reactor. Using oxygen as ozonizer material gas, ozone concentration was high enough to treat NO initial concentration of 200 ppm. Both dry and wet reactors successfully treated the NO in this simulated gas. DeNOx was about 100% for wet reactor and 80% for dry reactor.

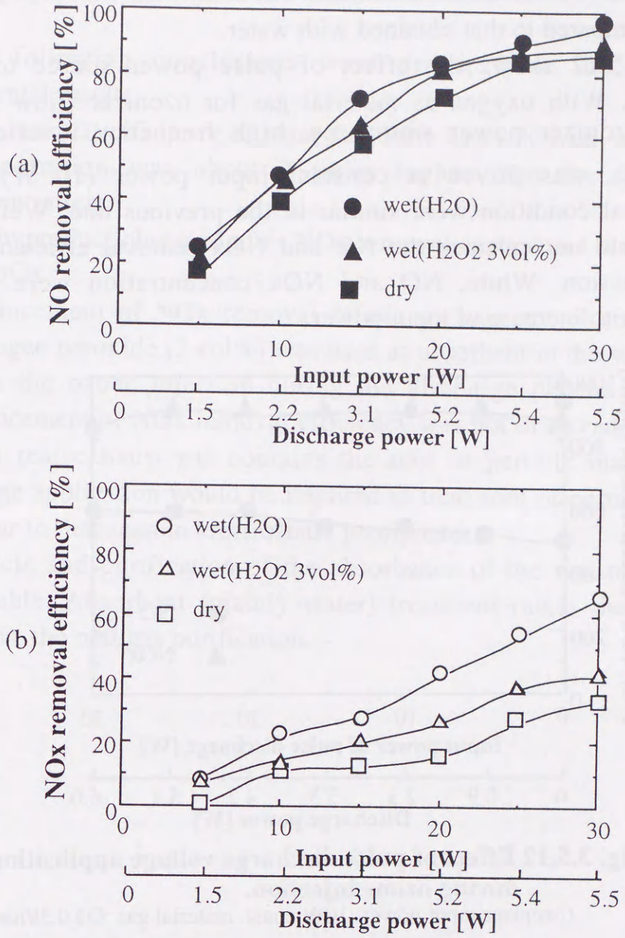

Fig.3.5.11 Effect of absorbent on NO(a) and NOx(b) removal efficiency.

Fig. 3.5.11(a) and (b) shows NO and NOx removal efficiencies for different absorbents. Water and H_2O_2 were used as the main absorbents. The simulated gas composition was maintained similar to the previous experiment except initial NO concentration was 1000 ppm. When alkaline absorbent was used, no absorbance enhancement was observed as mentioned in section 3.3.5.

When H_2O_2 (3 vol%), which is having a high oxidizing effect, was used as absorbent and with oxygen as material ozonizer gas, NOx removal for dry and wet reactors were respectively 30 and 70%.

However, no absorbance enhancement was confirmed with H_2O_2 3 vol% solution compared to that obtained with water.

Fig. 3.5.12 shows the effect of pulse power source to ozone production. With oxygen as material gas for ozonizer (flow rate 0.3 ℓ/min.), ozonizer power source i.e. high frequency inverted neon transformer, was driven at constant input power (10 W). Other experimental condition were similar to the previous one. Wet plasma reactor could not enhance the NO and NOx removal efficiency with ozone injection. While, NO and NOx concentration were slightly increased with increase of input power.

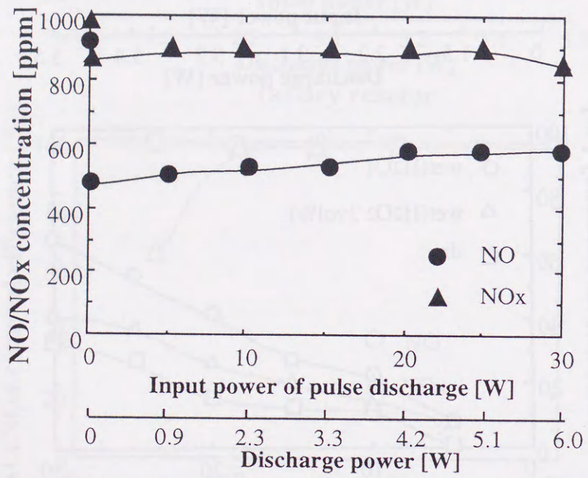

Fig. 3.5.12 Effect of pulse discharge voltage application during ozone injection.
(ozonizer input power :10W const. material gas :O2 0.3l/min)

3.5.4 Main inferences

The following conclusions were drawn from the foregoing experimental results.

(1) NOx removal efficiency of more than 80% was achieved, when ozone concentration was about 2 times higher than the NO initial concentration.
(2) The byproduct observed after NOx removal experiment was found to be N_2O_5.
(3) Enhancement of NOx removal efficiency was not observed when hydrogen peroxide (3 vol%) was used as absorbent in the wet reactor.
(4) With the ozone injection during the discharge plasma treatment, enhancement of NOx removal efficiency was not observed. However, when real exhaust gas contains the soot or particle matter, pulse voltage application would be required to treat soot or particle matter, similar to that seen in electrostatic precipitators.
(5) Recycle and purification of the absorbance of the wet reactor was desirable. Absorbent (mainly water) treatment raises the hopes to achieve the real gas purification.

3.6 Cigarette smoke removal using pulsed discharge plasma

Room air can be polluted by cigarette smoke which contains various poisonous gases including NH_3. Animal farms can also emit ammonia. It has unpleasant odour, unhygienic and should be removed together with other pollutants like NO_X, SO_X, particles etc.

However, there has been very little work done to evaluate the performance of plasma discharge reactors or to optimize parameters when it comes to household use that requires city air cleaning having low concentration of pollutants. Because of greater public awareness of the danger associated with inhaling polluted air, there may be a great demand for such simple pollution control devices in ordinary households, perhaps, to handle much less concentration of the above mentioned pollutants than the industry.

In this section, using a simulated gas mixture, the performance of a streamer corona plasma reactor consisting of a coaxial wire to cylinder electrode geometry has been studied. The initial concentration of the pollutant gases has been set low, in the range 10 - 40ppm. The residence time has been varied in the range 0.6 - 2.4s. The reactor performance has been studied for dry and semi-wet conditions and the results compared.

There has been some work already on wet reactors that show better performance in removal of NO_X compared to dry reactors as shown in section 3.3, 3.4, and 3.5. Here, a different version of wet reactor has been employed and its performance in lightly polluted air containing NO, NH_3 and submicron particles have been studied.

The main study has been carried out using a positive square pulse produced by a rotating pulse generator. However, in order to compare the effectiveness of other type of voltages, some experiments have also been done with 60Hz and 18 kHz alternating voltage applications.

3.6.1 Experimental procedure

NO and NH_3 contents in the gas mixture were adjusted by controlling the flow rate of air and premixed constituent NO and NH_3 gases. The premixed gas cylinders were supplied with about 1000 ppm of NH_3 or NO in air. This mixture was further diluted by dry air to give the pollutant gas content in the final mixture any desired value in the range

10~40 ppm. Normally, the outlet pressure of the regulators of the gas cylinders was adjusted to ~ 0.5 kg/cm^2. The gas pressure inside the reactor was slightly above the atmospheric pressure and no attempt has been made to heat or cool the reactor externally. The room temperature varied in the range of 10~ 25°C.

The gases from the two cylinders were mixed and then fed into the reactor where a streamer corona discharge was initiated. The current and the voltage of the pulses were recorded. Also, the input power to the high voltage transformer was measured. The outgoing gas from the reactor passes through a NO_X detector or, it was desired, diverted for analysis by a gas chromatography. NH_3 and its discharge products were analyzed by FTIR as described above.

In case of particle experiment, an incense was used as a particle source. Air containing particles was drawn in through the semi-wet reactor by a pump. Voltage was applied in the same way as before and the performance of the reactor was studied by recording the particle counter.

3.6.2 Removal of NO_X

1) Features of NO_X reduction: Fig. 3.6.1 presents the variation of input power with voltage for pulse applications. This power, measured by the power meter (Yokogawa, 2534) consisted of the power input into the discharge and the losses in the electrical circuit. To estimate the power going into the discharge the input power to two identical reactors, connected in parallel, was measured. Power input is noted again after removing one of the reactors. The discharge power was calculated by taking the difference of the two power readings, assuming that the losses remain constant and depend only on the applied voltage. In the semi-wet reactor, the input power was higher than that of the dry reactor. This is due to the increase in the capacitance of the reactor having a conductive layer. The relation between the power going into the discharge and the pulse amplitude is shown in Fig. 3.6.2 for the dry and the semi-wet reactors.

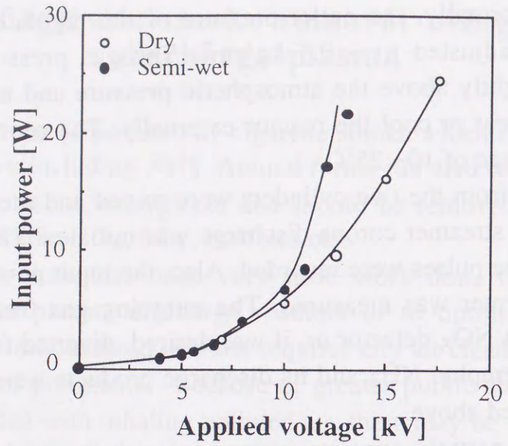

Fig. 3.6.1 Variation of input power with pulse voltage amplitude.

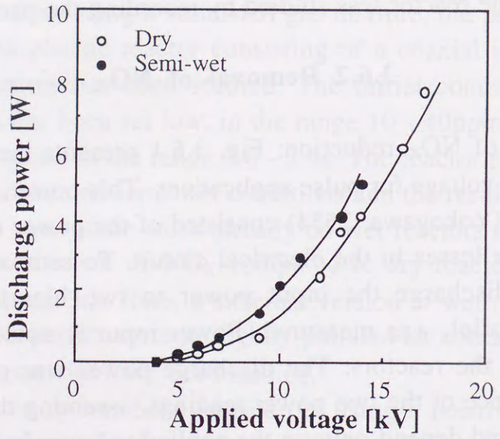

Fig. 3.6.2 Variation of discharge power with applied voltage.
frequency of pulse voltage : 250Hz

Fig. 3.6.3 and 3.6.4 summarize the results on NO reduction for different initial gas concentrations of the gas in a mixture of air and NO in the dry reactor. As mentioned earlier, the study concentrates on very dilute mixtures of NO in air. The effect of residence time is also presented in these figures.

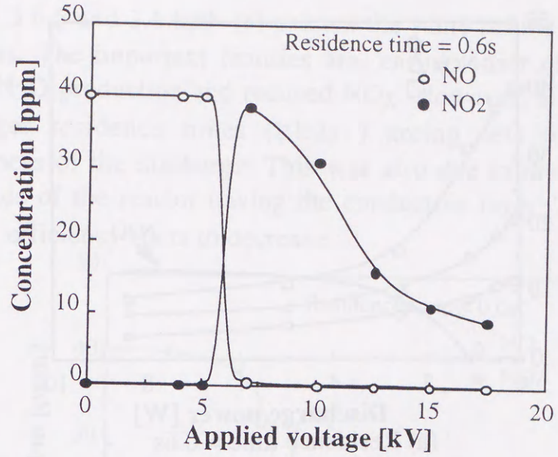

Fig. 3.6.3 Typical variation of NO and NO_2 concentration with the pulse voltage in a dry reactor.

Fig. 3.6.3 depicts the variation of NO and the formation of NO_2 with pulse amplitude. The initial NO concentration in this case was 40 ppm. This is representative of the type of variation seen in all other cases. It can be seen that NO reduction starts at about 5 kV. The reduction rate was very sharp with increasing voltage. However, this was accompanied by rapid increase in NO_2 production. NO_2 also decreased with further increase in applied voltage, thus enabling effective reduction in NO_X level. From Fig. 3.6.4(a)~(c), it appears that the removal efficiency of NO_X at high voltage and relatively high power was, generally, higher for longer residence time. However, N_2O production was less for shorter residence time. The power going into the discharge appears to be quite low and usually less than 10 W.

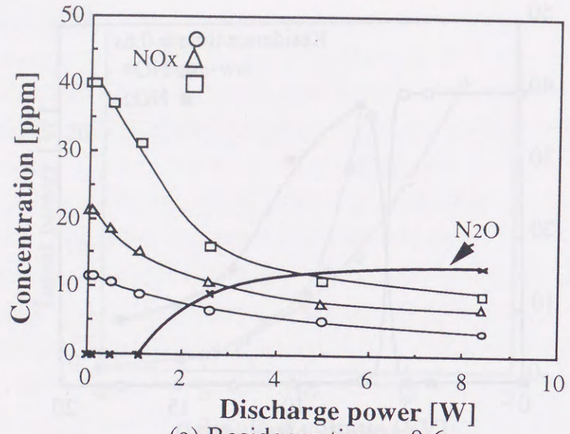

(a) Residence time = 0.6s

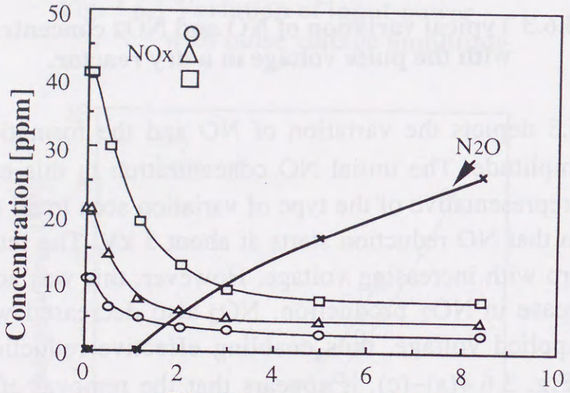

(b) Residence time = 1.2s

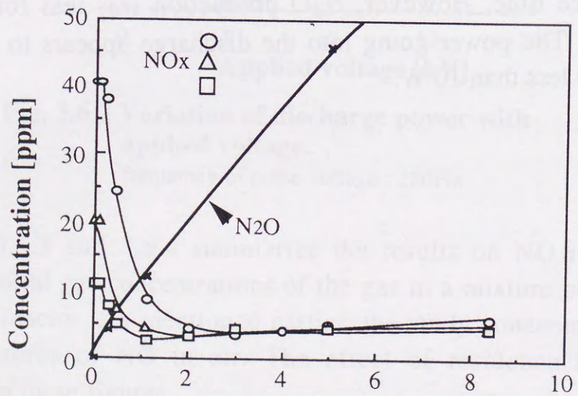

(c) Residence time = 2.4s

Fig. 3.6.4 NOx and N2O concentration with discharge power for different residence time in a dry reactor.

Fig. 3.6.5 and 3.6.6(a)~(c) present the same results under semi-wet conditions. The important features are, earlier onset of the discharge, reduced N_2O production and reduced NO_X. However, at higher voltages and longer residence times (≥1.2s) arcing sets in reducing the effectiveness of the discharge. This was also due to the increase in the capacitance of the reactor having the conductive layer. Therefore, NO_X reduction efficiency starts to decrease.

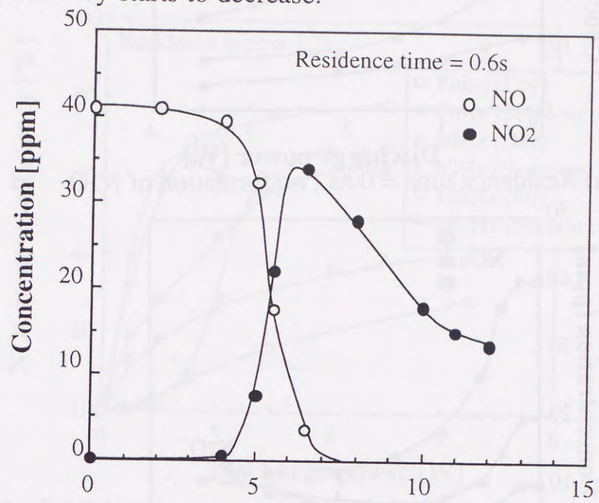

Fig. 3.6.5 Typical variation of NO and NO2 concentration with the pulse voltage in a semi-wet reactor.

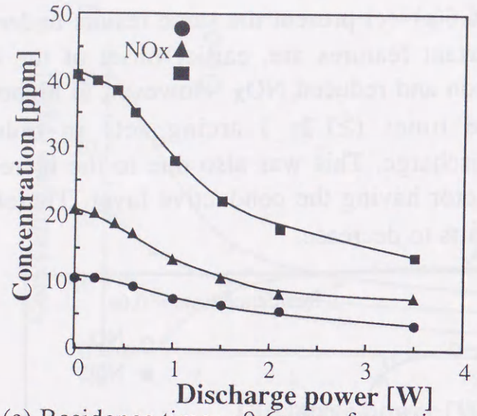

(a) Residence time = 0.6s ; no formation of N2O

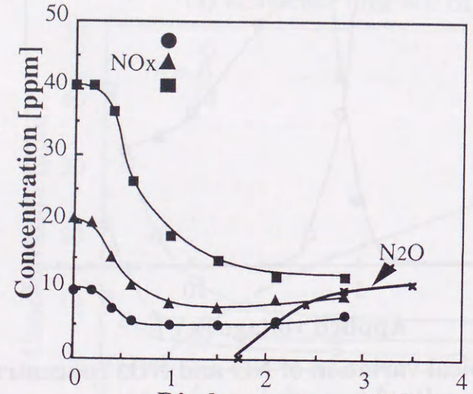

(b) Residence time = 1.2s

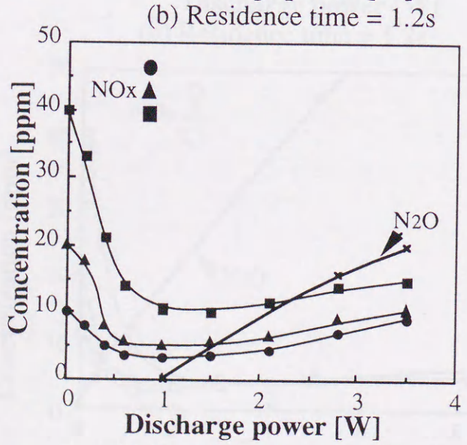

(c) Residence time = 2.4s

Fig. 3.6.6 NOx and N2O concentration with discharge power for different residence time in a semi-wet reactor.

2) Effect of the type of voltage: In the present work, positive polarity rectangular pulses were mainly used. This was done in view of an earlier work [68] that showed high efficiency for NO_X removal with a similar type of voltages. In order to compare the NO_X removal efficiencies, different type of applied voltages were also used in some cases.

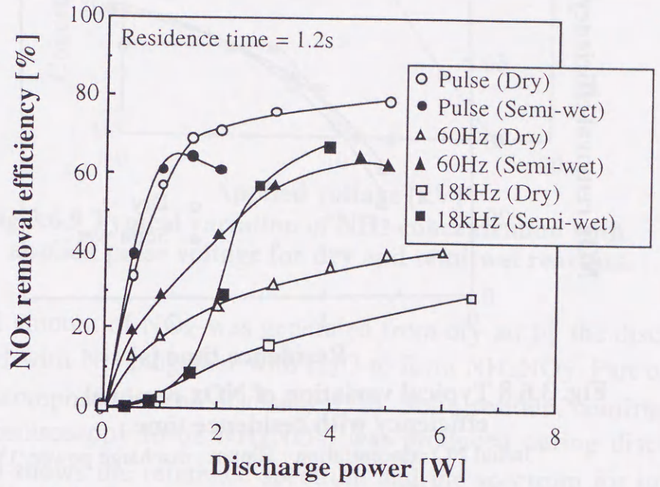

Fig. 3.6.7 NOx removal efficiency in air with discharge power for different type of applied voltage ;
initial NO concentration : 20ppm

Fig. 3.6.7 shows NO_X removal efficiency for the dry and the semi-wet reactors plotted as a function of average power input into the discharge for 1.2 s residence time. It appears that positive pulses in the semi-wet reactor gave the best performance although there was no significant difference between dry and semi-wet test results in this case. The semi-wet reactor outperformed the dry reactor by a wide margin in the case of 60 Hz and 18 kHz voltages. Reason for this better performance may be NO_2 and/or N_2O_4 absorption in water [69]. $CaCl_2$ solutions kept moisture, and semi-wet condition could be achieved with less supply of water. The author considers that H_2O emission and surface absorption were main roles of this solution, and that Cl_2 was not likely to play an important role.

3) Residence time: As initial concentration of NO was very low, residence time (Fig. 3.6.3 and 3.6.5) did not seem to influence NO

removal significantly. However, after the inception of the discharge, at a fixed value of input power, NO_X removal efficiency was better for longer residence time. This is depicted in Fig. 3.6.8. Here again, the semi-wet reactor performed better than the dry reactor till arcing sets in.

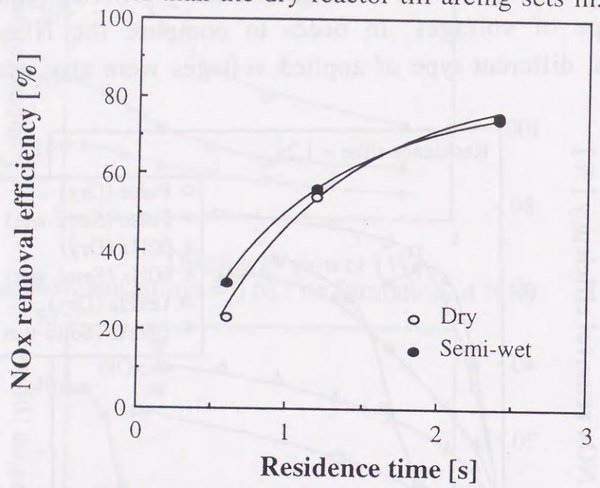

Fig. 3.6.8 Typical variation of NOx removal efficiency with residence time ;
initial NO concentration : 40ppm , discharge power :1W

3.6.3 Removal of ammonia

1) Features of NH_3 reduction: A typical curve showing the variation of the NH_3 concentration with applied voltage for pulse voltage application is presented in Fig. 3.6.9 for both dry type and semi-wet type reactors. The initial NH_3 concentration for the dry reactor was 25 ppm and that for the semi-wet reactor was 19 ppm. The figure shows that the slope of the reduction curves was about the same for both but a ~60% reduction was achieved in semi-wet condition even without any voltage application. NH_3 was easily absorbed in water and, therefore, can be removed under wet condition. To remove all NH_3, discharge power required in semi-wet condition is ~2.5W compared to ~8W in dry condition. With the increase in residence time, the decrease of NH_3 concentration with voltage has been observed to be steeper.

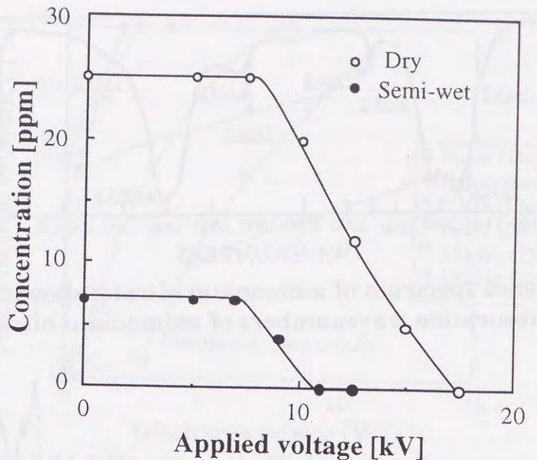

Fig.3.6.9 Typical variation of NH3 concentration with applied pulse voltage for dry and semi-wet reactors.

Small amount of NO_X was generated from dry air by the discharge, and reacted with NH_3 together with H_2O to form NH_4NO_3. Part of NH_3 may be decomposed by the discharge [70]. Solid residue, confirmed by infrared spectroscopy to be NH_4NO_3, was produced during discharge. Fig. 3.6.10 shows the reference spectrum and the spectrum for infrared transmission obtained from the solid residue collected from the reactor after experiment.

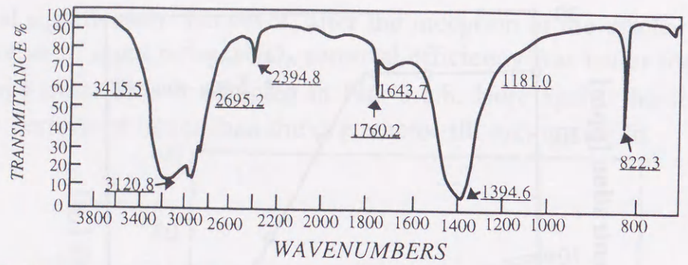

(a) Reference spectrum of ammonium nitrate; showing peak absorption wavenumbers of ammonium nitrate.

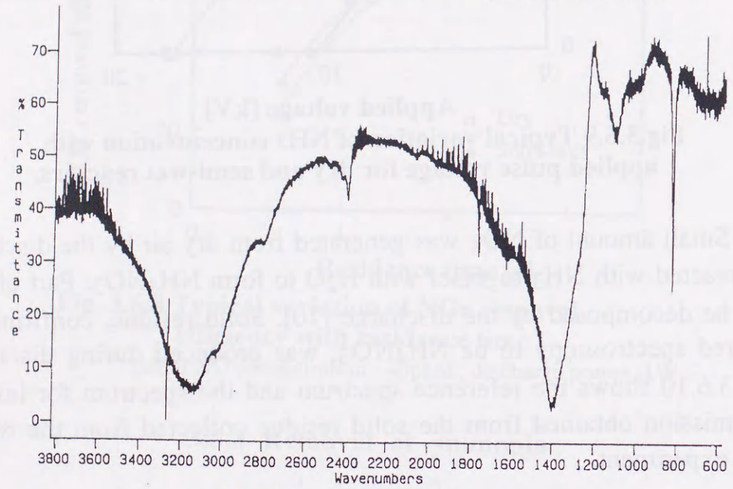

(b) Measured spectrum

Fig. 3.6.10 Infra-red transmission spectrum of the solid residue in ammonia discharge experiment.

2) Effect of the type of voltage: Fig. 3.6.11 summarizes all the result of dry and wet tests with different type of voltages for a fixed residence time of ~0.6s and for an initial NH_3 concentration of 18~25 ppm. It shows the advantage of using the semi-wet reactor for NH_3 removal. Even without any applied voltage, 50~60% of ammonia could be removed by the semi-wet reactor. The figure also shows that pulse and high frequency voltages perform better in ammonia removal than power frequency voltage. It is, however, to be noted that almost 80% could be removed at ~9.5W with power frequency voltage. This was also a significant reduction.

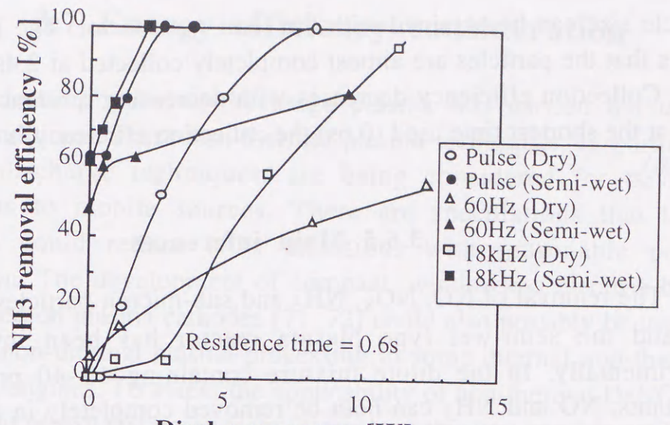

Fig.3.6.11 NH_3 removal efficiency in air with discharge power for different type of applied voltage ; initial NH_3 concentration :18-25ppm.

In both the cases of NH_3 and NO_X removal, significant O_3 generation has been observed. Ozone can, however, be easily removed by catalytic reaction [70].

3.6.4 Removal of particles

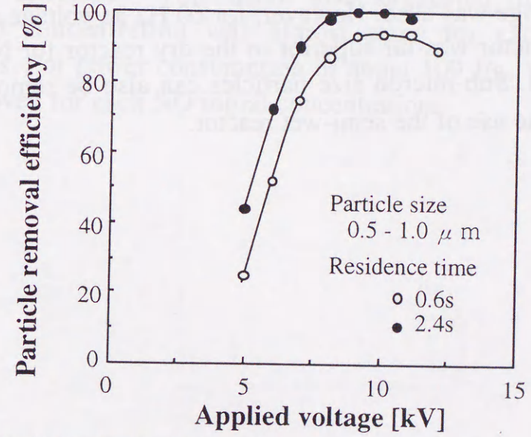

Fig.3.6.12 Variation of particle removal efficiency in air with applied pulse voltage to the semi-wet reactor for different residence time.

The removal efficiencies of particles of 0.5 - 1.0μm size are shown in Fig. 3.6.12 for pulse voltage applications and for two different residence times. Very high collection efficiencies for these range of

particle size can be obtained with the semi-wet reactor. The Fig. 3.6.12 shows that the particles are almost completely collected at 2.4s residence time. Collection efficiency decreases with decreasing residence time but even at the shortest time used (0.6s) the collection efficiency is quite good (~93%).

3.6.5 Main inferences

The removal of NO, NO_X, NH_3 and sub-micron particles using the dry and the semi-wet type plasma reactor has been investigated experimentally. In the dilute mixture containing 10~40 ppm of the pollutants, NO and NH_3 can both be removed completely in a streamer corona discharge. However, in case of NH_3, significant O_3 and NH_4NO_3 formation were taken place. With NO, the formation of NO_2 increases with the decrease in NO level. At higher input power, however, NO_X level went down reaching a saturation value of the order of a few ppm. N_2O formation has been found to be significant with the dry reactor at long residence time. But with semi-wet reactor and short residence time (0.6s) no N_2O has been detected. As a result, the semi-wet type reactor has been found to be more efficient than the dry type reactor. For NO_X removal, the semi-wet reactor is marginally better than the dry reactor when pulse voltage was used. However, for 60 Hz ac voltage application, the semi-wet reactor was far superior to the dry reactor for NH_3 as well as NO_X removal. Sub-micron size particles can also be removed almost completely by the use of the semi-wet reactor.

3.7 Energy efficiency consideration

Gas cleaning utilizing discharge plasma was carried out under various conditions. These non-thermal plasma techniques, in particular electrical discharge techniques, are being considered for possible applications to mobile sources. There are speculations that these techniques could reduce NOx emissions with reasonable power consumption. The development of compact, windowless electron-beam sources based on plasma cathodes [71, 72] could also possibly be used to implement non-thermal plasma processing in some internal non-thermal combustion engines. To assess the applicability of non-thermal DeNOx to the treatment of exhaust gases from internal combustion engines could be one of the important factors to realize this process.

Fig. 3.7.1 shows the NO and NOx (=NO + NO_2) removal efficiency for various power consumptions of the dry reactor. Gas temperature was 150°C. Discharge power required for treatment of 1 gram of gas is referred to as the "*discharge power ratio*". Three kinds of initial NO concentration were investigated, i.e. 200, 600, and 1000 ppm. Maximum NO removal efficiency was about 55 % and obtained for an initial NO concentration of 200 ppm. Higher the NO initial concentration, lower the NO removal efficiency. This result also suggested that amount of removed NO concentration was almost same for each NO initial concentrations. For power consumption of about 100 J/g, 120 - 150 ppm NO was removed for each NO initial concentrations.

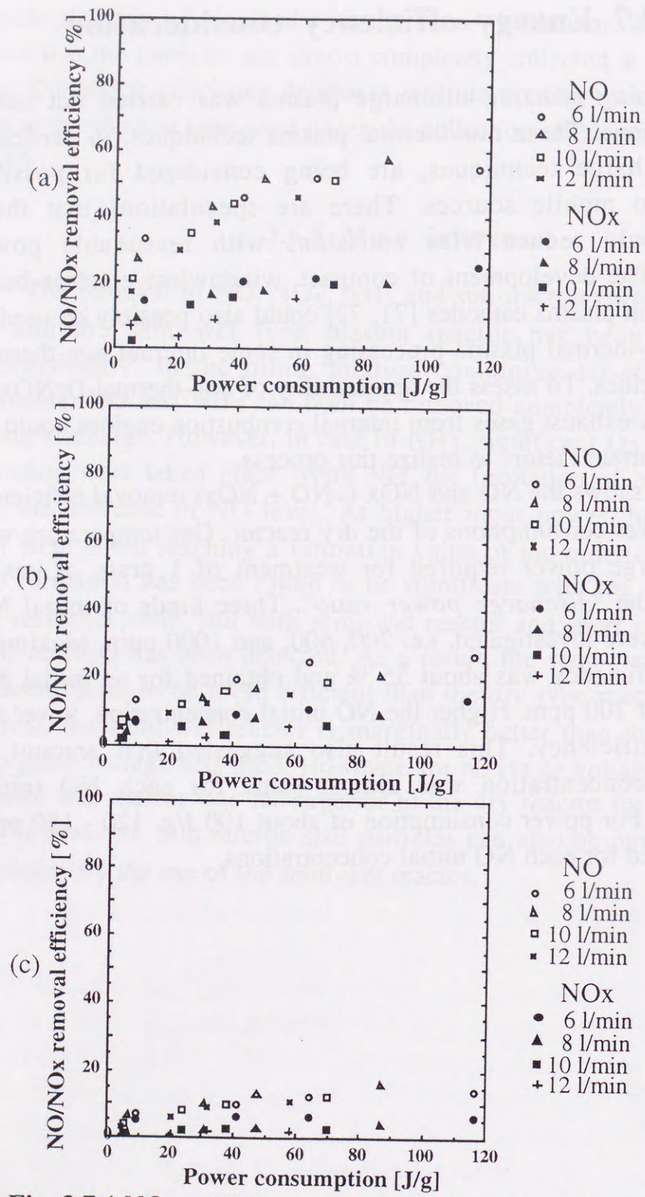

Fig. 3.7.1 NO and NOx removal efficiency for various power consumptions of the dry reactor.

Gas temperature :150 °C, CO_2 :10%, balance gas: dry air
(a) NO initial concentration 200 ppm
(b) NO initial concentration 600 ppm
(c) NO initial concentration 1000 ppm

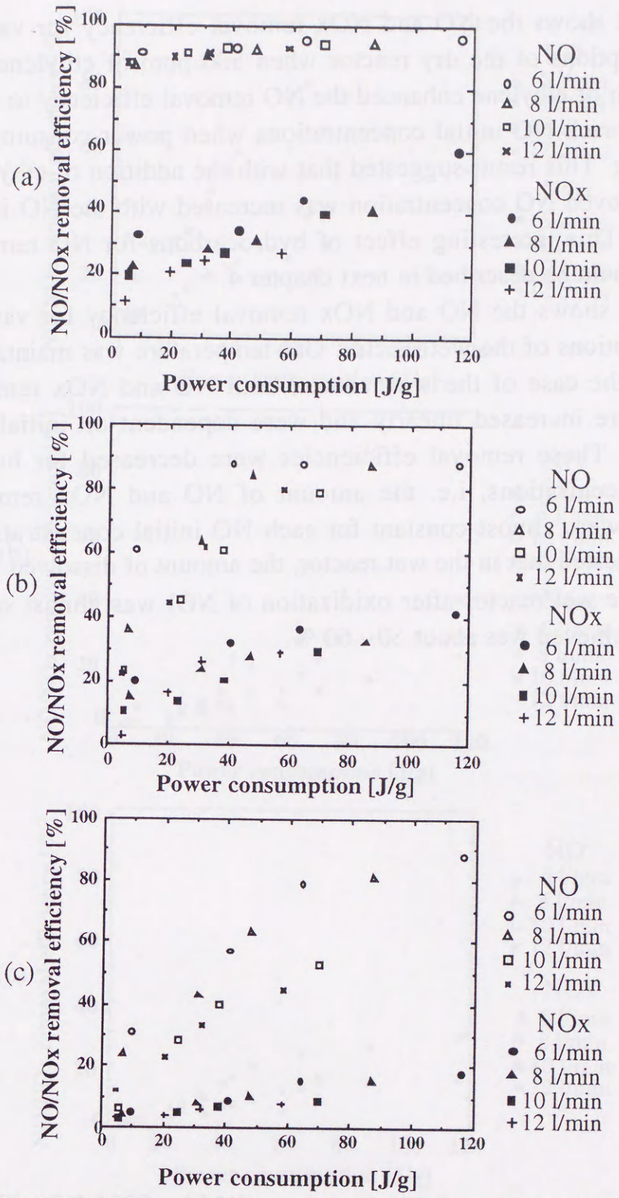

Fig. 3.7.2 NO and NOx removal efficiency for various power consumptions of the dry reactor.

Gas temperature :150 °C, CO_2 :10%, balance gas: dry air, C_2H_4 :500 ppm
(a) NO initial concentration 200 ppm
(b) NO initial concentration 600 ppm
(c) NO initial concentration 1000 ppm

Fig. 3.7.2 shows the NO and NOx removal efficiency for various power consumptions of the dry reactor when 500 ppm of ethylene was added. Addition of ethylene enhanced the NO removal efficiency to more than 80 % for each NO initial concentrations when power consumption was 50 - 60 J/g. This result suggested that with the addition of ethylene, amount of removed NO concentration was increased with the NO initial concentration. This interesting effect of hydrocarbons for NO removal mechanisms would be described in next chapter 4.

Fig. 3.7.3 shows the NO and NOx removal efficiency for various power consumptions of the wet reactor. Gas temperature was maintained at 150 °C. In the case of the wet reactor, both NO and NOx removal efficiencies were increased linearly and were dependent on initial NO concentrations. These removal efficiencies were decreased for higher initial NO concentrations, i.e. the amount of NO and NOx removal concentrations were almost constant for each NO initial concentrations. This result suggested that in the wet reactor, the amount of dissolved NO_2 (produced in the wet reactor after oxidization of NO) was almost same. NOx removal achieved was about 50 - 60 %.

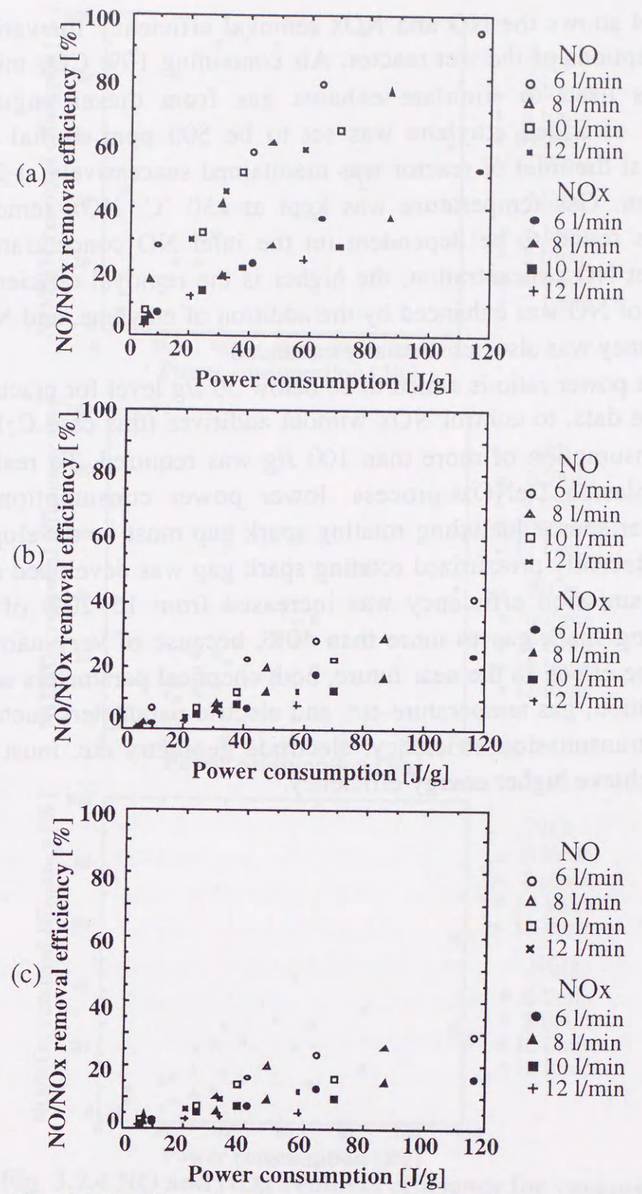

Fig. 3.7.3 NO and NOx removal efficiency for various power consumptions of the wet reactor.

Gas temperature :150 °C, CO_2 :10%, balance gas: dry air
(a) NO initial concentration 200 ppm
(b) NO initial concentration 600 ppm
(c) NO initial concentration 1000 ppm

Fig. 3.7.4 shows the NO and NOx removal efficiency for various power consumptions of the wet reactor. Air containing 10% CO_2 mixed with NO was used to simulate exhaust gas from diesel engines. Concentration of added ethylene was set to be 500 ppm. Initial NO concentration at the inlet of reactor was maintained successively at 200, 600, 1000 ppm. Gas temperature was kept at 150 °C. NOx removal efficiency was found to be dependent on the inlet NO concentration. Lower the inlet NO concentration, the higher is the removal efficiency. The oxidation of NO was enhanced by the addition of ethylene, and NOx removal efficiency was also substantially enhanced.

Discharge power ratio is aimed to be below 30 J/g level for practical use. With these data, to control NOx without additives (this case C_2H_4) the energy consumption of more than 100 J/g was required. To realize non-thermal plasma DeNOx process, lower power consumption is desirable. Power source including rotating spark gap must be developed for this sake. Recently pressurized rotating spark gap was developed and its power transmission efficiency was increased from 15~20% of an ordinary rotating spark gap to more than 40%, because of very narrow voltage rise time effect. In the near future, both chemical parameters such as gas composition, gas temperature etc. and electric parameters such as power source transmission efficiency, electrode geometry etc. must be developed to achieve higher energy efficiency.

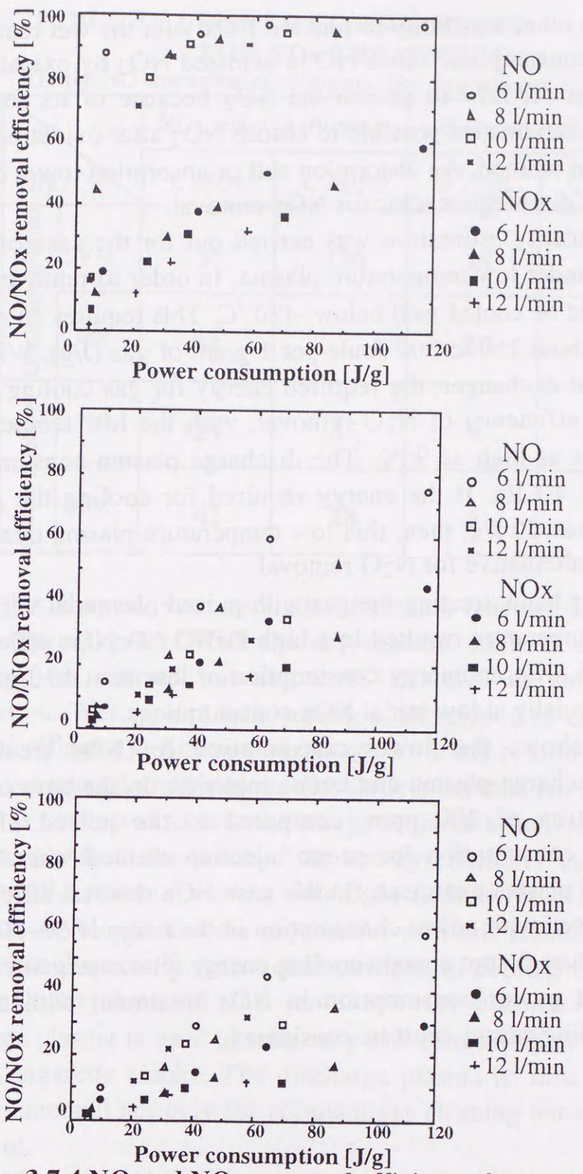

Fig. 3.7.4 NO and NOx removal efficiency for various power consumptions of the wet reactor.

Gas temperature :150 °C, CO_2 :10%, balance gas: dry air, C_2H_4 :500 ppm

(a) NO initial concentration 200 ppm

(b) NO initial concentration 600 ppm

(c) NO initial concentration 1000 ppm

It seems the other feasibility to remove NOx with the wet reactor to save the energy consumption. Once NO is oxidized NO_2 by oxidation, it is only the matter for how to absorb the NO_2 because of its solvable characteristics. It can be also possible to absorb NO_2 after oxidation even by ozone injection method. An absorption cell or absorption tower can be attached after the discharge reactor for NO_2 removal.

Also, the energy estimation was carried out for the case of N_2O removal treated under low temperature plasma. In order to remove N_2O, the flue gas should be cooled well below -130 °C. This requires an energy consumption of about 150 to 300 Joule per 1 gram of gas (J/g). With the heat-pump or heat exchanger, the required energy for gas cooling could be reduced. The efficiency of N_2O removal, with the low temperature plasma reactor, is as high as 90%. The discharge plasma consumes an energy as low as 40 J/g. If the energy required for cooling the gas is reduced to less than 50 J/g, then, this low temperature plasma treatment could be a better alternative for N_2O removal.

On the other hand, treating the gas with pulsed plasma at very low liquid nitrogen temperature resulted in a high DeNO / DeNOx efficiency of more than 90% with an energy consumption of less than 10 J/g. This was observed especially at low initial NOx concentrations.

Table 3.7.1 shows the power consumption for NOx treatment comparing the discharge plasma and ozone injection. In the case of NO initial concentration of 200 ppm, compared to the pulsed plasma treatment, power consumption for ozone injection method was almost half that of pulsed plasma treatment. (In this case NOx removal efficiency of 80% was achieved with power consumption in the range of 30~50 J/g.) However these values do not contain cooling energy for ozone generation. Therefore for net power consumption in NOx treatment with ozone injection, this cooling energy must be considered.

TABLE 3.7.1 POWER CONSUMPTION FOR NOx TREATMENT.

(Initial NO concentration: 200 ppm, Gas temperature: 150 °C)

		NOx removal efficiency		NO removal efficinecy	
(J/g)		η =50%	η =80%	η =50%	η =80%
Discharge plasma	wet	**37**	**126**	**18**	**21**
	dry	**84**	—	**20**	**46**
Ozone injection	wet	**29**	**35**	**6**	**9**
	dry	**42**	**48**	**6**	**12**

In this chapter, various kinds of plasma reactors are introduced to treat pollutant gases. With the dry reactor, addition of hydrocarbons (ethylene) is carried out and it is effective to enhance the NOx oxidization. Wet type plasma reactor is developed to enhance the NOx removal efficiency. Another advantage with this reactor is that the NO_2 which is produced under plasma discharge is soluble. Also ozone injection method is conducted to save the energy required to remove NOx.

Not only from the point of the energy efficiency consideration, but also from the point of treating stable gas such as N_2O, low temperature reactor is developed and the experiment with this reactor is successively carried out. Especially with liquid nitrogen as cooling agent, both NOx and N_2O are clustered and removed with plasma discharge. Also discharge plasma is used to treat very low concentration gas components such as cigarette smoke. The discharge plasma is, thus found to be an effective method not only for pollutant gas cleaning but also for the odor treatment.

Finally to conclude this chapter, the wet type reactor is the most efficient ones to treat the pollutant gases (in the range of this study) from the point of power consumption. For real exhaust gas treatment, soot or dust particles have to be collected and ozone injection method may not be suitable for treating these dusts. Pulsed plasma treatment which has precipitation effect must be used in such cases.

4 PLASMA CHEMICAL REACTIONS OF NOx WITH WATER VAPOR / HYDROCARBONS AND BY-PRODUCT ANALYSIS

Many theoretical models have been proposed to explain the mechanisms of the radical generations in the pulsed streamer discharge. The mean energy of electrons in the pulsed streamer discharge is almost proportional to the ratio of the electric field and the gas density (E/N), but independent of the gas composition [73]. Electrons contribute to the generation of OH, O, and N radicals. These radicals can be generated by $e + H_2O$, $e + O_2$, and $N^+ + O_2$, respectively. NO is then oxidized into reactive species such as NO_2, HNO_3, etc. These reactions and scheme have been introduced in the appendix I [60a, 60b].

In the previous chapter, effect of addition of the hydrocarbons (ethylene) was studied to enhance the NOx removal. Though the effect of hydrocarbon such as ethylene to the NOx removal was significant, but the reports about its effect were very few [74]. If some of the by-products from discharge plasma treatment were poisonous, hydrocarbon addition could not be used for the actual exhaust gas treatment. To confirm the safety from the by-products of this method, in this chapter, the by-products analysis will be presented. Some chemical reactions with ethylene will be discussed to highlight the effects of hydrocarbon.

4.1 Effect of additives on the NOx removal

4.1.1 NOx removal with addition of hydrocarbons

Many tests have been made on NOx removal both from the simulated gas and from the diesel engine exhaust using various hydrocarbon additives, including C_2H_4, C_3H_8, and CH_4 as shown in Fig. 4.1.1. The pulse power source was the same as used in the previous section 3.2.

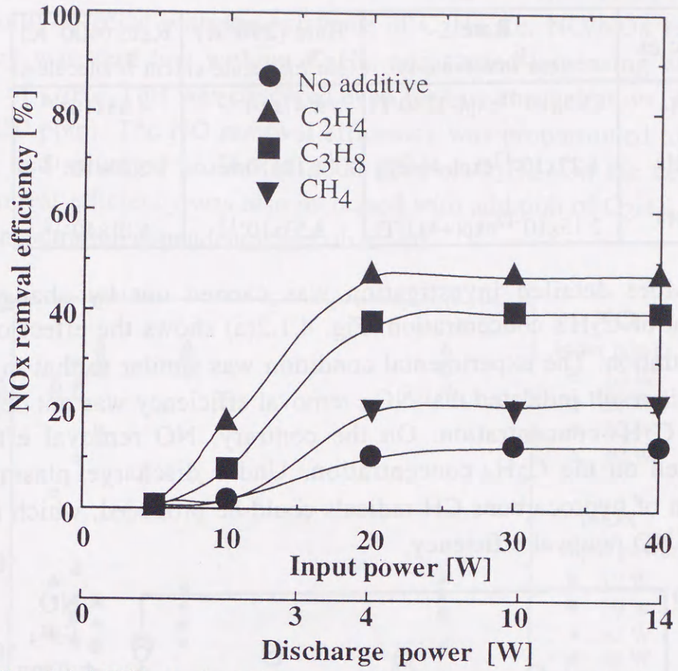

Fig. 4.1.1 Effect of additives on the NOx removal efficiency.
T = 240 °C, Gas flow rate=8 ℓ/min, Initial NO concentration = 600 ppm, Initial NO_2 concentration =30 ppm.

Among the additives, C_2H_4 was found to be most efficient. For example, at the gas temperature of 30°C, 70% NOx removal efficiency was observed with 500 ppm C_2H_4 additive as shown in Fig. 3.2.9. The initial concentration of NO was 400 ppm. Based on a gas flow rate of 2 ℓ/min. and power input of 20 W (corresponding to about 4 W of power dissipated in the discharge), the energy consumption was about 150 J/g to reduce 280 ppm of NOx for dry reactor. (In the wet or semi-wet reactor case energy consumption could be decreased.). Table 4.1 [74, 75] shows the reaction rates for a variety of hydrocarbons.

Note that at higher gas temperature, C_2H_4 becomes less effective because of its negative activation energy as shown in Table 4.1.

TABLE 4.1 INTERACTION OF HYDROXYL RADICALS WITH HYDROCARBONS

Species	Rate (cm^3/molecule-s)	Rate (298°K) (cm^3/molecule-s)	Rate (400°K) (cm^3/molecule-s)
CH4	$6.95x10^{-18}exp(-1280/T)$	$8.41x10^{-15}$	$4.53x10^{-14}$
C3H8	$1.27x10^{-17}exp(-444/T)$	$1.18x10^{-12}$	$2.10x10^{-12}$
C2H4	$2.15x10^{-12}exp(+411/T)$	$8.53x10^{-12}$	$6.01x10^{-12}$

More detailed investigation was carried out by changing the addition of C_2H_4 concentration. Fig. 4.1.2(a) shows the effect of C_2H_4 concentration. The experimental condition was similar to that in section 3.2. This result indicated that NOx removal efficiency was not dependent on the C_2H_4 concentration. On the contrary, NO removal efficiency depended on the C_2H_4 concentration. Under discharge plasma, with addition of hydrocarbons CH radicals could be produced, which resulted in high NO removal efficiency.

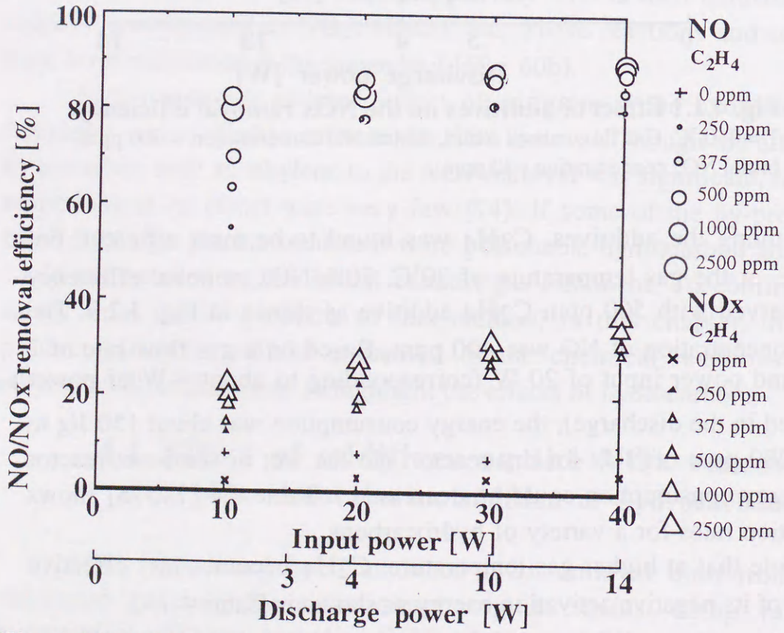

Fig. 4.1.2(a) Effect of C_2H_4 concentration on the NO/NOx removal efficiency.

T= 150°C, Gas flow rate = 2l/min, Initial NO concentration = 1000 ppm

Fig. 4.1.2(b) shows NO/NOx removal efficiency as a function of C_2H_4 concentration. Both NO/NOx removal efficiencies were significantly affected with the existence of C_2H_4, i.e. NO/NOx removal efficiency was very low without C_2H_4, and started increasing with the addition of C_2H_4. This was observed even for low concentration of C_2H_4 (about 250 ppm). The NO removal efficiency was proportioned to C_2H_4 addition and saturated around of 1000 ppm of C_2H_4. On the contrary, NOx removal efficiency was also increased with addition of C_2H_4, but no C_2H_4 concentration dependency was observed.

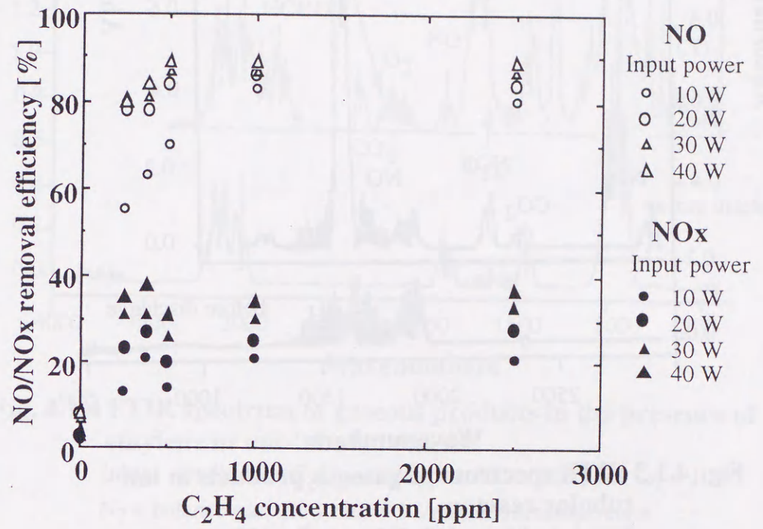

Fig. 4.1.2(b) NO/NOx removal efficiency as a function of C_2H_4 concentration.

T= 150°C, Gas flow rate = 2l/min, Initial NO concentration = 1000 ppm

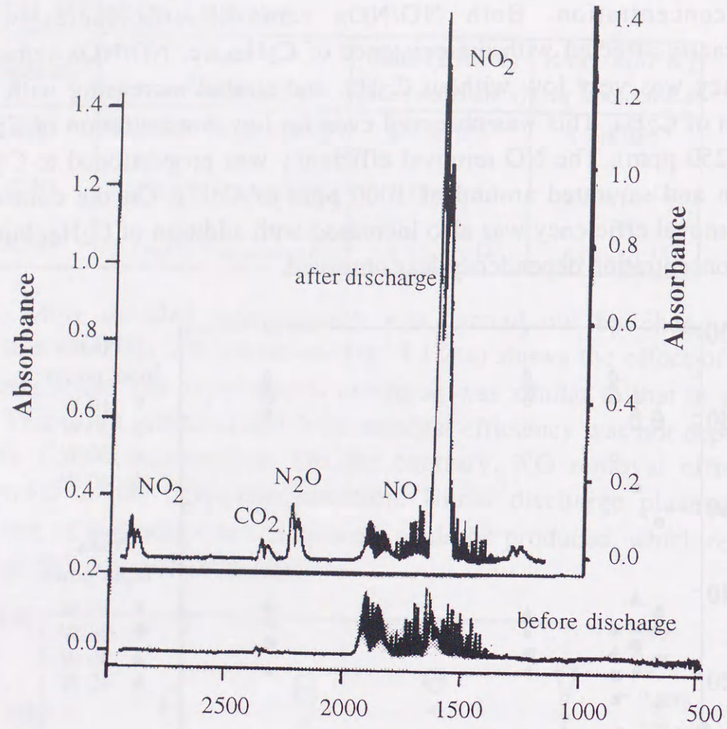

Fig. 4.1.3 FTIR spectrum of gaseous products in uni - tubular reactor.

Initial conditions: NO=200 ppm, O_2=10%, N_2=balance gas, flow rate =2 ℓ/min, room temperature.

The results of Fourier Transform Infrared Spectroscopy (FTIR), presented in Fig. 4.1.3, confirmed that NO reacted with the ozone generated by the discharge (input power of 30 W) and was oxidized to NO_2. The presence of N_2O was also observed in the output of the plasma chemical process. It shold be noted that a small amount (less than 30 ppm) of N_2O can also be generated from pure dry air. NO in the range of 200 ppm with an addition of 500 ppm C_2H_4 did not enhance the generation of N_2O. When NH_3 was added, large amount of N_2O generation (about 10 ppm) was confirmed [76].

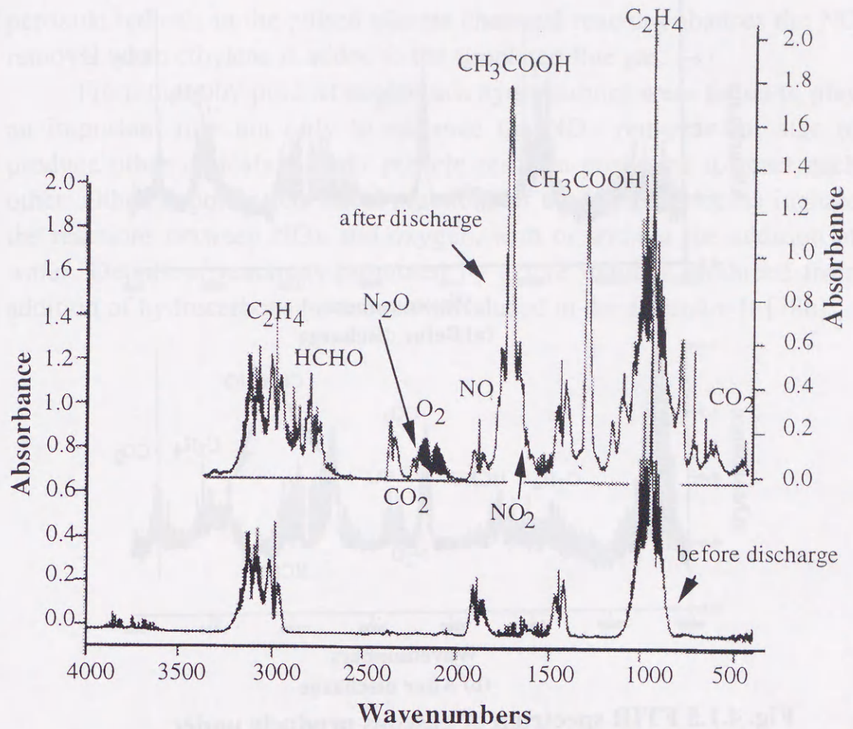

Fig. 4.1.4 FTIR spectrum of gaseous products in the presence of ethylene in uni-tubular reactor.

Initial conditions: C_2H_4 = 500 ppm, NO = 200 ppm, O_2 = 10%, N_2 = balance gas, flow rate = 2 ℓ/min, room temperature.

The FTIR analysis (Fig. 4.1.4) shows the by-products under plasma discharge when C_2H_4 was added to the simulated flue gas (input power = 30 W). NO_2, O_3, acetic acid (CH_3COOH) and formaldehyde (HCHO) along with some CO_2, were identified in the output gas of the reactor. Concentrations of these gaseous components were not quantitatively evaluated in the present study.

Usually addition of hydrocarbons comes to produce abundant radicals. However, the mechanisms of the plasma chemical reactions are in still uncertain. It is very hard to measure or specify these radicals directly because their life time are usually very short. In order to investigate these reactions, relatively simple gas composition (750 ppm of C_2H_4 in air without NO) was subjected to plama treatment as very low input power of about 6 W.

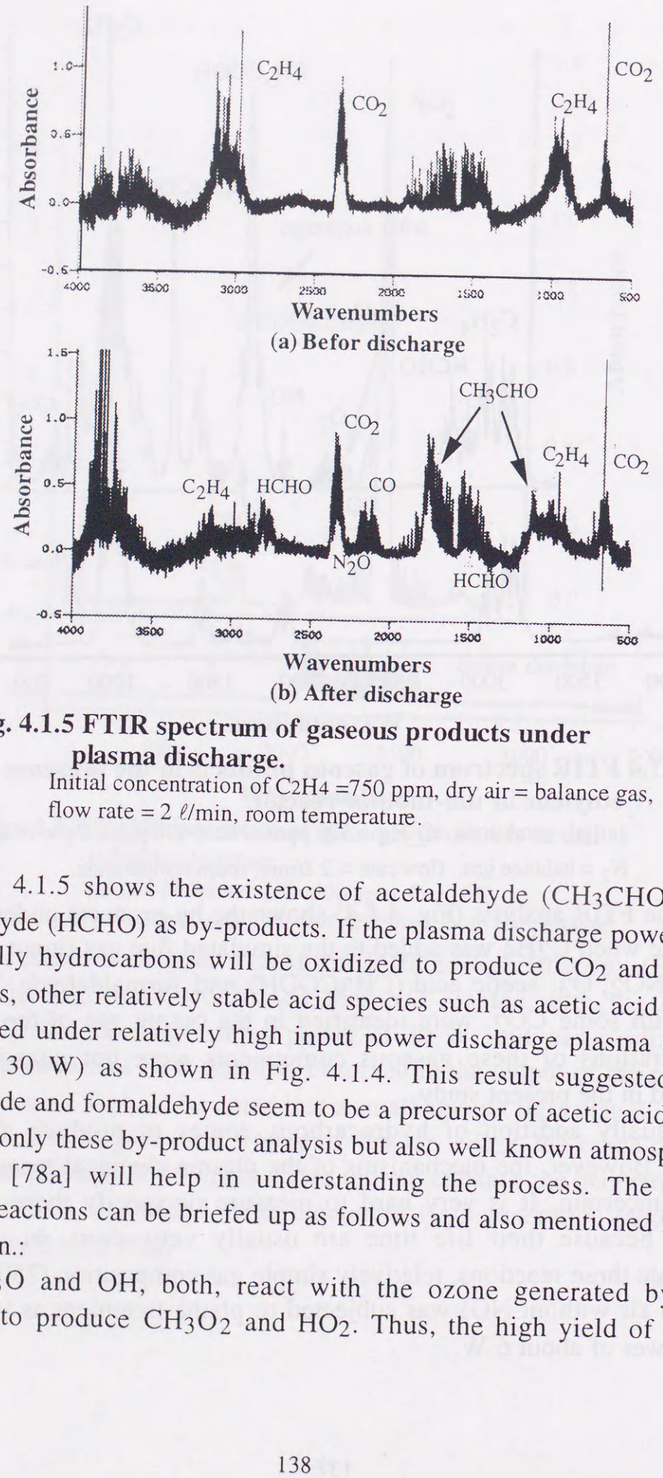

Fig. 4.1.5 FTIR spectrum of gaseous products under plasma discharge.

Initial concentration of C_2H_4 =750 ppm, dry air = balance gas, flow rate = 2 ℓ/min, room temperature.

Fig. 4.1.5 shows the existence of acetaldehyde (CH_3CHO) and formaldehyde (HCHO) as by-products. If the plasma discharge power was high, finally hydrocarbons will be oxidized to produce CO_2 and H_2O. Before this, other relatively stable acid species such as acetic acid could be produced under relatively high input power discharge plasma (input power of 30 W) as shown in Fig. 4.1.4. This result suggested that acetaldehyde and formaldehyde seem to be a precursor of acetic acid.

Not only these by-product analysis but also well known atmospheric chemistry [78a] will help in understanding the process. The main chemical reactions can be briefed up as follows and also mentioned in the next section.:

CH_3O and OH, both, react with the ozone generated by the discharge to produce CH_3O_2 and HO_2. Thus, the high yield of these

peroxide radicals in the pulsed plasma chemical reactor enhances the NO removal when ethylene is added to the simulated flue gas.

From these by-product analysises, hydrocarbons were found to play an important role not only to enhance the NOx removal but also to produce other radicals in their recycle reaction processes to react each other. Other important chemical reactions of the plasma process include the reactions between NOx and oxygen, with or without the addition of water. Details of reactions promoted by active radicals produced from addition of hydrocarbons have been introduced in the appendix II [78b].

4.1.2 NOx removal with addition of water vapor

Though the effect of OH radical is not clear at present stage, it may play a major role in NOx removal chemical reactions. Because usually, the real exhaust gas contains 5-10% water vapor and OH radicals can be produced from water vapor by the plasma in the reacor [79]. However, previous DeNOx studies were carried out without water vapor in the feedgas to make the other gas composition effect such as C_2H_4 more clearly which is the motivation for the present study.

In this section, the effect of water vapor concentration on NOx removal were presented. This could give some information on the OH radical effect. Details on the effect of OH radicals produced from water vapor under plasma discharge have been investigated by varying the water vapor concentration.

Fig. 4.1.6 shows the effect of water vapor concentration on the NO/NOx removal efficiency.

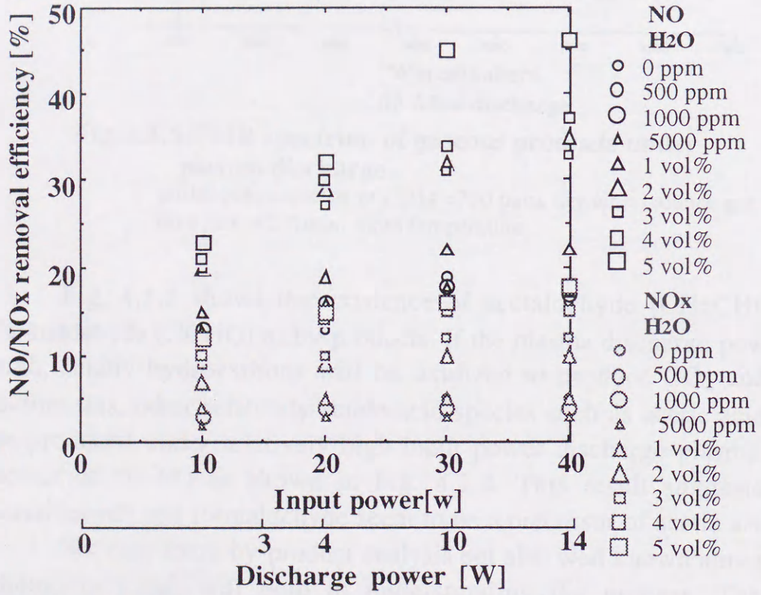

Fig. 4.1.6 Effect of water vapor concentration on NO/NOx removal efficiency.

T = 150℃, Gas flow rate = 2 l/min, Initial NO concentration = 1000ppm

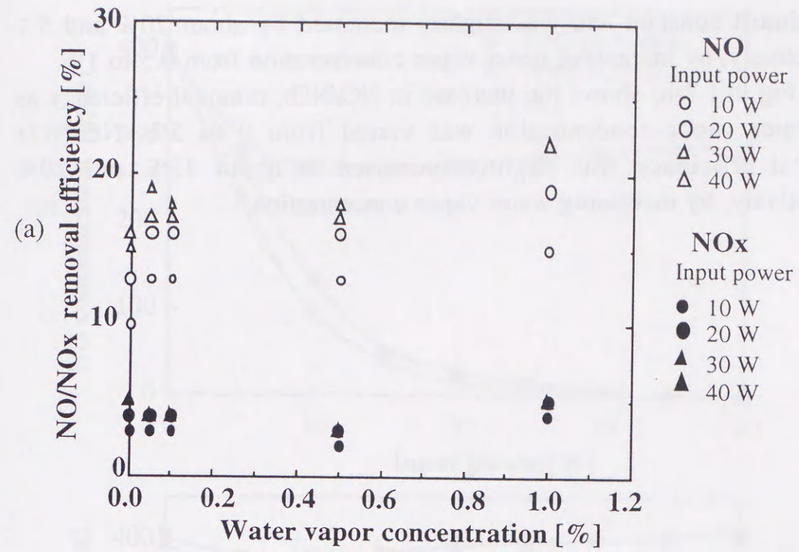

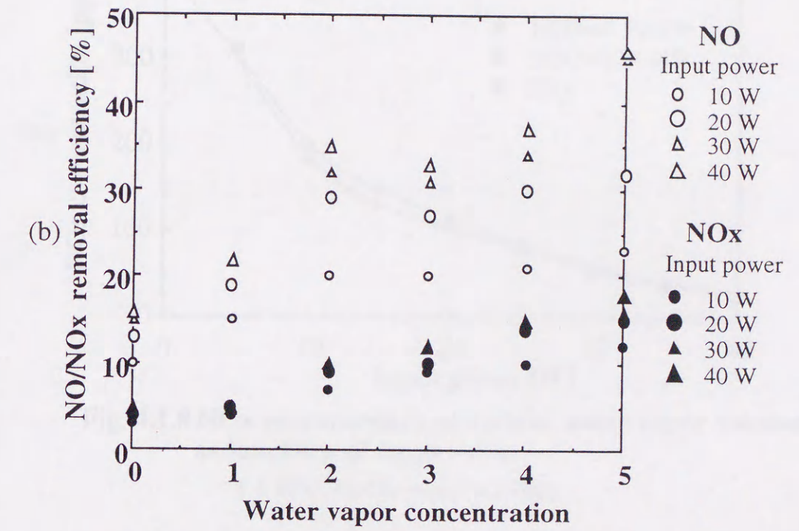

Fig. 4.1.7 NO/NOx removal efficiency as a function of water vapor concentration.

T = 150°C, Gas flow rate = 2 l/min, Initial NO concentration = 1000ppm

Fig. 4.1.7(a) shows the NO/NOx removal efficiency as a function of water vapor concentration varied from 0 to 1%. In the range of water vapor concentration 0 to 0.5% (5000 ppm), NO/NOx removal efficiency

was almost constant and was slightly increased by about 20% and 5% respectively, by increasing water vapor concentration from 0.5 to 1%.

Fig. 4.1.7(b) shows the increase in NO/NOx removal efficiency as the water vapor concentration was varied from 0 to 5%. NO/NOx removal efficiency was slightly increased to about 45% and 20% respectively, by increasing water vapor concentration.

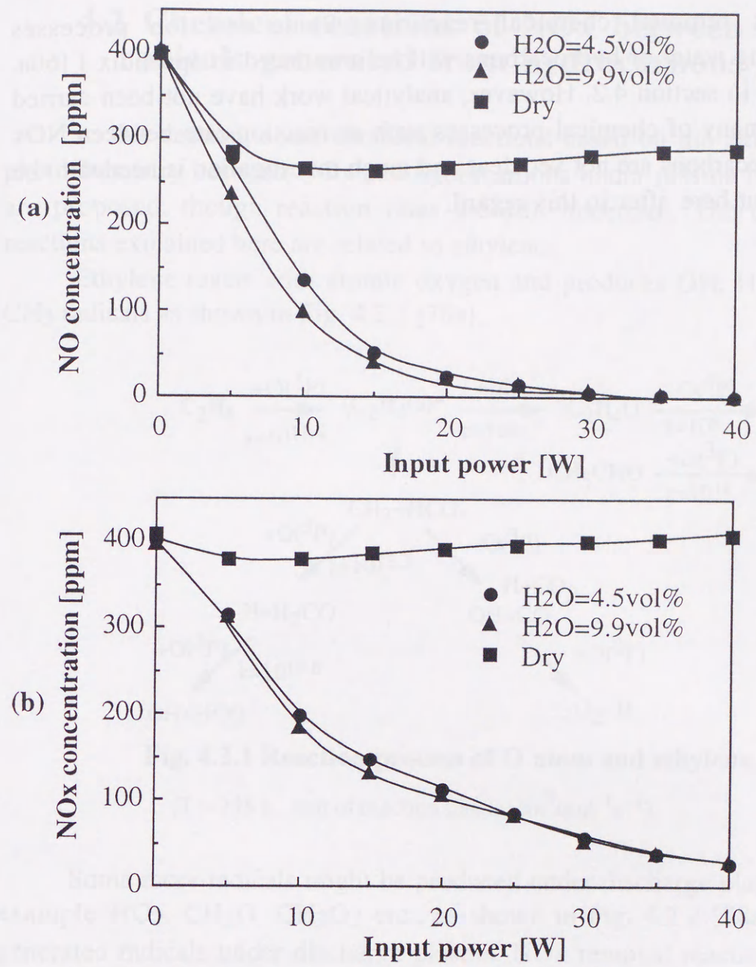

Fig. 4.1.8 NOx concentration at various water vapor volume as functions of input power.

T = 80°C, Gas flow rate = 2 l/min

To check the effect of relatively higher water vapor concentration, for example 4.5 and 9.9 vol% water vapor was studied as shown in Fig. 4.1.8(a), (b). There was no difference between two water vapor concentrations. This suggests that increasing water vapor concentration will only result in saturation of NO/NOx concentration characteristics.

Comparing the results between addition of C_2H_4 and water vapor, (In other words, this could be considered comparing the effect of CH radicals and OH radicals) effect of C_2H_4 addition is predominant in

NO/NOx removal chemical reactions. Some reaction processes concerning water or hydrocarbons will be introduced in appendix I [60a, 60b] and in section 4.2. However, analytical work have not been carried out and many of chemical processes such as reaction rate between NOx and hydrocarbons are not yet clear and much investigation is needed to be carried out here after in this regard.

4.2 Chemical reactions of NOx between active radicals generated from hydrocarbons

In this section, some chemical reactions based on the atmosphere photochemistry between NOx and hydrocarbons under plasma discharge are proposed, though reaction rates are still uncertain. The chemical reactions explained here are related to ethylene.

Ethylene reacts with atomic oxygen and produces OH, HCO, and CH_3 radicals as shown in Fig. 4.2.1 [78a].

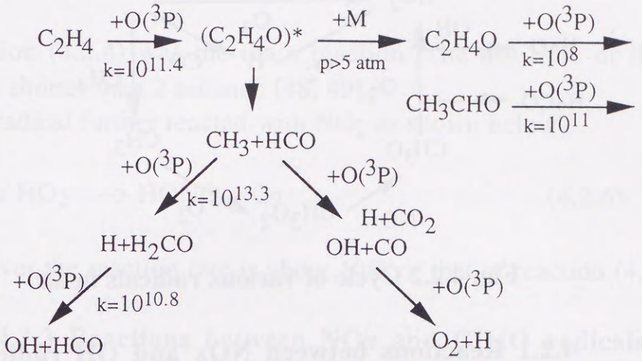

Fig. 4.2.1 Reaction process of O atom and ethylene.

(T = 298 k , unit of reaction rate is $cm^3mol^{-1}s^{-1}$)

Some more radicals might be produced under discharge plasma, for example HO_2, CH_3O, CH_3O_2 etc., as shown in Fig. 4.2.2 [78a]. With generated radicals under discharge plasma, NOx removal reaction could be occurred as explained below.

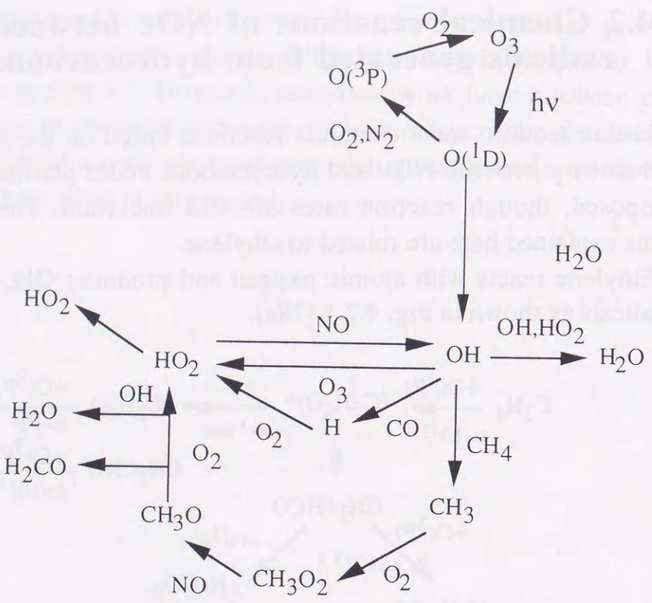

Fig. 4.2.2 Cycle of various radicals in air.

4.2.1 Reactions between NOx and OH radicals

An explanation of reactions the between NOx and OH radicals are given as below:

NO can be oxidized to NO_2 with OH radicals through the following reaction.

$NO + OH + M \text{ ----> } HONO + M$ (4.2.1)
($k = 2.8 \times 10^{-17}$ cm^6/s, $M=N_2$, 296 K)

$NO + OH \text{ ----> } NO_2 + H$ ($k = 6.6 \times 10^{-12}$ cm^3/s) (4.2.2)

Of oxidization of NO_2 with radicals such as O, O_3 or OH etc. i.e., because NO_2 oxidization reaction between NO and O, O_3, and OH could be removed as shown below.

$NO_2 + OH + M \text{ ----> } HNO_3 + M$ (4.2.3)

NO_2 was converted to HNO_3 through this recombination reaction with OH.

4.2.2 Reactions between NOx and HO_2 radicals

Reactions between NOx and HO_2 radicals are also important from the view point of NOx removal as well as the re-productivity of OH radicals.

$NO + HO_2 \text{ ----> } NO_2 + OH$ (4.2.4)
($k = 1.2 \times 10^{-13}$ $\exp(-2400/RT)$ cm^3/s)

$NO + HO_2 + M \text{ ----> } HONO_2$ (4.2.5)

Reaction (4.2.4) was the main reaction. The life time of the by-product was shorter than 2 seconds [48, 49].

HO_2 radical further reacted with NO_2 as shown below.

$NO_2 + HO_2 \text{ ----> } HONO + O_2$ (4.2.6)

However the reaction rate is about 10% of that of reaction (4.2.4).

4.2.3 Reactions between NOx and CH_3O radicals

Under plasma discharge, CH_3O radicals were also produced. Reaction between NOx and CH_3O was less compared to that of OH, and HO_2.

$NO + CH_3O \text{ ----> } CH_3ONO$ (4.2.7)
$\text{ ----> } HNO + CH_2O$ (4.2.8)

Reaction was occurred not only with NO but also with NO_2 as shown below.

$NO_2 + CH_3O \text{ ----> } CH_3ONO_2$ (4.2.9)
$\text{ ----> } HONO + CH_2O$ (4.2.10)

Reactions (4.2.7) and (4.2.9) are recombination reactions, and reactions (4.2.8) and (4.2.10) are hydrogenation reactions. Though the reaction rate of these reactions was very low, CH_3O radical plays an important role in plasma chemical reactions because of its recycle

characteristics with other radicals to produce HO_2 radicals as shown in Fig. 4.2.2.

$$O_2 + CH_3O \text{----> } CH_2O + HO_2 \quad (4.2.11)$$

4.2.4. Reactions between NOx and CH_3O_2 radicals

Reactions between NOx and CH_3O_2 radicals are similar to that with CH_3O radicals. However, these reactions produced nitric acid (HNO_3) and nitrous acid (HNO_2).

$$NO + CH_3O_2 \text{----> } CH_3O_2NO \quad (4.2.12)$$
$$\text{----> } CH_2O + HONO \text{ (nitrous acid)} \quad (4.2.13)$$
$$\text{----> } CH_3O + NO_2 \quad (4.2.14)$$

$$NO_2 + CH_3O_2 \text{----> } CH_3O_2NO_2 \quad (4.2.15)$$
$$\text{----> } CH_2O + HONO_2 \text{ (nitric acid)} \quad (4.2.16)$$

Note that radicals such as CH_3O were produced in this reaction's cycle.

4.2.5 Reactions between NOx and CH_3 radicals

Reactions between CH_3 radicals and NOx can occur in the followng manner..

$$NO + CH_3 \text{----> } CH_3NO \ (k = 1.2\sim3.2 \times 10^{-11} \text{ cm}^3/\text{s}) \quad (4.2.17)$$

Also CH_3 and NO_2 are reacted by recombination. Recombination with either N atom or O atom of NO_2 is occurred.

$$NO_2 + CH_3 \text{----> } CH_3NO_2 \quad (4.2.18)$$
$$\text{----> } CH_3ONO \text{----> } CH_3O + NO \quad (4.2.19)$$

4.2.6 Reactions between NOx and HCO radicals

Reactions of HCO radicals are important for radicals recycle process rather than NOx removal process as shown in the Fig. 4.2.1.

$$HCO + O \text{----> } CO_2 + H. \quad (4.2.20)$$
$$\text{----> } CO + OH \quad (4.2.21)$$

$$HCO + O_2 \text{-----> } CO + HO_2 \quad (4.2.22)$$

Further, NOx removal reactions were also occurred.

$$HCO + NO \text{----> } HNO + CO \ (k = 8.4 \times 10^{-12} \text{ cm}^3/\text{s}) \quad (4.2.23)$$

Among the foregoing reactions, especially reactions concerning sub sections (4.2.5) and (4.2.6) likely to produce peroxide radicals HO_2 and CH_3O_2, which then oxidize NO to NO_2:

$$HO_2 + NO \text{----> } NO_2 + OH$$

$$CH_3O_2 + NO \text{----> } NO_2 + CH_3O$$

CH_3O and OH, both, react with the ozone generated in the discharge to produce CH_3O_2 and HO_2. Thus, the high yield of these peroxide radicals in the pulsed plasma chemical reactor enhances the NO removal when ethylene is added to the simulated flue gas.

4.3 Main inference

Comparing the various kinds of hydrocarbons used in the present study, ethylene is found to be one of the best additive. This result is supported and associated with the interaction of hydroxyl radicals [74, 75]. By-product analysis using FTIR is carried out to confirm the safety of the addition of the hydrocarbons. Some simple aldehyde species and carbon dioxids are found out as by-products. No hazardous gas such as HCN, is detected with this analysis. From this by-product analysis, hydrocarbons are considered to be oxidized to produce CO_2, H_2O and other relatively stable acid species.

Chemical reactions between NOx and hydrocarbons are proposed. From these considerations, it can be concluded that hydrocarbons plays an important role not only to enhance the NOx removal but also to produce other radicals in their recycle reaction processes to react with each other.

Other important chemical reactions of the plasma process such as reactions between NOx and oxygen, with or without the addition of water will be introduced in appendix I [60a, 60b]. Also appendix II [78b] present some chemical reactions involved in non-thermal DeNOx process. These chemical processes are computed and simulated in other works concerning the streamer development [73, 80-82].

5. CONCLUSIONS

Conventional gas cleaning methods like selective catalytic reduction, low NOx burner etc., are although economical for large scale power plants, they are expensive and sometimes dangerous for the case of a small plant or mobile emission source. In this regard plasma discharge or non-thermal plasma (sometimes called *non-thermal* or *non-equilibrium plasma*), comprising of electrical discharges, is gaining popularity as it has a potential to treat the gas at relatively lower energy and is less hazardous.

In this work, gas treatment utilizing pulsed discharge plasma has been studied and some advantages of this technique have been found. There are many works done by others using this discharge plasma, but the parametric study and other applications which enable increasing the energy efficiency have not been reported. In the present study the main emphasis had been laid on pollutant gas (many cases NOx) removal efficiency as well as on energy efficiency considerations. Further, in this work the effect of E/N and addition of hydrocarbons on NOx removal efficiency had been emphasized. The major conclusions of the present work can be reported as follows:

Experimental estimation of electron energy from direct measurement of the electron current showed that electron had higher energy when E/N value was higher. This higher E/N value might have energized only by the pulsed streamer discharge. Though the dc voltage was tend to cause breakdown in the gap, high E/N could not be achieved. The electron energy was also dependent on the gas composition. Further, to clarify the relatively high electron energy of non-thermal plasma, energy estimation was done by light emission of the N_2^+ first negative band (391.4 nm) and N_2 second positive band (337.1 nm) with spectroscopy.

The N_2^+ first negative band and the N_2 second positive band could be produced through the collisions of high energy electrons. Also higher E/N value gave the higher light emission signal peak suggesting that the

electron energy was significantly affected by E/N value of given pulse voltage. This further strengthens the fact that the pulsed streamer discharge is superior to the dc corona discharge. The optical studies indicate that under the discharge plasma, some electrons had enough energy to produce the so called "seed radicals" for promoting the plasma chemical reactions. Because of the high electric field the energy levels of the electron densities were high enough to ionize or dissociate the gas molecules and produce the active radical species which enhance the plasma chemical reactions.

Main and the most important part of present work is experimental study of NOx removal. The work has been carried out on simulated flue gas and diesel engine exhaust gas as feed gases. Several gas conditions were investigated. Various kinds of plasma reactors were studied to treat pollutant gases. With the dry reactor, addition of hydrocarbons (ethylene) was carried out and it was effective to enhance the NOx oxidation particularly for gas temperatures above 200 °C. Wet type plasma reactor was developed to enhance the NOx removal efficiency. This reactor was also effective for NOx removal since NO_2 which was produced under plasma discharge was soluble. Also ozone injection method was conducted to save the energy required to remove NOx.

Energy considerations were studied to estimate these techniques suited for practical use of gas cleaning. Calculation results showed that with addition of hydrocarbons (ethylene), use of semi-wet or wet reactors, instead of dry reactor, significantly decreased the power consumption. This suggested that energy efficiency can be improved by one of these methods described above. Use of ozonizer gives better energy efficiency compared to the discharge plasma. However to treat soot and particle matters simultaneously, pulse voltage application which had electrostatic precipitator effect could be required. Therefore idea are necessary for whole systems that include type of gas, purpose of purification level etc.

Not only from the view point of the energy efficiency, but also from the point of treating stable gas such as N_2O, a low temperature reactor was developed. With liquid nitrogen as cooling agent, both NOx and N_2O were clustered and removed with plasma discharge. The addition of hydrocarbons further improved the NOx removal efficiency. Also the discharge plasma can be used to treat very low concentration gas components such as cigarette smoke. Particles from cigarette smoke were removed from simulated gas at very high removal efficiency. However,

the recycle and purification of the absorbent of the wet reactor was desirable. The discharge plasma is thus an effective method not only for pollutant gas cleaning but also for the deodorization.

Power consumption for NOx treatment with ozone injection method was almost half of that with pulsed plasma treatment. However these values do not contain cooling energy for ozone generation. Therefore for net power consumption in NOx treatment with ozone injection, this cooling energy must be considered.

From the present work, it can be concluded that the wet type reactor is the most efficient one to treat the pollutant gases (within the range of this study) from the point of power consumption. For real exhaust gas treatment, soot or dust particles have to be collected and ozone injection method may not be suitable for treating these dusts. Pulsed plasma treatment which has precipitation effect must be used in such cases.

By-product analysis using FTIR confirmed safety of the addition of the hydrocarbons. Some simple aldehyde species and carbon dioxide were found out as by-products. No hazardous gas such as HCN, was detected. From this by-product analysis result, hydrocarbons is considered to be oxidized to produce CO_2, H_2O and other relatively stable acid species. From the proposed chemical reactions between NOx and hydrocarbons, it can be concluded that hydrocarbons plays an important role not only to enhance the NOx removal but also to produce other radicals in their recycle reaction processes to react with each other.

. To conclude, this work, hopefully, will make a contribution on the development of non-thermal plasma technique and will be realized to solve the various environmental problems in near future.

REFERENCES

[1] O. Tokunaga and N. Suzuki, "Radiation Chemical Reactions in NOx and SO_2 Removals from Flue Gas", Radiat. Phys. Chem., vol. 24, pp. 145-165, 1984.

[2] N. W. Frank and S. Hirano, "The history of electron beam processing for environmental pollution control and work performed in the united statre", Non-Thermal Plasma Techniques for Pollution Control-Part B, Springer-Verlag Pub., pp.1-26, 1993.

[3] A. Maezawa and M. Izutsu, "Application of E-beam treatment to flue gas cleanup in Japan", Non-Thermal Plasma Techniques for Pollution Control-Part B, Springer-Verlag Pub., pp.47-54, 1993.

[4] H.R. Paur, "Removal of volatile hydrocarbons from industrial off-gas", Non-Thermal Plasma Techniques for Pollution Control-Part B, Springer-Verlag Pub., pp.77-90, 1993.

[5] H. Scheytt, H. Esrom, L. Prager, R. Mehnet, and C. von Sonntag, "Ultraviolet light and electron beam induced degradation of trichloroethene", Non-Thermal Plasma Techniques for Pollution Control-Part B, Springer-Verlag Pub., pp.91-102, 1993.

[6] A. Mizuno, J. S. Clements, and R. H. Davis, "A Device for The Removal of Sulfur Dioxide from Exhaust Gas by Pulsed Energization of Free Electrons", Conf. Rec. of IEEE/IAS Annual Meeting, pp.1015-1020, 1984.

[7] S. Masuda and H. Nakao, " Control of NOx by Positive and Negative Pulsed Corona Discharges", in Conf. Rec IEEE/IAS Annual Meeting, pp. 1173-1182, 1986.

[8] J. S. Clements, A. Mizuno, W.C. Finney, and R. H. Davis, "Combined Removal of SO_2, NOx, and Fly Ash from Simulated Flue Gas Using Pulsed streamer corona", IEEE Trans. Ind. Appl., vol. 25, pp. 62-69, 1989.

[9] G. Dinelli, L. Civitano, and M. Rea, "Industrial Experiments on Pulse Corona Simultaneous Removal of NOx and SO_2 from Flue Gas", IEEE Trans. Ind. Appl., vol. 25, pp. 535-541, 1990.

[10] T. Ohkubo, S. Kanazawa, Y. Nomoto, J. S. Chang, and T. Adachi, "Time dependence of NOx removal rate by a corona radical shower system", in Conf. Rec. of IEEE/IAS Annual Meeting, pp. 1570-1574, 1994.

[11] T. Oda, T. Takahashi, H. Nakano, and S. Masuda, "Decomposion of fluorocarbon gaseous cntaminants by surface discharge-induced plasma chemical processing", IEEE Trans. Ind. Appl., vol. 29, pp. 787-792, 1993.

[12] K. Jogan, A. Mizuno, T. Yamamoto, and J. S. Chang, "The effect of residence time on the CO_2 reduction from combustion flue gases by an AC ferroelectric packed bed reactor", IEEE Trans. Ind. Appl., vol. 29, pp. 876-881, 1993.

[13] T. Yamamoto, K. Ramanathan, P. A. Lawless, D. S. Ensor, J. R. Newsome, G. H. Ramsey, and N. Plaks, "Control of volatile organic compounds by an AC energized ferroelectric pellet reactor and a pulsed corona reactor", IEEE Trans. Ind. Appl., vol. 28, pp. 528-534, 1992.

[14] J. S. Chang, "Energetic Electron Induced Plasma Processes for Reduction of Acid and Greenhouse Gases in Combustion Flue Gas", Non-Thermal Plasma Techniques for Pollution Control-Part A, Springer-Verlag Pub., pp.1-32, 1993.

[15] L. Civitano, "Industrial application of pulsed corona processing to flue gas", Non-Thermal Plasma Techniques for Pollution Control-Part B, Springer-Verlag Pub., pp.103-130, 1993.

[16] T. Yamamoto, P. A. Lawless, M. K. Owen, D.S. Ensor, and C. Boss, "Decomposition of volatile organic compounds by a packed-bed rector and a pulsed-corona plasma reactor", Non-Thermal Plasma Techniques for Pollution Control-Part B, Springer-Verlag Pub., pp.223-238, 1993.

[17] Handbook of electrical discharge, Inst. of Elect. Engineers Japan, p.263 ,1973.

[18] K. Fujii, M. Sugaya, R. Tsuji, Y. Yokosawa, and M. Higashi, "Plasma Creation for Efficient NOx Reductions in Exhaust Gas from A Diesel Engine", 8th Int. Symp. Plasma Chem., Tokyo, pp. 840-844, 1987.

[19] B. Eliasson, F. G. Simon, and W. Egli, "Hydrogenation of CO2 in a silent discharge", Non-Thermal Plasma Techniques for Pollution Control-Part B, Springer-Verlag Pub., pp. 321-338, 1993.

[20] U. Kogelschatz, "UV production in dielectic barrier discharges for pollution control", Non-Thermal Plasma Techniques for Pollution Control-Part B, Springer-Verlag Pub., pp. 339-355, 1993.

[21] A. Mizuno, Y. Yamazaki, H. Ito, H. Yoshida, "AC Energized Ferroelectric Pellet Bed Gas Cleaner", IEEE Trans. on IAS, Vol.28, No.3, p.535-540, 1992.

[22] T. Yamamoto, K. Mizuno, I. Tamori, A. Ogata, M. Nifuku, M. Michalska, and G. Prieto, "Catalysis-assisted plasma technology for carbon tetrachloride destruction", in Conf. Rec. of IEEE/IAS Annual Meeting, pp. 1556-1562, 1994.

[23] S. Futamura, T. Yamamoto, and P. A. Lawless, "Towards understanding of VOC decomposition mechanisms using non-thermal plasmas", in Conf. Rec. of IEEE/IAS Annual Meeting, pp. 1453-1458, 1995.

[24] S. Masuda et. al., "Characteristics of Ceramic Ozonizer Using Surface Discharge", Proc. Inst. of Electrostatics Jpn., pp.174-177, 1985.

[25] T. Oda, R. Yamashita, T. Takahashi, and S. Masuda, "Atmospheric Pressure Discharge Plasma Processing for gaseous air contaminants", in Conf. Rec. of IEEE/IAS Annual Meeting, pp. 1983-1988, 1993.

[26] T. Oda, R. Yamashita, and T. Takahashi, "Studies on atmospheric low temperature discharge plasma decompositon of VOCs", in Conf. Rec. of IEEE/IAS Annual Meeting, pp. 1440-1444, 1995.

[27] K. Tamaki, et al. "Effect of Discharge Mode of DC Corona on Oxidization of Carbon Oxide", in Proc. Chem. Soc. Japan, vol. 11, p. 1582-1588, 1979.

[28] T. Adachi, "Absorption of SO_2 in A Wet-Type Electrostatic Precipitator- Effect of Ionic Wind", J. of IEEJ-B, 63, p.512-517, 1977.

[29] I. Gallimberti, "Impulse corona simulation for flue gas treatment", Pure & Appl. Chem., Vol. 60, No. 5, pp. 663-674, 1988.

[30] E. Nasser, "Fundamentals of gaseous ionization & plasma electronics", John Wiley & Sons, Inc, 1971.

[31] J. M. Meek, and J. D. Craggs, "Electrical breakdown of gases", John Wiley & Sons, Inc, 1978.

[32] Sanborn C. Brown, "Basic data of plasma physics", The technology press, John Wiley & Sons, Inc., 1959.

[33] K. Yan, E. M. van Veldjuizen, A. H. F. M. Baede, Y. L. M. Creyghton, W. R. rutgers, "Electron energy for primary and secondary streamers of pulsed corona in relation with flue gas cleaning", in Conf. Rec. of 11th Intl. Symp. on Plasma Chemistry in U. K., 1993.

[34] T. H. Teich and M. Jacob, "Optical diagnostics of some reactions in corona discharges", in Conf. Rec. of 11th Intl. Conf. on Gas Discharge and their applications in Tokyo, Jpn., vol. I, pp. 172-175, 1995.

[35] E. M. van Veldhuizen, A. H. F. M. Baede, Y. L. M. Creyghton, W. R. Rutgers, and K. Yan, "Electrical and spectroscopic investigation of positive pulse corona in air and in flue gas", in Conf. Rec. of 6th Asian Conf. on Electrical Discharge in Oita, Jpn, pp.1-4, A-1, 1993.

[36a] M. P. Sarma and W. Janischewskyj, " DC corona on smooth conductors in air", Proc. IEE, Vol. 116, No. 1, pp. 161-166, 1969.

[36b] M. Ogasawara, "Analysis of formation stage of corona discharge", J. Phys. Soc. Japan, Vol. 21, No. 11, pp. 2360-2372, 1966.

[36c] B. S. Rajanikanth, and B. R. Prabhaker, "Modeling of prebreakdown VI characteristics of a wire-plate electrostatic precipitator operating under combined dc-pulse energization", IEEE Trans. on DEI, vol. 1 No. 6, pp. 1058-1067, 1994.

[36d] S. Oglesby, Jr. and G. B. Nichols, Electrostatic Precipitation, Marcel Dekker Inc., NY, USA, 1978.

[36e] G. N. Aleksandrov, "On the nature of current pulses of a negative corona", Sov. Phys. Tech. Phys., Vol. 8, No. 2, pp. 161-166, 1963.

[37] Y. Kamase, M. Shimizu, T. Nagahama, and A. Mizuno, "Pulsed high voltage source for ozone generator", in Conf. Rec. of IEEE/IAS Annual Meeting, pp. 693-697, 1991.

[38] Sanborn C. Brown, "Introduction to electric discharges in gases", John Wiley & Sons, Inc., p. 7, 1966.

[39] R. B. Brode, Rev. Mod. Phys., Vol. 5, 257, 1933.

[40] T. H. Teich, "Emission spectroscopy of corona discharges", Non-Thermal Plasma Techniques for Pollution Control-Part A, Springer-Verlag Pub., pp. 231-248, 1993.

[41] T. Yoshida, F. Tochikubo, and T. Watanabe, "Diagnostics of pulsed corona discharge for DeNOx process", in Conf. Rec. of 11th Intl. Conf. on Gas Discharge and their applications in Tokyo, Jpn., vol. II, pp. 410-413, 1995.

[42] Y. L. M. Creyghton, E. M. van Veldhuizen, W. R. Rutgers, "Streamer charracteristics of positive pulsed corona", in Conf. Rec. of 10th Intl. Symp. on Plasma Chemistry, pp.1-6, 1991.
[43] M. B. Awad and G. S. P. Castle, APCA Journal, Vol. 25, pp. 369-374, 1975.
[44] G. S. P. Castle, I. I. Inculet and K. I. Burgess, IEEE Trans., Vol. IGA-5, pp. 489-496, 1969.
[45] R. Peyrous and C. Lacaze, Ozone Science & engineering.
[46] K. Shitara, M. Shimizu, K. Yamamoto, O. Hara and A. Mizuno, Proc.12th Ozone World Congress, 1993.
[47] R. Peyrous and R. -M.Millot, Gas Disch. Conl.Proc., pp.173-176, 1982.
[48] A. Goldman and J. Amouroux, "Plasma Chemistry" in Electrical Breakdown and Discharges in gases: Pt B : Macroscopic Processes and Discharges (eds. Kunhard and Luessen), New York, Plenum, pp. 293-346, 1983.
[49] L. B. Loeb, Electrical Coronas, Univ. of California Press, Berkely, 1965.
[50] B. Eliasson, M. Hirth and U. Kogelshaty, J. Phys.D. Appl. Phys., Vol. 20, pp. 1421-,1987.
[51] Y. Nomoto, T. Okhubo, S. Kanazawa and T. Adachi, IEEE-IAS Conf. Record, pp. 1995-1999, 1993.
[52] M.Khaliba, "Electrical Coronas" in High Voltage Engineering: Theory and Practice", Marcel Dekker, New York, 1990.
[53] B. Makin and I. I. Inculet, IEEE-IAS Conf. Record, pp. 381-389, 1973.
[54] M. Khalifa, M. Abdel-Salam and M. Abon-Seada, IEEE-PES paper, 1973.
[55] A. S. Viner, Ph. A. Lawless, D. S. Ensor and L. E. Sparks, IEEE Trans, IA Vol. 28, pp. 504-512, 1992.
[56] B. Eliasson and U. Kogelschatz,"Basic data for modelling of electrical discharges in gases: oxygen", Brown Boveri forschungszentrum, CH-5405 Baden, Jun., 1986
[57] S. Masuda and W. Yan, "Removal of NOx from combustion gas by corona discharge induced by very sharp pulse voltage, "Proc. Inst. Electrostat. Jpn., vol.12,pp 277-283, 1988(in Japanese).
[58] T. Matsuoka, K. Shimizu, and A. Mizuno, "NOx removal using a water-filmed electrostatic precipitator," in Proc. 1992 Ann. Meeting

Inst. Electrostat. Jpn., Tokyo, Oct. 20-22, 1992, pp.495-498(in Japanese).
[59] A.Chakrabarti, A.Mizuno, K.Shimizu, T.Matsuoka, and S. Furuta, "Gas Cleaning with a Puls-Energized Semi-Wet Type Plasma Reactor", in Conf.Rec.IEEE/IAS Annual Meeting pp.1989-1994, 1993.
[60a] J.S.Chang, "The role of H_2O and NH_3 on the formation of NH_4NO_3 aerosol particles and De-NOx under the corona discharge treatment of combustion flue gases," J. Aerosol Sci., Vol. 20, No.8, pp.1087-1090, 1989.
[60b] J. S. Chang and S. Masuda, "Mechanism of pulse corona induced plasma chemical process for removal of NOx and SO2 from combustion gases", in Conf.Rec.IEEE/IAS Annual Meeting pp. 1628-1635, 1988.
[61] A.L.Goldsmith, N.S. Holt, and A.P. Jeapes, "Removal of iodine from nuclear fuel reprocessing plant off-gases by corona discharge," Joint Int. Waste Management Conf. Oct. 29, 1991
[62] A. Chakrabarti, A. Mizuno, K. Okazaki, E. Suzuki, and S. Furuta, "Removal of N_2O from simulated flue gas," in Proc.1992 Annual Meeting of IESJ, pp.1-5, 1992.
[63] A. Mizuno, S. Katsura, K. Shimizu, M. Okumoto and B. S. Rajanikanth, "Study of energy efficiency hydrocarbon fuels by plasma chemical reaction process," Report on regeneration, Fukuoka, Japan, p12, 1995 *(aided by the ministry of education, science and culture, Japan, under the scheme grant-in-aid for scientific research on priority areas, No: 06246103).*
[64] A. Mizuno, K. Shimizu, T. Matuoka, and S. Furuta, "Reactive absorbtion of NOx using discharge plasma," in Conf. Rec. IEEE IAS Annual Meeting pp.1550-1555, 1994.
[65] A. Watanabe, "Generation and measurements of particles in plasma CVD processes for semiconductor-manufacturing,", Journal of aerosol research, Japan, vol. 10, No. 1, pp.13-19, 1995.
[66] S. Masuda , S. Hosokawa, X. L. Tu, K. Sakakibara, S. Kitoh, and S. Sasaki, "Destrucion of gaseous pollutants by surface-induced plasma chemical processes (SPCP)", IEEE Trans. on IAS, Vol. 29, No. 4, pp.781-786, 1993.
[67] K. Shimizu, K. Tsunoda, and A. Mizuno, "NOx removal using wet-type plasma reactor", in Proc. 1995 Ann. Meeting Inst. Electrostat. Jpn., 1995, pp.387-390(in Japanese).

[68] K. Okazaki, A. Mizuno, K. Shimizu and T. Niwa, "Application of semi-wet type corona discharge reactor to the simulteneous removal of NO_X, SO_X and fly ash in pulverized coal combustion", presented at Int. Conf. on power Eng.-93, Sep. 12-16, 1993, Tokyo, Jpn.

[69] A. Mizuno, J. S. Clements and R. H. Davies, "A method for the removal of sulpher dioxide from exhaust gas utilizing pulsed streamer corona for electron energization", IEEE Trans. on IAS, Vol. 22, No. 3, pp. 516 - 522, 1986.

[70] H. Yoshida, Z. Marui, M. Aoyama, J. Sugira and A. Mizuno, "Removal of odor gas component utilizing plasma chemical reactions promoted by the partial discharge in a ferroelectric pellet layer," *IES Japan*, 13, 5, pp.425-430, 1989

[71] S. J. Scott, "A long life, high repetition rate electron beam source", Non-Thermal Plasma Techniques for Pollution Control-Part A, Springer-Verlag Pub., pp. 339-344, 1993.

[72] S. Pekarek, J. Rosenkranz, and H. Lonekova, "Generation of electron beam for technological processes", Non-Thermal Plasma Techniques for Pollution Control-Part A, Springer-Verlag Pub., pp. 345-354, 1993.

[73] B. M. Penetrante, "Plasma Chemistry And Power Comsumption in Non-thermal DeNOx", Non-Thermal Plasma Techniques for Pollution Control, Part A, Springer-Verlag Pub., Oxford, pp.65-89, 1993.

[74] G. E. Vogtlin and B. M. Penetrante, "Pulsed corona discharge for removal of NOx from flue gas", Non-Thermal Plasma Techniques for Pollution Control, Part B, Springer-Verlag Pub., Oxford, pp.187-198, 1993.

[75] R. Atkinson, "Kinetics and mechanisms of the gas-phase reactions of the hydroxyl radical with organic compounds under atmospheric conditions", Chem. Rev. Vol. 86, 69, 1986.

[76] S. Furuta, "Nitrogen oxide removal utilizing discharge plasma chemical reaction", Master's thesis, Toyohashi Univ. Tech., 1994, (in Japanese).

[77] R. Atkinson, and J. N. Pitts Jr., "Absolute rate constants for the reaction of $O(^3P)$ atoms with allene, 1, 3-butadience, and vinyl methyl ether over the temperature range 297-439 K", J. Chem. Phys., Vol. 67, 2493, 1977.

[78a] S. Suzuki, Y. Yamamoto, "Photochemistry of atmosphere", Tokyo University Press, 1979.

[78b] H. Mätzing, "Chemical kinetics of flue gas cleaning by irradiation with electrons", Advances in Chemical Physics Volume LXXX, John Wiley & Sons. Inc., pp. 315-402, 1991.

[79] S. Kawabata, Y. Mochizuki, and T. Misaka, "Gas cleaning technique by pulse corona discharge", IEJ symposium 1995 on non-thermal plasma technique for pollution control, pp. 72-76, 1995

[80] P. A. Vitello, B. M. Penetrante, and J. N. Bardsley, "Simulation of negative-streamer dynamics in nitrogen", Phys. Rev. E, Vol. 49, No. 6, pp. 5574-5598, 1994.

[81] N. Yu. Babaeva and G. V. Naidis, "2D model of streamer porpagation in nonuniform electric fields", in Conf. Rec. of 11th Intl. Conf. on Gas Discharge and their applications in Tokyo, Jpn., vol. II, pp. 488-491, 1995.

[82] D. Djermounve, S. Samson, E. Marode, and P. Ségur, "A time resolved two dimensional modelling of the electrical behaviour and the chemical yield of streamer induced discharge", in Conf. Rec. of 11th Intl. Conf. on Gas Discharge and their applications in Tokyo, Jpn., vol. II, pp. 484-487, 1995.

ACKNOWLEDGMENTS

I am highly indebted to my guide Professor Akira Mizuno for suggesting an interesting and a challenging research problem. I wholeheartedly thank him for his fruitful advice and guidance throughout my research work.

I would also like to thank Prof. Masamitsu Kosaki, Prof. Tateki Sakakibara, and Prof. Kazuo Onda judging my thesis and giving me beneficial opinions.

I wish to express my thanks to Dr. Shinji Katsura for his valuable suggestions on plasma chemical reactions and for constantly encouraging me in my research career.

I wish to thank Prof. Ken Okazaki of Tokyo Institute of Technology for providing me the working facilities related to coal exhaust gas treatment experiment and for his valuable discussions.

I would like to express my thanks to Prof. Jae-Duk Moon of Kyungpook National University, Korea for his fruitful discussions.

My sincere thanks belong to Assistant Prof. Saburo Tanaka and Dr. Yukiko Matsuzawa, for providing me the useful information.

I wish to express my thanks to Prof. Lucian Dascalescu, Dr. Alok Chakrabarti, and Professor Mazen Abdel-Salam for guiding me during the course of my experiments and giving me useful suggestions.

Thanks are also extended to my close colleague Mr. Masateru Nishioka who has provided constant encouragement all along my stay in this university.

I am grateful to my co-workers Mr. Yasuo Sakaguchi, Mr. Hiroaki Nagura, Mr. Hideki Yamamoto, Mr. Satoshi Furuta, Mr. Tsutomu Matsuoka, Mr. Hiroyuki Sone, Mr. Thoru Miyamoto, Mr. Kouich Fukuta, Mr. Katsuhiro Kinoshita, Mr. Kenya Yanagihara, Mr. Seigo Sakata, and Mr. Mamoru Okumoto, for their extensive help in making and carrying out the experiments and supporting me throughout my work. Furthermore, I owe a great deal of gratitude to Mr. Kazuhiko Tsunoda for helping me not only in the experiments but also in drawing the figures.

Thanks are also due to my senior co-workers, Mr. Sadami Obama and Mr. Eiki Suzuki for providing a moral support during my stay at the university.

Thanks are also extended to Dr. Tomonori Kawakami of Hamamatsu Photonics K. K. and Mr. Tetsuo Horino of Amano Co.

My gratitude is also given to Dr. B. S. Rajanikanth for helping me in writing and revising this thesis.

Assistant Prof. Xilu Wang, Mr. Masato Kurahashi, they are members of our laboratory and also good friends of mine, supporting and cheering me up the during this laboratory life. My thanks to them.

Finally, I would like to express my sincere thanks to my parents for their understanding and economic support.

APPENDIX I

A.1 Classical models of reactions concerned to NOx

A.1.1 Plasma chemical reactions of NOx in air

The chemical reactions promoted by pulsed plasma discharge are usually significantly affected by the gas temperature as explained in section 3.3. The chemical reactions are processed by oxidizing agent or radical species such as O_3, O, OH etc. In the non-thermal plasma abundant electrons are generated. Even though the electrons are short lived under atmospheric pressure and rarely collide with a pollutant molecule, they undergo many collisions with the dominant background gas molecules, thus producing radicals which lead to the decomposition of the toxic molecules. The efficiency of the decomposition arises from the fact that the radicals have long lifetimes and react selectivlely with the pollutant molecules.

Classical models of discharge chemistry are based on the fact that the electron is the main source of radical generations as indicated in the following reactions:

$$O_2 + e \text{ ---> } O^* + O^* + e \quad \text{(A1.1)}$$

$$N_2 + e \text{ ---> } N^* + N^* + e \quad \text{(A1.2)}$$

The following reactions occur rarely because of the relatively low NO density when compared to the other background gas.

$$NO + e \text{ ---> } N^* + O^* + e \text{ (electron impact dissociation)} \quad \text{(A1.3)}$$

$$\text{---> } N^+ + O + 2e \text{ (dissociative ionization)} \quad \text{(A1.4)}$$

$$\text{---> } NO^+ + 2e \text{ (ionizaions)} \quad \text{(A1.5)}$$

$NO + e + N_2 \text{ ---> } NO^- + N_2$ (three body attachment) (A1.6)

$NO^+ + e \text{ -> } N + O$ (dissociative recombination) (A1.7)

$NO^- + NO^+ + M \text{ ---> } N_2 + O_2 + M$ (A1.8)
(three body recombination)

The radical particles formed will be reacting with each other to generate active species such as O_3, OH etc. which in turn help in the removal of NOx. The possible radical reactions are NO to NO_2 conversion as shown:

$NO + O + M \text{ ---> } NO_2 + M$ ($k= 6.9 \times 10^{-32}$ cm^6/s) (A1.9)

$NO + O_3 \text{ ---> } NO_2 + O_2$ ($k= 1.8 \times 10^{-14}$ cm^3/s) (A1.10)

Where k is the reaction rate. This being followed by O and O_3 productions via electron impact processes. Net loss of NO and NO_2 can be, thus explained and the associated are:

$NO + N^* \text{ ---> } N_2 + O$ ($k= 5.9 \times 10^{-11}$ cm^3/s) (A1.11)

$NO + NO^+ \text{ ---> } N_2 + O_2^+$ ($k= 4.5 \times 10^{-10}$ cm^3/s) (A1.12)

$NO_2 + O \text{ ---> } NO + O_2$ ($k= 6.3 \times 10^{-12}$ cm^3/s) (A1.13)

$NO_2 + N^* \text{ ---> } 2NO$ ($k= 9.0 \times 10^{-12}$ cm^3/s) (A1.14)

$NO_2 + O_3^- \text{ ---> } NO_3^- + O_2$ ($k= 2.8 \times 10^{-10}$ cm^3/s) (A1.15)

and other associated ion-molecule reactions. N* indicates the electronically excited nitrogen species. As shown in the previous session, decomposition of NO_2 could be very less. However, O_3 can oxidize or decompose NO_2 when O_3 concentration is at least 2 times higher than that of NO.

More recently, it was suggested that radical species can be generated through the dissociative recombination of the positive and negative species via formations of ion-molecular reactions. The order of the two body reaction rate for electron-ion related reaction is 10 to 10^8 times larger compared with neutral species. The effective production or

loss of each species becomes comparable in spite of the density of ions being much less than neutral species as shown in Table A.1.

TABLE A.1 REACTION RATE EQUATION FOR NEUTRAL AND IONIC EQUATIONS

$$\frac{\partial N}{\partial t} = K_1[A][B] + K_2[C^+][B] - \cdots$$

$$A + B \xrightarrow{K1} N + M \qquad [A] \gg [C^+]$$

$$C^+ + B \xrightarrow{K2} N + L \qquad K_1 \ll K_2$$

$$K_1[A] \approx K_2[C^+]$$

A.1.2 Atomic and molecule processes in a N_2-O_2-NOx mixtured ionized gas

For the N_2-O_2-NOx mixtured gas, the radical reactions are summarized in Fig. A.1.1. The existence of NH_3 will generate HNO_m (m= 0 to 3) free radicals shown in the figure. Formation and loss of NO gas is summarized in Fig. A.1.2. It is clear that the NO will be converted into NO_2 without NH_3 gas, and depend on the concentration of oxygen free radicals and gas pressure, NO will be generated or eliminated by gas discharges.

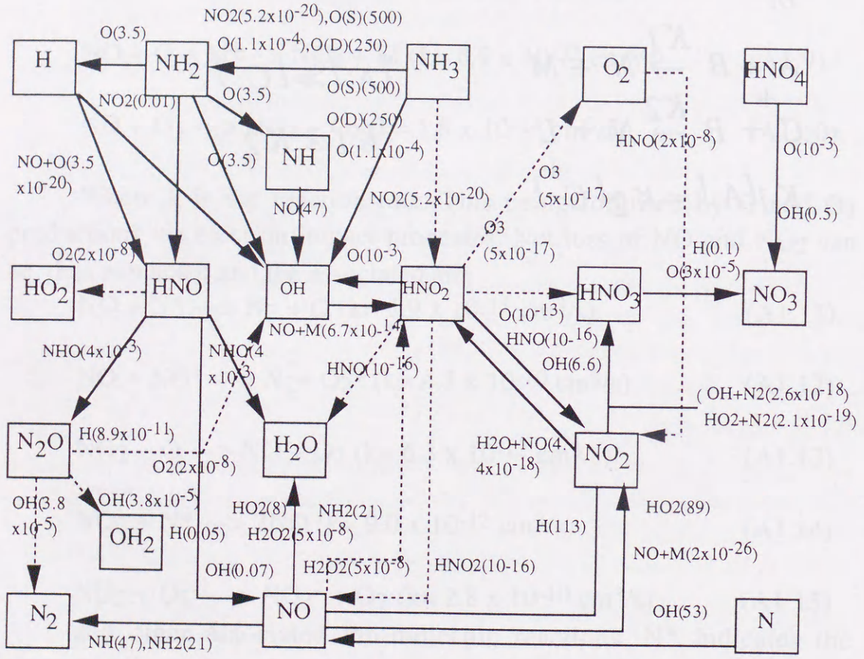

Fig. A.1.1 Radical reactions for N2-O2-NOx system.

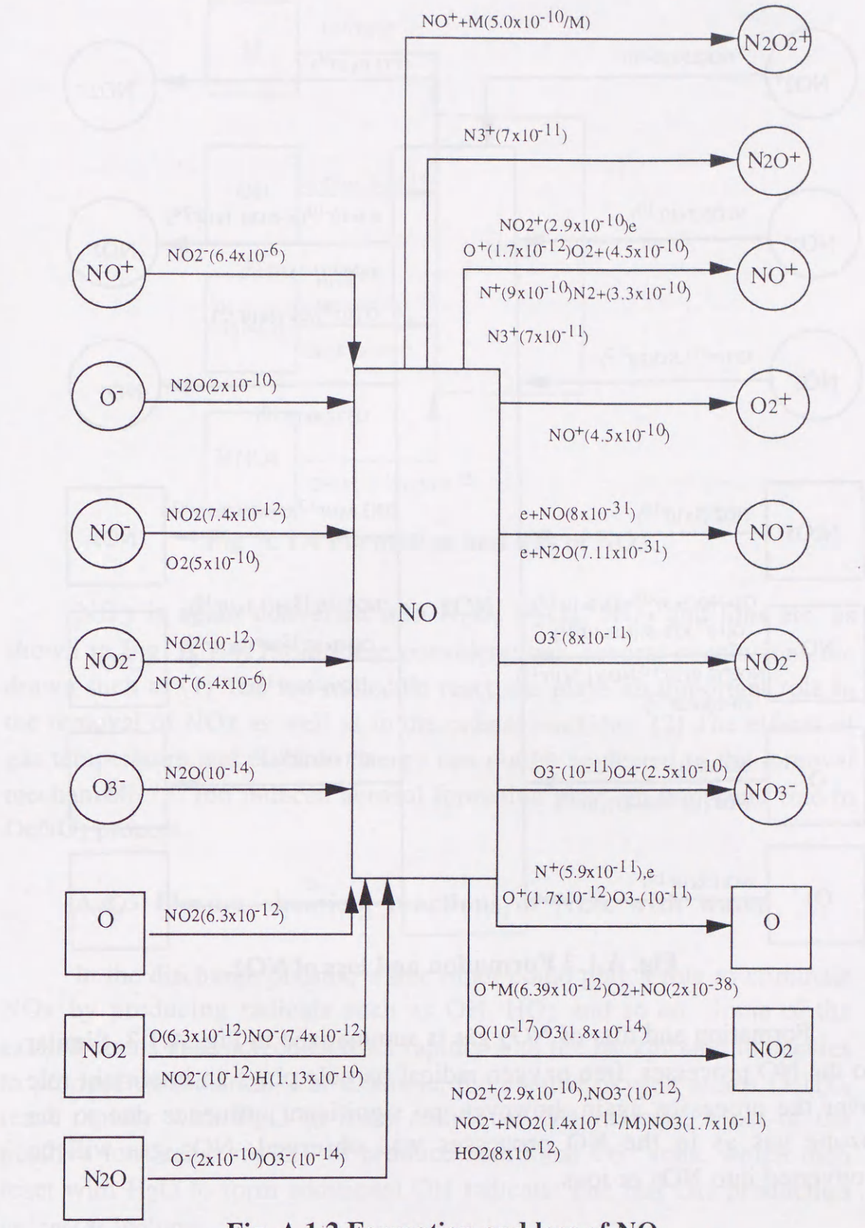

Fig. A.1.2 Formation and loss of NO.

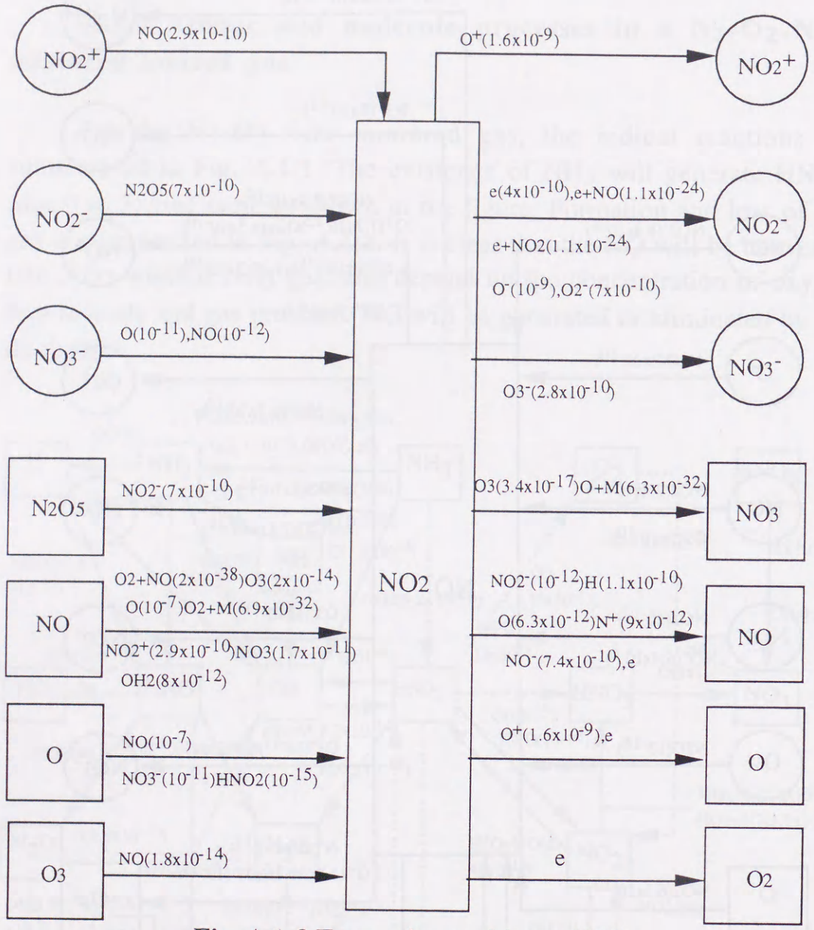

Fig. A.1.3 Formation and loss of NO_2.

Formation and loss of NO_2 gas is summarized in Fig. A.1.3. Similar to the NO processes, free oxygen radical particle plays an important role over the processes again, however, no significant influence due to the ozone gas as in the NO processes was observed. NO_2 gas will be converted into NO_3 or ions.

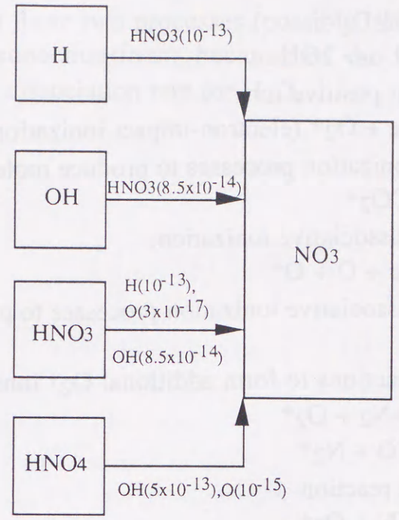

Fig. A.1.4 Formation and loss of NO_3.

NO_3 is again converted into N_2O, N_2O_5, NO_2 and ions etc. as shown in Fig. A.1.4. From these considerations, several conclusions are drawn such as:(1) The ion-molecule reactions plays an important role in the removal of NOx as well as in the radical reactions; (2) The effects of gas temperature and electron energy can not be neglected in the removal mechanism; (3) Ion induced aerosol formation plays an important role in $DeNO_2$ process.

A.1.3 Plasma chemical reactions of NOx with water

In the discharge plasma, water vapor could play a role to eliminate NOx by producing radicals such as OH, HO_2 and so on. Some of the excited atoms and molecules react rapidly with the background molecules to produce dissociation. For example, the excited oxygen atoms O(1D), react rapidly with H_2O to form additional OH radicals. Most of the positive ions react rapidly to produce additional O_2^+ ions, which then react with H_2O to form additional OH radicals. The fast OH production processes include:

Electron attachment:

$$e + H_2O \text{ ---> } H^- + OH \qquad \text{(A1.16)}$$

Direct dissociation by electron impact:

$$e + H_2O \text{ --->} e + H + OH \qquad \text{(A1.17)}$$

Dissociation by $O(^1D)$

$O(^1D) + H_2O$ ---> 2OH (A1.18)

Contribution from positive ions

$e + O_2$ ---> $2e + O_2^+$ (electron-impact ionization) (A1.19)

and similar ionization processes to produce molecular ions N_2^+, H_2O^+, CO_2^+

Electron-impact dissociative ionization:

$e + O_2$ ---> $2e + O + O^+$ (A1.20)

and similar dissociative ionization processes to produce N^+, H^+

Charge transfer reactions to form additional O_2^+ ions:

$N_2^+ + O_2$ --->$N_2 + O_2^+$ (A1.21)

also $O^+ + N_2$ ---> $O + N_2^+$ (A1.22)

followed by above reaction

$N^+ + O_2$ ---> $N + O_2^+$ (A1.23)

$O^+ + O_2$ ---> $O + O_2^+$ (A1.24)

$H^+ + O_2$ ---> $H + O_2^+$ (A1.25)

$N_2^+ + CO_2$ ---> $N_2 + CO_2^+$ (A1.26)

and $N^+ + CO_2$ --->$N + CO_2^+$ (A1.27)

and $H^+ + CO_2$ ---> $H + CO_2^+$ (A1.28)

followed by $CO_2^+ + O_2$ ---> $CO_2 + O_2^+$ (A1.29)

Formation of water cluster ions:

$O_2^+ + H_2O$ ---> $O_2^+(H_2O)$ (A1.30)

Dissociative reactions of water cluster ions to form OH

$O_2^+(H_2O) + H_2O$ ---> $H_3O^+ + O_2 + OH$ (A1.31)

---> $H_3O^+(OH) + O_2$ (A1.32)

followed by

$H_3O^+(OH) + H_2O$ ---> $H_3O^+ + H_2O + OH$ (A1.33)

The corresponding reverse reactions are small. Electronically excited states of nitrogen, such as $N_2(A^3\Sigma_u^+)$, could not also lead to the dissociation of H_2O. However, this reaction is slower and there are more competing processes for quenching the electronically excited N_2 molecules; nevertheless, the reactions of excited species are included in the chemical kinetics calculations.

In all the reactors studied, it was observed that only if the simulated gas or exhaust gas contains water vapor, then the OH radicals are formed both by electrons and by excited oxygen atoms from direct dissociation of H_2O. But there is still a large uncertainty in evaluating the relative

contributions of these two processes (possibly, these are functions of the O_2 and H_2O concentrations) because of the limited knowledge of electron-impact dissociation rate for H_2O.

APPENDIX II

A.2 Data representation

During the plasma discharge treatment, various chemical reactions take place. The typical reactions concerning NOx removal in air are shown below. These include positve ion and neutral reactions, negative ion and neutral reactions, ionic recombinations in the gas phase, and reactions of excited species.

A.2.1 Positive ion - neutral reactions

1	$N_2^+ + O_2$	$\rightarrow O_2^+ + N_2$	$K= 3.9\times10^{-10}\exp(-T/143)$
2	$N_2^+ + O_2$	$\rightarrow NO^+ + NO$	$K= 1.0\times10^{-17}$
3	$N_2^+ + H_2O$	$\rightarrow H_2O^+ + N_2$	$K= 2.0\times10^{-9}$
4	$N_2^+ + CO_2$	$\rightarrow CO_2^+ + N_2$	$K= 8.3\times10^{-10}$
5	$N_2^+ + NO$	$\rightarrow NO^+ + N_2$	$K= 3.3\times10^{-10}$
6	$N_2^+ + NO_2$	$\rightarrow NO_2^+ + N_2$	$K= 3.0\times10^{-10}$
7	$N_2^+ + SO_2$	$\rightarrow SO_2^+ + N_2$	$K= 5.0\times10^{-10}$
8	$N_2^+ + NH_3$	$\rightarrow NH_3^+ + N_2$	$K= 1.9\times10^{-9}$
9	$N_2^+ + O_3$	$\rightarrow O_2^+ + O + N_2$	$K= 1.0\times10^{-10}$
10	$N_2^+ + H_2O$	$\rightarrow H_2O^+ + N_2$	$K= 3.0\times10^{-10}$
11	$N_2^+ + H_2$	$\rightarrow H_2^+ + N_2$	$K= 3.0\times10^{-10}$
12	$N_2^+ + CO$	$\rightarrow CO^+ + N_2$	$K= 7.0\times10^{-11}$
13	$N_2^+ + OH$	$\rightarrow OH^+ + N_2$	$K= 4.6\times10^{-10}$
14	$N_2^+ + H$	$\rightarrow H^+ + N_2$	$K= 2.5\times10^{-10}$
15	$N_2^+ + O$	$\rightarrow NO^+ + N$	$K= 1.4\times10^{-10}$
16	$N_2^+ + O$	$\rightarrow NO^+ + N(^2D)$	$K= 1.8\times10^{-10}(300/T)$
17	$N_2^+ + O$	$\rightarrow O^+ + N_2$	$K= 6.0\times10^{-12}$
18	$N_2^+ + N$	$\rightarrow N^+ + N_2$	$K= 1.0\times10^{-11}$
19	$N_2^+ + N + M$	$\rightarrow N_3^+ + M$	$K= 1.0\times10^{-29}(300/T)$
20	$N_2^+ + N_2 + M$	$\rightarrow N_4^+ + M$	$K= 5.0\times10^{-29}(300/T)$

21	$N^+ + O_2$	$\rightarrow NO^+ + O$	$K= 2.6\times10^{-10}$
22	$N^+ + O_2$	$\rightarrow N + O_2^+$	$K= 3.0\times10^{-10}$
23	$N^+ + O_2$	$\rightarrow O^+ + NO$	$K= 3.6\times10^{-11}$
24	$N^+ + H_2O$	$\rightarrow H_2O^+ + N$	$K= 2.4\times10^{-9}$
25	$N^+ + H_2O$	$\rightarrow NO^+ + H_2$	$K= 2.4\times10^{-10}$
26	$N^+ + CO_2$	$\rightarrow CO_2^+ + N$	$K= 1.3\times10^{-9}$
27	$N^+ + CO_2$	$\rightarrow CO^+ + NO$	$K= 2.5\times10^{-10}$
28	$N^+ + NO$	$\rightarrow NO^+ + N$	$K= 4.1\times10^{-10}$
29	$N^+ + NO$	$\rightarrow N_2^+ + O$	$K= 5.0\times10^{-11}$
30	$N^+ + NO_2$	$\rightarrow NO^+ + NO$	$K= 5.0\times10^{-10}$
31	$N^+ + NO_2$	$\rightarrow NO_2^+ + N$	$K= 3.0\times10^{-10}$
32	$N^+ + NH_3$	$\rightarrow NH_3^+ + N$	$K= 1.7\times10^{-9}$
33	$N^+ + O_3$	$\rightarrow NO^+ + O_2$	$K= 5.0\times10^{-10}$
34	$N^+ + N_2O$	$\rightarrow NO^+ + N_2$	$K= 5.5\times10^{-10}$
35	$N^+ + H_2$	$\rightarrow H_2^+ + N$	$K= 2.0\times10^{-10}$
36	$N^+ + CO$	$\rightarrow CO^+ + N$	$K= 4.9\times10^{-10}$
37	$N^+ + OH$	$\rightarrow OH^+ + N$	$K= 3.4\times10^{-10}$
38	$N^+ + OH$	$\rightarrow NO^+ + H$	$K= 3.4\times10^{-10}$
39	$N^+ + H$	$\rightarrow H^+ + N$	$K= 3.0\times10^{-10}$
40	$N^+ + O$	$\rightarrow O^+ + N$	$K= 1.0\times10^{-12}$
41	$N^+ + O + M$	$\rightarrow NO^+ + M$	$K= 1.0\times10^{-29}(300/T)$
42	$N^+ + N + M$	$\rightarrow N_2^+ + M$	$K= 1.0\times10^{-29}(300/T)$
43	$N^+ + N_2 + M$	$\rightarrow N_3^+ + M$	$K= 1.8\times10^{-29}(300/T)$
44	$O_2^+ + N_2$	$\rightarrow NO^+ + NO$	$K= 1.0\times10^{-16}$
45	$O_2^+ + NO$	$\rightarrow NO^+ + O_2$	$K= 3.5\times10^{-10}$
46	$O_2^+ + NO_2$	$\rightarrow NO_2^+ + O_2$	$K= 6.0\times10^{-10}$
47	$O_2^+ + NH_3$	$\rightarrow NH_3^+ + O_2$	$K= 2.4\times10^{-9}$
48	$O_2^+ + N_2O_5$	$\rightarrow NO_2^+ + NO_3 + O_2$	$K= 8.8\times10^{-10}$
49	$O_2^+ + N$	$\rightarrow NO^+ + O$	$K= 1.8\times10^{-10}$
50	$O_2^+ + 2O_2$	$\rightarrow O_4^+ + O_2$	$K= 2.8\times10^{-30}(300/T)$
51	$O_2^+ + H_2O + M$	$\rightarrow O_2^+(H_2O) + M$	$K= 2.8\times10^{-28}(300/T)$
52	$O^+ + N_2$	$\rightarrow N_2^+ + O$	$K= 9.0\times10^{-11}T^{-0.7}$
53	$O^+ + N_2$	$\rightarrow NO^+ + N$	$K=1.2\times10^{-12} + 5.4\times10^{-29}(300/T)M$
54	$O^+ + O_2$	$\rightarrow O_2^+ + O$	$K= 6.6\times10^{-10}T^{-0.55}$
55	$O^+ + H_2O$	$\rightarrow H_2O^+ + O$	$K= 2.7\times10^{-9}$
56	$O^+ + CO_2$	$\rightarrow O_2^+ + CO$	$K= 1.0\times10^{-9}$
57	$O^+ + NO$	$\rightarrow NO^+ + O$	$K= 1.0\times10^{-12}$
58	$O^+ + NO_2$	$\rightarrow NO_2^+ + O$	$K= 1.6\times10^{-9}$

59	$O^+ + NO_2$	$\rightarrow NO^+ + O_2$	$K= 5.0\times10^{-10}$
60	$O^+ + SO_2$	$\rightarrow O_2^+ + SO$	$K= 8.0\times10^{-10}$
61	$O^+ + NH_3$	$\rightarrow NH_3^+ + O$	$K= 1.2\times10^{-9}$
62	$O^+ + O_3$	$\rightarrow O_2^+ + O_2$	$K= 1.1\times10^{-10}$
63	$O^+ + N_2O$	$\rightarrow N_2O^+ + O$	$K= 5.0\times10^{-10}$
64	$O^+ + H_2$	$\rightarrow OH^+ + H$	$K= 1.8\times10^{-9}$
65	$O^+ + OH$	$\rightarrow OH^+ + O$	$K= 3.3\times10^{-10}$
66	$O^+ + OH$	$\rightarrow H^+ + O_2$	$K= 2.7\times10^{-11}(300/T)$
67	$O^+ + OH$	$\rightarrow O_2^+ + H$	$K= 3.6\times10^{-10}$
68	$O^+ + H$	$\rightarrow H^+ + O$	$K=6.8\times10^{-11}$
69	$O_2^+(H_2O) + H_2O$	$\rightarrow H_3O^+ + OH + O_2$	$K=2.0\times10^{-10}$
70	$O_2^+(H_2O) + H_2O$	$\rightarrow H_3O^+(OH) + O_2$	$K=1.5\times10^{-9}$
71	$O_2^+(H_2O) + NO_2$	$\rightarrow NO_2^+ + H_2O + O_2$	$K=3.0\times10^{-10}$
72	$O_2^+(H_2O) + NO$	$\rightarrow NO^+ + H_2O + O_2$	$K=1.0\times10^{-10}$
73	$H_2O^+ + O_2$	$\rightarrow O_2^+ + H_2O$	$K=2.6\times10^{-10}$
74	$H_2O^+ + H_2O$	$\rightarrow H_3O^+ + OH$	$K=1.7\times10^{-9}$
75	$H_2O^+ + NO$	$\rightarrow NO^+ + H_2O$	$K=6.0\times10^{-10}$
76	$H_2O^+ + NO_2$	$\rightarrow NO_2^+ + H_2O$	$K=3.0\times10^{-10}$
77	$H_2O^+ + NH_3$	$\rightarrow NH_3^+ + H_2O$	$K=2.2\times10^{-9}$
78	$H_2O^+ + NH_3$	$\rightarrow NH_4^+ + OH$	$K=9.0\times10^{-10}$
79	$H_2O^+ + H_2$	$\rightarrow H_3O^+ + H$	$K=8.7\times10^{-10}$
80	$H_2O^+ + OH$	$\rightarrow H_3O^+ + O$	$K=6.9\times10^{-10}$
81	$H_2O^+ + O$	$\rightarrow O_2^+ + H_2$	$K=5.5\times10^{-11}$
82	$H^+ + O_2$	$\rightarrow O_2^+ + H$	$K=1.2\times10^{-9}$
83	$H^+ + H_2O$	$\rightarrow H_2O^+ + H$	$K=8.2\times10^{-9}$
84	$H^+ + H_2O + M$	$\rightarrow H_3O^+ + M$	$K=2.7\times10^{-27}$
85	$H^+ + CO_2$	$\rightarrow CO_2^+ + H$	$K=1.2\times10^{-9}\exp(-1942/T)$
86	$H^+ + NO$	$\rightarrow NO^+ + H$	$K=7.0\times10^{-10}$
87	$H^+ + NO_2$	$\rightarrow NO_2^+ + H$	$K=3.0\times10^{-10}$
88	$H^+ + NH_3$	$\rightarrow NH_3^+ + H$	$K=5.2\times10^{-9}$
89	$H^+ + N_2O$	$\rightarrow N_2O^+ + H$	$K=3.0\times10^{-10}$
90	$H^+ + OH$	$\rightarrow OH^+ + H$	$K=2.0\times10^{-9}$
91	$H^+ + O$	$\rightarrow O^+ + H$	$K=3.8\times10^{-10}$
92	$H_2^+ + O_2$	$\rightarrow O_2^+ + H_2$	$K=8.0\times10^{-10}$
93	$H_2^+ + O_2$	$\rightarrow H_2O^+ + O$	$K=1.9\times10^{-9}$
94	$H_2^+ + H_2O$	$\rightarrow H_2O^+ + H_2$	$K=3.9\times10^{-9}$
95	$H_2^+ + H_2O$	$\rightarrow H_3O^+ + H$	$K=3.4\times10^{-9}$
96	$H_2^+ + CO_2$	$\rightarrow CO_2^+ + H_2$	$K=1.4\times10^{-9}$
97	$H_2^+ + CO_2$	$\rightarrow CO^+ + H_2O$	$K=1.4\times10^{-9}$

98	$H_2^+ + CO$	$\rightarrow CO^+ + H_2$	$K=6.44\times10^{-10}$
99	$H_2^+ + NO$	$\rightarrow NO^+ + H_2$	$K=1.1\times10^{-9}$
100	$H_2^+ + NH_3$	$\rightarrow H_3O^+ + H_2$	$K=5.7\times10^{-9}$
101	$H_2^+ + OH$	$\rightarrow H_2O^+ + H$	$K=7.5\times10^{-10}$
102	$H_2^+ + OH$	$\rightarrow OH^+ + H_2$	$K=7.5\times10^{-10}$
103	$H_2^+ + H$	$\rightarrow H^+ + H_2$	$K=6.4\times10^{-10}$
104	$OH^+ + O_2$	$\rightarrow O_2^+ + OH$	$K=2.0\times10^{-10}$
105	$OH^+ + H_2O$	$\rightarrow H_3O^+ + O$	$K=1.5\times10^{-9}$
106	$OH^+ + H_2O$	$\rightarrow H_2O^+ + OH$	$K=1.5\times10^{-9}$
107	$OH^+ + NO$	$\rightarrow NO^+ + OH$	$K=4.6\times10^{-10}$
108	$OH^+ + NO_2$	$\rightarrow NO_2^+ + OH$	$K=3.0\times10^{-10}$
109	$OH^+ + NH_3$	$\rightarrow H_3O^+ + OH$	$K=1.2\times10^{-9}$
110	$OH^+ + NH_3$	$\rightarrow H_4O^+ + O$	$K=1.2\times10^{-9}$
111	$OH^+ + N_2O$	$\rightarrow N_2O^+ + OH$	$K=5.0\times10^{-10}$
112	$OH^+ + N_2O$	$\rightarrow NO^+ + HNO$	$K=1.7\times10^{-10}$
113	$OH^+ + H_2$	$\rightarrow H_2O^+ + H_2$	$K=1.3\times10^{-9}$
114	$OH^+ + OH$	$\rightarrow H_2O^+ + O$	$K=7.0\times10^{-10}$
115	$NO^+ + H_2O + M$	$\rightarrow NO^+(H_2O) + M$	$K=1.5\times10^{-28}(300/T)$
116	$NO^+ + O_3$	$\rightarrow NO_2^+ + O_2$	$K=1.0\times10^{-14}$
117	$NO^+ + N_2O_5$	$\rightarrow NO_2^+ + 2NO$	$K=5.9\times10^{-10}$
118	$NO^+ + N + M$	$\rightarrow N_2O^+ + M$	$K=1.0\times10^{-29}(300/T)$
119	$NO^+(H_2O) + H_2O + M$	$\rightarrow NO^+(H_2O)_2 + M$	$K=1.0\times10^{-27}(300/T)$
120	$NO^+(H_2O) + NO_2$	$\rightarrow NO_2^+(H_2O) + NO$	$K=2.0\times10^{-15}$
121	$NO^+(H_2O) + NH_3$	$\rightarrow NH_4^+ + HNO_2$	$K=1.0\times10^{-9}$
122	$NO^+(H_2O)_2 + M$	$\rightarrow NO^+(H_2O) + H_2O + M$	$K=1.0\times10^{-14}$
123	$NO^+(H_2O)_2 + H_2O + M$	$\rightarrow NO^+(H_2O)_3 + M$	$K=2.0\times10^{-27}(300/T)$
124	$NO^+(H_2O)_2 + NH_3$	$\rightarrow NH_4^+ + HNO_2 + H_2O$	$K=1.0\times10^{-9}$ NH_4^+/H_2O clusters neglected
125	$NO^+(H_2O)_3 + M$	$\rightarrow NO^+(H_2O)_2 + H_2O + M$	$K=1.5\times10^{-12}$
126	$NO^+(H_2O)_3 + H_2O$	$\rightarrow H_3O^+(H_2O)_2 + HNO_2$	$K=2.0\times10^{-6}\exp(-3000/T)$
127	$NO^+(H_2O)_3 + NH_3$	$\rightarrow NH_4^+ + HNO_2 + 2H_2O$	$K=1.0\times10^{-9}$ NH_4^+/H_2O clusters neglected
128	$NO_2^+ + NO$	$\rightarrow NO^+ + NO_2$	$K=2.9\times10^{-10}$
129	$NO_2^+ + H_2O + N_2$	$\rightarrow NO_2^+(H_2O) + N_2$	$K=5.0\times10^{-28}$

130 $NO_2^+(H_2O) + NH_3 \rightarrow NH_4^+ + HNO_3$ $K=6.4\times10^{-10}$

131 $NO_2^+(H_2O) + N_2 \rightarrow NO_2^+ + H_2O + N_2$ $K=5.0\times10^{-15}$

132 $NO_2^+(H_2O) + NO \rightarrow NO^+(H_2O) + NO_2$ $K=3.1\times10^{-11}$

133 $NO_2^+(H_2O) + H_2O + N_2 \rightarrow NO_2^+(H_2O)_2 + N_2$ $K=2.0\times10^{-27}$

134 $NO_2^+(H_2O)_2 + H_2O \rightarrow H_3O^+(H_2O) + HNO_3$ $K=2.0\times10^{-10}$

A.2.2 Negative ion - neutral reactions

135 $e^-(hot) \rightarrow e^-(thermal)$ $K=1.0\times10^{+9}$

136 $e^- + 2O_2 \rightarrow O_2^- + O_2^*$ $K=1.2\times10^{-29}(300/T)^{1.38} \times \exp(-6602/T)$

137 $e^- + O_2 + M \rightarrow O_2^- + M$ $K=3.0\times10^{-31}$ M is not O_2

138 $e^- + NO + M \rightarrow NO^- + M$ $K=8.0\times10^{-31}$

139 $e^- + NO_2 + M \rightarrow NO_2^- + M$ $K=1.5\times10^{-30}$

140 $e^- + HNO_3 \rightarrow NO_2^- + OH$ $K=5.0\times10^{-8}$

141 $e^- + O_3 \rightarrow O^- + O_2$ $K=9.0\times10^{-12}(300/T)^{1.5}$

142 $e^- + O_3 + M \rightarrow O_3^- + M$ $K=1.0\times10^{-30}$

143 $e^- + NO_3 + M \rightarrow NO_3^- + M$ $K=1.0\times10^{-30}$

144 $O^- + O_2 + M \rightarrow O_3^- + M$ $K=1.1\times10^{-12}(300/T)$

145 $O^- + O_2^* \rightarrow e^- + O_3$ $K=3.0\times10^{-10}$

146 $O^- + CO_2 + M \rightarrow CO_3^- + M$ $K=8.0\times10^{-29}(300/T)$

147 $O^- + NO \rightarrow e^- + NO_2$ $K=3.1\times10^{-10}(300/T)0.83$

148 $O^- + NO + M \rightarrow NO_2^- + M$ $K=1.0\times10^{-29}(300/T)$

149 $O^- + NO_2 \rightarrow NO_2^- + O$ $K=1.2\times10^{-9}$

150 $O^- + N_2O \rightarrow NO^- + NO$ $K=2.3\times10^{-10}$

151 $O^- + O_3 \rightarrow O_3^- + O$ $K=6.5\times10^{-10}$

152 $O^- + CO \rightarrow e^- + CO_2$ $K=6.0\times10^{-10}(300/T)0.32$

153 $O^- + H_2 \rightarrow e^- + H_2O$ $K=6.5\times10^{-10}(300/T)0.19$

154 $O^- + O \rightarrow e^- + O_2$ $K=1.9\times10^{-10}$

155 $O^- + N \rightarrow e^- + NO$ $K=2.0\times10^{-10}$

156 $O_2^- + O_2 + M \rightarrow O_4^- + M$ $K=3.5\times10^{-31}(300/T)$

157 $O_2^- + O_2^* \rightarrow e^- + 2O_2$ $K=2.0\times10^{-10}$

158 $O_2^- + H_2O + M \rightarrow O_2^-(H_2O) + M$ $K=3.0\times10^{-28}(300/T)$

159 $O_2^- + NO_2 \rightarrow NO_2^- + O_2$ $K=8.0\times10^{-10}$

160 $O_2^- + HNO_3 \rightarrow NO_3^- + HO_2$ $K=2.8\times10^{-10}$

161 $O_2^- + O_3 \rightarrow O_3^- + O_2$ $K=5.0\times10^{-10}$

162 $O_2^- + H_2 \rightarrow e^- + H_2O_2$ $K=1.0\times10^{-9}$

163 $O_2^- + O \rightarrow O^- + O_2$ $K=1.5\times10^{-10}$

164 $O_2^- + O \rightarrow e^- + O_3$ $K=1.5\times10^{-10}$

165 $O_2^- + H \rightarrow e^- + HO_2$ $K=1.0\times10^{-9}$

166 $O_2^- + N \rightarrow e^- + NO_2$ $K=5.0\times10^{-10}$

167 $O_2^- + NO_3 \rightarrow NO_3^- + O_2$ $K=5.0\times10^{-10}$

168 $O_2^-(H_2O) + NO \rightarrow NO_3^- + H_2O$ $K=3.0\times10^{-10}$

169 $O_2^-(H_2O) + NO_2 \rightarrow NO_2^- + O_2 + H_2O$ $K=3.0\times10^{-10}$

170 $O_2^-(H_2O) + O_3 \rightarrow O_3^- + O_2 + H_2O$ $K=8.0\times10^{-10}$

171 $O_2^-(H_2O) + O \rightarrow O^- + O_2 + H_2O$ $K=3.0\times10^{-10}$

172 $O_2^-(H_2O) + NO_3 \rightarrow NO_3^- + O_2 + H_2O$ $K=3.0\times10^{-10}$

173 $O_2^-(H_2O) + N \rightarrow e^- + NO_2 + H_2O$ $K=1.0\times10^{-10}$

174 $O_3^- + CO_2 \rightarrow CO_3^- + O_2$ $K=4.8\times10^{-10}$

175 $O_3^- + NO \rightarrow NO_2^- + O_2$ $K=1.0\times10^{-11}$

176 $O_3^- + NO_2 \rightarrow NO_2^- + O_3$ $K=2.8\times10^{-10}$

177 $O_3^- + NO_2 \rightarrow NO_3^- + O_2$ $K=2.0\times10^{-11}$

178 $O_3^- + SO_2 \rightarrow SO_3^- + O_2$ $K=1.7\times10^{-9}$

179 $O_3^- + O \rightarrow O_2^- + O_2$ $K=2.5\times10^{-10}$

180 $O_3^- + O \rightarrow e^- + 2O_2$ $K=1.0\times10^{-11}$

181 $O_3^- + NO_3 \rightarrow NO_3^- + O_3$ $K=5.0\times10^{-10}$

182 $NO^- + M \rightarrow e^- + NO + M$ $K=2.1\times10^{-11}(300/T)^{1.54} \times \exp(-278/T)$

183 $NO^- + O_2 \rightarrow O_2^- + NO$ $K=5.0\times10^{-10}$

184 $NO^- + NO_2 \rightarrow NO_2^- + NO$ $K=3.0\times10^{-10}$

185 $NO^- + O_3 \rightarrow O_3^- + NO$ $K=3.0\times10^{-10}$

186 $NO^- + O \rightarrow O^- + NO$ $K=3.0\times10^{-10}$

187 $NO^- + NO_3 \rightarrow NO_3^- + NO$ $K=3.0\times10^{-10}$

188 $NO_2^- + NO_2 \rightarrow NO_3^- + NO$ $K=2.0\times10^{-13}$

189 $NO_2^- + HNO_3 \rightarrow NO_3^- + HNO_2$ $K=1.6\times10^{-9}$

190 $NO_2^- + N_2O_5 \rightarrow NO_3^- + 2NO_2$ $K=6.5\times10^{-10}$

191 $NO_2^- + O_3 \rightarrow NO_3^- + O_2$ $K=5.0\times10^{-11}$

192 $NO_2^- + NO_3 \rightarrow NO_3^- + NO_2$ $K=5.0\times10^{-10}$

193 $NO_3^- + NO \rightarrow NO_2^- + NO_2$ $K=4.3\times10^{-11}(300/T)^{0.35} \times \exp(-3788/T)$

194 $NO_3^- + O + CO_2 \rightarrow CO_3^- + NO_3$ $K=8.2\times10^{-34}(300/T)^{1.16} \times \exp(-2619/T)$

A.2.3 Ionic recombination reactions in the gas phase

195 $N_2^+ + e^-$ --->$N + N(^2D)$
$K=2.2\times10^{-7}(300/T)^{0.39}+6.0\times10^{-27}(300/T)^{2.5}M$

196 $N_2^+ + e^-$ --->N_2
$K=4.0\times10^{-12}(300/T)^{0.7}+6.0\times10^{-27}(300/T)^{2.5}M$

197 $N_2^+ + O_2^-$ --->$N_2 + O_2$
$K=1.6\times10^{-7}(300/T)^{0.5}+3.0\times10^{-25}(300/T)^{2.5}M$

198 $N_2^+ + O^-$ --->$N_2 + O$
$K=4.0\times10^{-7}(300/T)^{0.5}+3.0\times10^{-25}(300/T)^{2.5}M$

199 $N_2^+ + O_3^-$ --->$N_2O + O_2$
$K=4.0\times10^{-7}(300/T)^{0.5}+3.0\times10^{-25}(300/T)^{2.5}M$

200 $N_2^+ + NO^-$ --->$N_2 + NO$
$K=4.0\times10^{-7}(300/T)^{0.5}+3.0\times10^{-25}(300/T)^{2.5}M$

201 $N_2^+ + NO_2^-$ --->$NO_2 + N_2$
$K=4.0\times10^{-7}(300/T)^{0.5}+3.0\times10^{-25}(300/T)^{2.5}M$

202 $N_2^+ + NO_3^-$ --->$NO_2 + N_2O$
$K=4.0\times10^{-7}(300/T)^{0.5}+3.0\times10^{-25}(300/T)^{2.5}M$

203 $N_2^+ + CO_3^-$ --->$CO_2 + N_2 + O$
$K=4.0\times10^{-7}(300/T)^{0.5}+3.0\times10^{-25}(300/T)^{2.5}M$

204 $N_2^+ + O_4^-$ --->$N_2 + 2O_2$
$K=4.0\times10^{-7}(300/T)^{0.5}+3.0\times10^{-25}(300/T)^{2.5}M$

205 $N_2^+ + O_2^-(H_2O)$ --->$N_2 + O_2 + H_2O$
$K=5.0\times10^{-7}(300/T)^{0.5}+6.0\times10^{-27}(300/T)^{2.5}M$

206 $N^+ + O^-$ --->$N + O$
$K=2.6\times10^{-7}(300/T)^{0.5}+3.0\times10^{-25}(300/T)^{2.5}M$

207 $N^+ + O_2^-$ --->$N + O_2$
$K=4.0\times10^{-7}(300/T)^{0.5}+3.0\times10^{-25}(300/T)^{2.5}M$

208 $N^+ + O_3^-$ --->$NO + O_2$
$K=4.0\times10^{-7}(300/T)^{0.5}+3.0\times10^{-25}(300/T)^{2.5}M$

209 $N^+ + NO^-$ --->$O + N_2$
$K=4.0\times10^{-7}(300/T)^{0.5}+3.0\times10^{-25}(300/T)^{2.5}M$

210 $N^+ + NO_2^-$ --->$2NO$
$K=4.0\times10^{-7}(300/T)^{0.5}+3.0\times10^{-25}(300/T)^{2.5}M$

211 $N^+ + NO_3^-$ --->$NO + NO_2$
$K=4.0\times10^{-7}(300/T)^{0.5}+3.0\times10^{-25}(300/T)^{2.5}M$

212 $N^+ + CO_3^-$ --->$NO + CO_2$
$K=4.0\times10^{-7}(300/T)^{0.5}+3.0\times10^{-25}(300/T)^{2.5}M$

213 $N^+ + O_2^-(H_2O)$ --->$NO_2 + H_2O$
$K=5.0\times10^{-7}(300/T)^{0.5}+3.0\times10^{-25}(300/T)^{2.5}M$

214 $O_2^+ + e^-$ --->$O + O(^1D)$ $K=2.1\times10^{-7}(300/T)^{0.55}$

215 $O_2^+ + e^-$ --->O_2
$K=4.0\times10^{-12}(300/T)^{0.7}+6.0\times10^{-27}(300/T)^{2.5}M$

216 $O_2^+ + O^-$ --->$O_2 + O$
$K=9.6\times10^{-8}(300/T)^{0.5}+3.0\times10^{-25}(300/T)^{2.5}M$

217 $O_2^+ + O_2^-$ --->$2O_2$
$K=4.2\times10^{-7}(300/T)^{0.5}+3.0\times10^{-25}(300/T)^{2.5}M$

218 $O_2^+ + O_3^-$ --->$2O_2 + O$
$K=4.0\times10^{-7}(300/T)^{0.5}+3.0\times10^{-25}(300/T)^{2.5}M$

219 $O_2^+ + NO^-$ --->$NO + O_2$
$K=4.0\times10^{-7}(300/T)^{0.5}+3.0\times10^{-25}(300/T)^{2.5}M$

220 $O_2^+ + NO_2^-$ --->$NO_2 + O_2$
$K=4.1\times10^{-7}(300/T)^{0.5}+3.0\times10^{-25}(300/T)^{2.5}M$

221 $O_2^+ + NO_3^-$ --->$NO_2 + O_2 + O$
$K=1.3\times10^{-7}(300/T)^{0.5}+3.0\times10^{-25}(300/T)^{2.5}M$

222 $O_2^+ + CO_3^-$ --->$CO_2 + O_2$
$K=4.0\times10^{-7}(300/T)^{0.5}+3.0\times10^{-25}(300/T)^{2.5}M$

223 $O_2^+ + O_2^-(H_2O)$ --->$2O_2 + H_2O$
$K=5.0\times10^{-7}(300/T)^{0.5}+3.0\times10^{-25}(300/T)^{2.5}M$

224 $O^+ + e^-$ --->O
$K=4.0\times10^{-12}(300/T)^{0.5}+6.0\times10^{-27}(300/T)^{2.5}M$

225 $O^+ + O^-$ --->$2O$
$K=2.7\times10^{-7}(300/T)^{0.5}+3.0\times10^{-25}(300/T)^{2.5}M$

226 $O^+ + O_2^-$ --->$O + O_2$
$K=4.0\times10^{-7}(300/T)^{0.5}+3.0\times10^{-25}(300/T)^{2.5}M$

227 $O^+ + O_3^-$ --->$2O_2$
$K=4.0\times10^{-7}(300/T)^{0.5}+3.0\times10^{-25}(300/T)^{2.5}M$

228 $O^+ + NO^-$ --->$NO + O$
$K=4.0\times10^{-7}(300/T)^{0.5}+3.0\times10^{-25}(300/T)^{2.5}M$

229 $O^+ + NO_2^-$ --->$NO + O_2$
$K=4.0\times10^{-7}(300/T)^{0.5}+3.0\times10^{-25}(300/T)^{2.5}M$

230 $O^+ + NO_3^-$ --->$O_2 + NO_2$
$K=4.0\times10^{-7}(300/T)^{0.5}+3.0\times10^{-25}(300/T)^{2.5}M$

231 $O^+ + CO_3^-$ --->$O_2 + CO_2$
$K=4.0\times10^{-7}(300/T)^{0.5}+3.0\times10^{-25}(300/T)^{2.5}M$

232 $O^+ + O_2^-(H_2O)$ --->$O_3 + H_2O$

$K=2.0x10^{-6}(300/T)+6.0x10^{-27}(300/T)^{2.5}M$

233 $O4^+ + NO^-$ ---> $O2 + NO3$

$K=4.0x10^{-7}(300/T)^{0.5}+3.0x10^{-25}(300/T)^{2.5}M$

234 $O4^+ + NO2^-$ ---> $2O2 + NO2$

$K=4.0x10^{-7}(300/T)^{0.5}+3.0x10^{-25}(300/T)^{2.5}M$

235 $O4^+ + NO3^-$ ---> $O2 + NO2 + O3$

$K=4.0x10^{-7}(300/T)^{0.5}+3.0x10^{-25}(300/T)^{2.5}M$

236 $O4^+ + CO3^-$ ---> $O2 + CO2 + O3$

$K=4.0x10^{-7}(300/T)^{0.5}+3.0x10^{-25}(300/T)^{2.5}M$

237 $O4^+ + O2^-(H2O)$ ---> $3O2 + H2O$

$K=5.0x10^{-7}(300/T)^{0.5}+3.0x10^{-25}(300/T)^{2.5}M$

238 $O2^+(H2O) + e^-$ ---> $H2O + O2$

$K=1.5x10^{-6}(300/T)^{0.2}+5.0x10^{-26}(300/T)^{2.5}M$

239 $O2^+(H2O) + O^-$ ---> $H2O + O3$

$K=5.0x10^{-7}(300/T)^{0.5}+3.0x10^{-25}(300/T)^{2.5}M$

240 $O2^+(H2O) + O2^-$ ---> $H2O + 2O2$

$K=5.0x10^{-7}(300/T)^{0.5}+3.0x10^{-25}(300/T)^{2.5}M$

241 $O2^+(H2O) + O3^-$ ---> $H2O + O2 + O3$

$K=5.0x10^{-7}(300/T)^{0.5}+3.0x10^{-25}(300/T)^{2.5}M$

242 $O2^+(H2O) + O4^-$ ---> $H2O + 3O2$

$K=4.0x10^{-7}(300/T)^{0.5}+3.0x10^{-25}(300/T)^{2.5}M$

243 $O2^+(H2O) + NO^-$ ---> $H2O + NO3$

$K=5.0x10^{-7}(300/T)^{0.5}+3.0x10^{-25}(300/T)^{2.5}M$

244 $O2^+(H2O) + NO2^-$ ---> $H2O + O2 + NO2$

$K=5.0x10^{-7}(300/T)^{0.5}+3.0x10^{-25}(300/T)^{2.5}M$

245 $O2^+(H2O) + NO3^-$ ---> $H2O + O3 + NO2$

$K=5.0x10^{-7}(300/T)^{0.5}+3.0x10^{-25}(300/T)^{2.5}M$

246 $O2^+(H2O) + CO3^-$ ---> $H2O + O2 + CO2 + O$

$K=5.0x10^{-7}(300/T)^{0.5}+3.0x10^{-25}(300/T)^{2.5}M$

247 $O2^+(H2O) + O2^-(H2O)$ ---> $2O2 + H2O$

$K=5.0x10^{-7}(300/T)^{0.5}+3.0x10^{-25}(300/T)^{2.5}M$

248 $H2O^+ + e^-$ ---> $OH + H$ $K=6.6x10^{-6}T^{-0.5}$

249 $H2O^+ + e^-$ ---> $H2 + O$ $K=2.4x10^{-6}T^{-0.5}$

250 $H2O^+ + e^-$ ---> $2H + O$ $K=3.0x10^{-6}T^{-0.5}$

251 $H2O^+ + e^- + M$ --> $H2O + M$ $K=6.0x10^{-27}(300/T)^{2.5}$

252 $H2O^+ + O^-$ --> $H2O + O$

$K=4.0x10^{-7}(300/T)^{0.5}+3.0x10^{-25}(300/T)^{2.5}M$

253 $H2O^+ + O2^-$ --> $H2O + O2$

$K=4.0x10^{-7}(300/T)^{0.5}+3.0x10^{-25}(300/T)^{2.5}M$

254 $H2O^+ + O3^-$ --> $H2O + O3$

$K=4.0x10^{-7}(300/T)^{0.5}+3.0x10^{-25}(300/T)^{2.5}M$

255 $H2O^+ + O4^-$ ---> $2O2 + H2O$

$K=4.0x10^{-7}(300/T)^{0.5}+3.0x10^{-25}(300/T)^{2.5}M$

256 $H2O^+ + NO^-$ ---> $NO + H2O$

$K=4.0x10^{-7}(300/T)^{0.5}+3.0x10^{-25}(300/T)^{2.5}M$

257 $H2O^+ + NO2^-$ ---> $NO2 + H2O$

$K=4.0x10^{-7}(300/T)^{0.5}+3.0x10^{-25}(300/T)^{2.5}M$

258 $H2O^+ + NO3^-$ ---> $NO3 + H2O$

$K=4.0x10^{-7}(300/T)^{0.5}+3.0x10^{-25}(300/T)^{2.5}M$

259 $H2O^+ + CO3^-$ ---> $H2O + CO2 + O$

$K=4.0x10^{-7}(300/T)^{0.5}+3.0x10^{-25}(300/T)^{2.5}M$

260 $H2O^+ + O2^-(H2O)$ ---> $O2 + 2H2O$

$K=5.0x10^{-7}(300/T)^{0.5}+3.0x10^{-25}(300/T)^{2.5}M$

261 $H3O^+ + e^-$ ---> $H2O + H$

$K=6.5x10^{-7}(300/T)^{0.5}+6.0x10^{-27}(300/T)^{2.5}M$

262 $H3O^+ + e^-$ ---> $OH + 2H$ $K=6.5x10^{-7}(300/T)^{0.5}$

263 $H3O^+ + O^-$ ---> $H2O + OH$

$K=4.0x10^{-7}(300/T)^{0.5}+3.0x10^{-25}(300/T)^{2.5}M$

264 $H3O^+ + O2^-$ ---> $H2O + O2 + H$ $K=2.0x10^{-6}$

265 $H3O^+ + O2^-$ ---> $H2O + HO2$

$K=4.0x10^{-7}(300/T)^{0.5}+3.0x10^{-25}(300/T)^{2.5}M$

266 $H3O^+ + O3^-$ ---> $H2O + OH + O2$

$K=4.0x10^{-7}(300/T)^{0.5}+3.0x10^{-25}(300/T)^{2.5}M$

267 $CO^+ + O4^-$ ---> $CO2 + O2 + O$

$K=4.0x10^{-7}(300/T)^{0.5}+3.0x10^{-25}(300/T)^{2.5}M$

268 $CO^+ + NO^-$ ---> $CO + NO$

$K=4.0x10^{-7}(300/T)^{0.5}+3.0x10^{-25}(300/T)^{2.5}M$

269 $CO^+ + NO2^-$ ---> $CO2 + NO$

$K=4.0x10^{-7}(300/T)^{0.5}+3.0x10^{-25}(300/T)^{2.5}M$

270 $CO^+ + NO3^-$ ---> $CO2 + NO2$

$K=4.0x10^{-7}(300/T)^{0.5}+3.0x10^{-25}(300/T)^{2.5}M$

271 $CO^+ + CO3^-$ ---> $2CO2$

$K=4.0x10^{-7}(300/T)^{0.5}+3.0x10^{-25}(300/T)^{2.5}M$

272 $CO^+ + O2^-(H2O)$ ---> $CO2 + O + H2O$

$K=5.0x10^{-7}(300/T)^{0.5}+3.0x10^{-25}(300/T)^{2.5}M$

273 $H^+ + e^-$ ---> H

$K=3.5x10^{-12}(300/T)^{0.7}+6.0x10^{-27}(300/T)^{2.5}M$

274 $H^+ + O^-$ ---> $H + O$

$K=4.0x10^{-7}(300/T)^{0.5}+3.0x10^{-25}(300/T)^{2.5}M$

275 $H^+ + O2^-$ ---> $H + O2$

$K=4.0x10^{-7}(300/T)^{0.5}+3.0x10^{-25}(300/T)^{2.5}M$

276 $H^+ + O3^-$ ---> $OH + O2$

$K=4.0x10^{-7}(300/T)^{0.5}+3.0x10^{-25}(300/T)^{2.5}M$

277 $H^+ + NO^-$ ---> $NO + H$

$K=4.0x10^{-7}(300/T)^{0.5}+3.0x10^{-25}(300/T)^{2.5}M$

278 $H^+ + NO2^-$ ---> $NO + OH$

$K=4.0x10^{-7}(300/T)^{0.5}+3.0x10^{-25}(300/T)^{2.5}M$

279 $H^+ + NO3^-$ ---> $NO2 + OH$

$K=4.0x10^{-7}(300/T)^{0.5}+3.0x10^{-25}(300/T)^{2.5}M$

280 $H^+ + CO3^-$ ---> $CO2 + OH$

$K=4.0x10^{-7}(300/T)^{0.5}+3.0x10^{-25}(300/T)^{2.5}M$

281 $H^+ + O2^-(H2O)$ ---> $H2O + HO2$

$K=5.0x10^{-7}(300/T)^{0.5}+3.0x10^{-25}(300/T)^{2.5}M$

282 $H2^+ + e^-$ ---> $2H$ $K=2.3x10^{-8}(100/T)^{0.29}$

283 $OH^+ + e^-$ ---> $H + O$ $K=2.0x10^{-7}$

284 $OH^+ + e^- + M$ ---> $OH + M$ $K=6.0x10^{-27}(300/T)^{2.5}$

285 $OH^+ + O^-$ ---> $H + O2$

$K=4.0x10^{-7}(300/T)^{0.5}+3.0x10^{-25}(300/T)^{2.5}M$

286 $OH^+ + O2^-$ ---> $OH + O2$

$K=4.0x10^{-7}(300/T)^{0.5}+3.0x10^{-25}(300/T)^{2.5}M$

287 $OH^+ + O3^-$ ---> $HO2 + O2$

$K=4.0x10^{-7}(300/T)^{0.5}+3.0x10^{-25}(300/T)^{2.5}M$

288 $OH^+ + NO^-$ ---> $OH + NO$

$K=4.0x10^{-7}(300/T)^{0.5}+3.0x10^{-25}(300/T)^{2.5}M$

289 $OH^+ + NO2^-$ ---> $OH + NO2$

$K=4.0x10^{-7}(300/T)^{0.5}+3.0x10^{-25}(300/T)^{2.5}M$

290 $OH^+ + NO3^-$ ---> $HNO2 + O2$

$K=4.0x10^{-7}(300/T)^{0.5}+3.0x10^{-25}(300/T)^{2.5}M$

291 $OH^+ + CO3^-$ ---> $H + O2 + H2O$

$K=4.0x10^{-7}(300/T)^{0.5}+3.0x10^{-25}(300/T)^{2.5}M$

292 $OH^+ + O2^-(H2O)$

$K=5.0x10^{-7}(300/T)^{0.5}+3.0x10^{-25}(300/T)^{2.5}M$

293 $NO^+ + e^-$ ---> NO

$K=4.0x10^{-12}(300/T)^{0.7}+6.0x10^{-27}(300/T)^{2.5}M$

294 $NO^+ + e^- + M$ ---> $N + O + M$ $K=1.0x10^{-27}$

295 $NO^+ + e^-$ ---> $O + N(^2D)$ $K=4.3x10^{-7}(300/T)^{0.8}$

296 $NO^+ + O^-$ ---> $O + NO$

$K=4.9x10^{-12}(300/T)^{0.7}+3.0x10^{-25}(300/T)^{2.5}M$

297 $NO^+ + O2^-$ ---> $NO + O2$

$K=4.0x10^{-7}(300/T)^{0.5}+3.0x10^{-25}(300/T)^{2.5}M$

298 $NO^+ + O3^-$ ---> $NO + O + O2$

$K=4.0x10^{-7}(300/T)^{0.5}+3.0x10^{-25}(300/T)^{2.5}M$

299 $NO^+ + NO^-$ ---> $O2 + N2$

$K=4.0x10^{-7}(300/T)^{0.5}+3.0x10^{-25}(300/T)^{2.5}M$

300 $NO^+ + NO2^-$ ---> $NO2 + N + O$ $K=1.0x10^{-7}$

301 $NO^+ + NO2^-$ ---> $NO + NO2$

$K=3.5x10^{-7}(300/T)^{0.5}+3.0x10^{-25}(300/T)^{2.5}M$

302 $NO^+ + NO3^-$ ---> $NO3 + N + O$ $K=1.0x10^{-7}$

303 $NO^+ + NO3^-$ ---> $2NO2$

$K=4.0x10^{-7}(300/T)^{0.5}+3.0x10^{-25}(300/T)^{2.5}M$

304 $NO^+ + CO3^-$ ---> $NO2 + CO2$

$K=4.0x10^{-7}(300/T)^{0.5}+3.0x10^{-25}(300/T)^{2.5}M$

305 $NO^+ + O4^-$ ---> $2O2 + NO$

$K=4.0x10^{-7}(300/T)^{0.5}+3.0x10^{-25}(300/T)^{2.5}M$

306 $NO^+ + O2^-(H2O)$ ---> $NO3 + H2O$

$K=5.0x10^{-7}(300/T)^{0.5}+3.0x10^{-25}(300/T)^{2.5}M$

307 $NO^+(H2O) + e^- + M$ ---> $H2O + NO + M$

$K=1.0x10^{-6}(300/T)^{0.2}+5.0x10^{-26}(300/T)^{2.5}M$

308 $NO^+(H2O) + O^-$ ---> $H2O + NO2$

$K=5.0x10^{-7}(300/T)^{0.5}+3.0x10^{-25}(300/T)^{2.5}M$

309 $NO^+(H2O) + O2^-$ ---> $H2O + O2 + NO$

$K=5.0x10^{-7}(300/T)^{0.5}+3.0x10^{-25}(300/T)^{2.5}M$

310 $NO^+(H2O) + O3^-$ ---> $H2O + O2 + NO2$

$K=5.0x10^{-7}(300/T)^{0.5}+3.0x10^{-25}(300/T)^{2.5}M$

311 $NO^+(H2O) + NO^-$ ---> $H2O + O2 + N2$

$K=5.0x10^{-7}(300/T)^{0.5}+3.0x10^{-25}(300/T)^{2.5}M$

312 $NO^+(H2O) + NO2^-$ ---> $H2O + NO2 + NO$

$K=5.0x10^{-7}(300/T)^{0.5}+3.0x10^{-25}(300/T)^{2.5}M$

313 $NO^+(H2O) + NO3^-$ ---> $H2O + 2NO2$

$K=5.0x10^{-7}(300/T)^{0.5}+3.0x10^{-25}(300/T)^{2.5}M$

314 $NO^+(H2O) + CO3^-$ ---> $H2O + CO2 + NO + O$

$K=5.0x10^{-7}(300/T)^{0.5}+3.0x10^{-25}(300/T)^{2.5}M$

315 $NO^+(H_2O) + O_2^-(H_2O)$
$K=5.0x10^{-7}(300/T)^{0.5}+3.0x10^{-25}(300/T)^{2.5}M$

316 $NO^+(H_2O)_2 + e^- + M \rightarrow H_2O + NO + M$
$K=2.0x10^{-6}(300/T)^{0.2}+5.0x10^{-26}(300/T)^{2.5}M$

317 $NO^+(H_2O)_2 + O^- \rightarrow 2H_2O + NO_2$
$K=5.0x10^{-7}(300/T)^{0.5}+3.0x10^{-25}(300/T)^{2.5}M$

318 $NO^+(H_2O)_2 + O_2^- \rightarrow 2H_2O + O_2 + NO$
$K=5.0x10^{-7}(300/T)^{0.5}+3.0x10^{-25}(300/T)^{2.5}M$

319 $NO^+(H_2O)_2 + O_3^- \rightarrow 2H_2O + O_2 + NO_2$
$K=5.0x10^{-7}(300/T)^{0.5}+3.0x10^{-25}(300/T)^{2.5}M$

320 $NO^+(H_2O)_2 + NO^- \rightarrow 2H_2O + O_2 + N_2$
$K=5.0x10^{-7}(300/T)^{0.5}+3.0x10^{-25}(300/T)^{2.5}M$

321 $NO^+(H_2O)_2 + NO_2^- \rightarrow 2H_2O + NO + N_2$
$K=5.0x10^{-7}(300/T)^{0.5}+3.0x10^{-25}(300/T)^{2.5}M$

322 $NO^+(H_2O)_2 + NO_3^- \rightarrow 2H_2O + 2NO_2$
$K=5.0x10^{-7}(300/T)^{0.5}+3.0x10^{-25}(300/T)^{2.5}M$

323 $NO^+(H_2O)_2 + CO_3^- \rightarrow 2H_2O + CO_2 + NO + O$
$K=5.0x10^{-7}(300/T)^{0.5}+3.0x10^{-25}(300/T)^{2.5}M$

324 $NO^+(H_2O)_2 + O_2^-(H_2O) \rightarrow NO_3 + 3H_2O$
$K=5.0x10^{-7}(300/T)^{0.5}+3.0x10^{-25}(300/T)^{2.5}M$

325 $NO^+(H_2O)_3 + e^- + M \rightarrow 3H_2O + NO + M$
$K=3.0x10^{-6}(300/T)^{0.2}+3.0x10^{-25}(300/T)^{2.5}M$

326 $NO^+(H_2O)_3 + O^- \rightarrow 3H_2O + NO_2$
$K=5.0x10^{-7}(300/T)^{0.5}+3.0x10^{-25}(300/T)^{2.5}M$

327 $NO^+(H_2O)_3 + O_2^- \rightarrow 3H_2O + O_2 + NO$
$K=5.0x10^{-7}(300/T)^{0.5}+3.0x10^{-25}(300/T)^{2.5}M$

328 $NO^+(H_2O)_3 + O_3^- \rightarrow 3H_2O + NO_2 + NO_2$
$K=5.0x10^{-7}(300/T)^{0.5}+3.0x10^{-25}(300/T)^{2.5}M$

329 $NO^+(H_2O)_3 + NO^- \rightarrow 3H_2O + O_2 + N_2$
$K=5.0x10^{-7}(300/T)^{0.5}+3.0x10^{-25}(300/T)^{2.5}M$

330 $NO^+(H_2O)_3 + NO_2^- \rightarrow 3H_2O + NO_2 + NO$
$K=5.0x10^{-7}(300/T)^{0.5}+3.0x10^{-25}(300/T)^{2.5}M$

331 $NO^+(H_2O)_3 + NO_3^- \rightarrow 3H_2O + 2NO_2$
$K=5.0x10^{-7}(300/T)^{0.5}+3.0x10^{-25}(300/T)^{2.5}M$

332 $NO^+(H_2O)_3 + CO_3^- \rightarrow 3H_2O + CO_2 + NO + O$
$K=5.0x10^{-7}(300/T)^{0.5}+3.0x10^{-25}(300/T)^{2.5}M$

333 $NO^+(H_2O)_3 + O_4^- \rightarrow 3H_2O + NO_3 + NO_2$
$K=5.0x10^{-7}(300/T)^{0.5}+3.0x10^{-25}(300/T)^{2.5}M$

334 $NO^+(H_2O)_3 + O_2^-(H_2O) \rightarrow 4H_2O + NO_3$
$K=5.0x10^{-7}(300/T)^{0.5}+3.0x10^{-25}(300/T)^{2.5}M$

335 $NO_2^+ + e^- \rightarrow NO + O$ $K=3.0x10^{-7}(300/T)^{0.5}M$

336 $NO_2^+ + e^- + M \rightarrow NO_2 + M$ $K=6.0x10^{-27}(300/T)^{0.5}M$

337 $NO_2^+ + O^- \rightarrow NO + O_2$
$K=4.0x10^{-7}(300/T)^{0.5}+3.0x10^{-25}(300/T)^{2.5}M$

338 $NO_2^+ + O_2^- \rightarrow NO_2 + O_2$
$K=4.0x10^{-7}(300/T)^{0.5}+3.0x10^{-25}(300/T)^{2.5}M$

339 $NO_2^+ + O_3^- \rightarrow NO_3 + O_2$
$K=4.0x10^{-7}(300/T)^{0.5}+3.0x10^{-25}(300/T)^{2.5}M$

340 $NO_2^+ + NO^- \rightarrow N_2O + O_2$
$K=4.0x10^{-7}(300/T)^{0.5}+3.0x10^{-25}(300/T)^{2.5}M$

341 $NO_2^+ + NO_2^- \rightarrow 2O_2 + N_2$
$K=4.0x10^{-7}(300/T)^{0.5}+3.0x10^{-25}(300/T)^{2.5}M$

342 $NO_2^+ + NO_3^- \rightarrow NO_2 + NO + O_2$
$K=4.0x10^{-7}(300/T)^{0.5}+3.0x10^{-25}(300/T)^{2.5}M$

343 $NO_2^+ + CO_3^- \rightarrow NO_3 + CO_2$
$K=4.0x10^{-7}(300/T)^{0.5}+3.0x10^{-25}(300/T)^{2.5}M$

344 $NO_2^+ + O_4^- \rightarrow 2O_2 + NO_2$
$K=4.0x10^{-7}(300/T)^{0.5}+3.0x10^{-25}(300/T)^{2.5}M$

345 $NO_2^+ + O_2^-(H_2O) \rightarrow NO_2 + O_2 + H_2O$
$K=5.0x10^{-7}(300/T)^{0.5}+3.0x10^{-25}(300/T)^{2.5}M$

A.2.4 Reactions of excited species

346 $N_2^* + N_2 \rightarrow 2N_2$ $K=2.7x10^{-11}$

347 $N_2^* + O_2 \rightarrow N_2 + O_2^*$ $K=1.0x10^{-12}$

348 $N_2^* + O_2 \rightarrow N_2 + 2O$ $K=2.0x10^{-12}$

349 $N_2^* + O_2 \rightarrow N_2O + O$ $K=3.0x10^{-14}$

350 $N_2^* + O_2 \rightarrow N_2O + O(^1D)$ $K=3.0x10^{-14}$

351 $N_2^* + H_2O \rightarrow OH + H + N_2$ $K=4.2x10^{-11}$

351 $N_2^* + CO_2 \rightarrow CO + O + N_2$ $K=1.5x10^{-10}$

352 $N_2^* + NO \rightarrow NO + N_2$ $K=1.5x10^{-10}$

353 $N_2^* + NO_2 \rightarrow NO + O + N_2$ $K=1.0x10^{-12}$

354 $N_2^* + SO_2 \rightarrow SO + O + N_2$ $K=5.0x10^{-11}$

355 $N_2^* + NH_3 \rightarrow NH_2 + H + N_2$ $K=4.6x10^{-11}$

356 $N_2^* + NH_3 \rightarrow NH + H_2 + N_2$ $K=9.0x10^{-11}$

357 $N_2^* + N_2O \rightarrow 2N_2 + O$ $K=8.0x10^{-11}$

358 $N_2^* + N_2O \rightarrow N_2 + N + NO$ $K=8.0x10^{-11}$

359	$N_2^* + H_2O_2$	$\rightarrow N_2 + 2OH$	$K=2.0\times10^{-11}$
360	$N_2^* + H_2$	$\rightarrow N_2 + 2H$	$K=3.8\times10^{-15}$
361	$N_2^* + N$	$\rightarrow N_2 + N$	$K=5.0\times10^{-11}$
362	$N_2^* + O$	$\rightarrow N_2 + O^*$	$K=2.3\times10^{-11}$
363	$N_2^* + NH_2$	$\rightarrow N_2 + NH + H$	$K=1.66\times10^{-11}$
364	$N(^2D) + N_2$	$\rightarrow N + N_2$	$K=9.4\times10^{-14}\exp(-510/T)$
365	$N(^2D) + O_2$	$\rightarrow NO + O$	$K=3.5\times10^{-13}T^{0.5}$
366	$N(^2D) + CO_2$	$\rightarrow NO + CO$	$K=4.0\times10^{-13}$
367	$N(^2D) + NO$	$\rightarrow N_2 + O$	$K=7.0\times10^{-11}$
368	$N(^2D) + NO_2$	$\rightarrow N_2O + O$	$K=1.5\times10^{-13}$
369	$N(^2D) + NO_2$	$\rightarrow 2NO$	$K=1.1\times10^{-13}$
370	$N(^2D) + N_2O$	$\rightarrow N_2 + NO$	$K=1.2\times10^{-11}\exp(-570/T)$
371	$N(^2D) + NH_3$	$\rightarrow NH + NH_2$	$K=7.0\times10^{-11}$
372	$N(^2D) + O$	$\rightarrow N + O$	$K=7.0\times10^{-13}$
373	$N(^2P) + N_2$	$\rightarrow N_2 + N$	$K=2.0\times10^{-18}$
374	$N(^2P) + O_2$	$\rightarrow NO + O$	$K=2.0\times10^{-12}$
375	$N(^2P) + NO_2$	$\rightarrow N_2O + O$	$K=1.5\times10^{-13}$
376	$N(^2P) + NO_2$	$\rightarrow 2NO$	$K=1.1\times10^{-13}$
377	$N(^2P) + NH_3$	$\rightarrow NH + NH_2$	$K=7.0\times10^{-11}$
378	$N(^2P) + O$	$\rightarrow N(^2D) + O$	$K=1.0\times10^{-11}$
379	$O_2^* + M$	$\rightarrow O_2 + M$	$K=5.0\times10^{-19}$
380	$O_2^* + O_3$	$\rightarrow 2O_2 + O$	$K=5.2\times10^{-11}\exp(-2840/T)$
381	$O_2^* + O$	$\rightarrow 2O_2 + O^*$	$K=1.7\times10^{-10}$
382	$O_2^* + H$	$\rightarrow OH + O$	$K=1.83\times10^{-13}\exp(-1550/T)$
383	$O_2^* + HO_2$	$\rightarrow O_2 + HO_2$	$K=1.66\times10^{-12}$
384	$O_2^* + HO_2$	$\rightarrow OH + O + O_2$	$K=1.66\times10^{-10}$
385	$O_2^* + NH_2$	$\rightarrow HNO + OH$	$K=1.0\times10^{-14}$
386	$O_2^* + NH$	$\rightarrow NO + OH$	$K=1.0\times10^{-14}$
387	$O_2^* + O^*$	$\rightarrow O_2 + O$	$K=1.7\times10^{-10}$
388	$O(^1D)$	$\rightarrow O + h\nu$	$K=6.3\times10^{-3}$
389	$O(^1D) + M$	$\rightarrow O + M$	$K=1.8\times10^{-11}\exp(+110/T)$ (M = N_2,CO_2)
390	$O(^1D) + N_2 + M$	$\rightarrow N_2O + M$	$K=3.5\times10^{-37}(300/T)^{0.6}$
391	$O(^1D) + O_2$	$\rightarrow O + O_2^*$	$K=2.7\times10^{-11}\exp(+67/T)$
392	$O(^1D) + O_2$	$\rightarrow O + O_2$	$K=5.0\times10^{-12}\exp(+67/T)$
393	$O(^1D) + H_2O$	$\rightarrow H_2 + O_2$	$K=2.3\times10^{-12}$
394	$O(^1D) + H_2O$	$\rightarrow 2OH$	$K=2.2\times10^{-10}$
395	$O(^1D) + H_2O$	$\rightarrow H_2O + O$	$K=1.2\times10^{-11}$
396	$O(^1D) + NH_3$	$\rightarrow NH_2 + OH$	$K=2.9\times10^{-11}$

397	$O(^1D) + NH_3$	$\rightarrow NH + H_2O$	$K=2.9\times10^{-11}$
398	$O(^1D) + O_3$	$\rightarrow 2O + O_2$	$K=1.2\times10^{-10}$
399	$O(^1D) + O_3$	$\rightarrow 2O_2$	$K=1.2\times10^{-10}$
400	$O(^1D) + H_2$	$\rightarrow H + OH$	$K=1.1\times10^{-10}$
401	$O(^1D) + N_2O$	$\rightarrow 2NO$	$K=6.7\times10^{-11}$
402	$O(^1D) + N_2O$	$\rightarrow N_2 + O_2$	$K=4.9\times10^{-11}$
403	$O(^1D) + NO_2$	$\rightarrow N_2 + O_2$	$K=1.4\times10^{-10}$
404	$O(^1D) + H_2O_2$	$\rightarrow OH + HO_2$	$K=5.2\times10^{-10}$
405	O^*	$\rightarrow O^+ + e^-$	$K=2.0\times10^{-7}$
406	$O^* + O_2$	$\rightarrow O_2^* + O$	$K=4.9\times10^{-12}\exp(-850/T)$
407	$O^+ + H_2O$	$\rightarrow H_2O + O$	$K=7.0\times10^{-11}$
408	$O^+ + CO_2$	$\rightarrow CO_2 + O$	$K=3.0\times10^{-11}\exp(-1315/T)$
409	$O^+ + NH_3$	$\rightarrow NH_3 + O$	$K=5.0\times10^{-10}$
410	$O^+ + O_3$	$\rightarrow 2O_2$	$K=1.2\times10^{-10}$